Study of Synchronization in Coupled Dynamical Systems

A THESIS

submitted for the award of Ph.D degree of

MOHANLAL SUKHADIA UNIVERSITY

in the

Faculty of Science

by

Suman Acharyya

Under the Supervision of

R. E. Amritkar

Professor

Theoretical Physics Division

Physical Research Laboratory

Ahmedabad, India

DEPARTMENT OF PHYSICS

MOHANLAL SUKHADIA UNIVERSITY

UDAIPUR

Year of Submission: 2012

To

My Family

DECLARATION

*I **Mr. Suman Acharyya**, S/o Mr. Debiprasad Acharyya, resident of C-9, PRL residences, Navrangpura, Ahmedabad 380009, hereby declare that the work incorporated in the present thesis entitled, **"Study of synchronization in coupled dynamical systems"** is my own and original. This work (in part or in full) has not been submitted to any University for the award of a Degree or a Diploma.*

Date :

(Suman Acharyya)

CERTIFICATE

I feel great pleasure in certifying that the thesis entitled, **"Study of synchronization in coupled dynamical systems"** embodies a record of the results of investigations carried out by Mr. Suman Acharyya under my guidance.

He has completed the following requirements as per Ph.D. regulations of the University.

(a) Course work as per the university rules.

(b) Residential requirements of the university.

(c) Presented his work in the departmental committee.

(d) Published minimum of two research papers in a referred research journal.

I am satisfied with the analysis of data, interpretation of results and conclusions drawn.

I recommend the submission of thesis.

Date :

R. E. Amritkar
Professor
(Thesis Supervisor)

Countersigned by

Head of the Department

Acknowledgements

This thesis is the outcome of my journey as a PhD student for past six years. There are many people who made this journey easier with their proper guidence, words of encouragement and generous help. And this is the place where I convey my thank and gratitude to all of them.

First of all I sincerely thank and express my gratitude to my thesis supervisor Prof. R. E. Amritkar for his excellent guidance and valuable suggestions during my doctoral studies. I have benefited immensely from his sound intuition and deep insight in the subject. I will always be indebted to him for what I have learned from him in these six years.

I thank Dr. Dilip Angom and Prof. V.K.B. Kota for periodically reviewing my thesis work and helping me with their critical and valuable suggestions. I thank Dr. M.S. Santhanam (now at IISER, Pune) for his valuable advices and suggestions on the subject. I thank Vimal and Resmi (IISER, Pune) for the useful discussions on the subject we have together. I thank Dr. Jitesh Bhatt for exploring the excitement of theoretical sciences to me and being my inspiration for joining Theoretical Physics Division. I thank Dr. H. Mishra, Prof. S. Rindani, Prof. S. Mohanty, Prof. A. Joshipura, Dr. Namit Mahajan, Dr. Navinder Singh, Dr. R. P. Singh, Prof. J. Banerjee for their help and the words of encouragements I have from them at various stages of my doctoral studies.

I thank all the staff members of PRL for their kind corporation at all stages. I specially acknowledge computer center staff, for providing excellent computational facilities and library staff for maintaining excellent on-line journal facilities.

I thank all my friends in PRL and outside for making my life delightful with their presence. I am blessed to have friends like Amzad, Anand, Arvind, Ashok, Jayati, Bhaswar, Tapas, Rabiul, Sandeep, Soumya, Vimal, Vineet, Sreekanth, Ketan, Patra, Pravin, Moumita, Khan, Sashi, Bhavik, Santosh, Akhilesh. I specially acknowledge the presence of my good old friends Tridib and Ipsita in my life. Even though staying miles away from me, they are the sources of energies and encouragements to me.

Lastly I express my sincere gratitude to the most important persons of my life, my parents, brother, my wife. Their constant love, support and encouragement help me to overcome the frustration and pain during my doctoral studies. Specially, Rupa for being with me at very crucial time of my life. I acknowledge the presence of two little persons in my life, Mainak and Babi. Their company always gives me the feelings of peace and euphoria.

– Suman Acharyya

Abstract

The work of this thesis can be divided into two parts. In the first part we study synchronization of coupled nonidentical dynamical systems and in the later part we analyze the desynchronization bifurcation of coupled dynamical systems.

When two or more identical systems are coupled then synchronization comes out as equality of the state variables of the coupled systems, which is known as complete (or identical) synchronization (CS). The conditions for stability of complete synchronization are well analyzed by the Master Stability Function (MSF). For coupled nonidentical systems it is not possible to get complete synchronization, instead one can find out a functional relationship between the state variables of the coupled systems which is known as generalized synchronization (GS). In this thesis we develop a theory to construct an approximate MSF for determining stability of GS for coupled nonidentical systems. Next, by using the stability criteria provided by the MSF we construct synchronized optimized network by rewiring the links of a given network. In the optimized network the nodes which have extreme values (maximum or minimum depending on the nature of MSF) of parameter mismatch are chosen as hubs and the pair of nodes having larger parameter mismatch are chosen to create links.

In the second part of this thesis we study desynchronization bifurcation of coupled dynamical systems. In some coupled dynamical systems one can find an interval of coupling strength where the synchronized state is stable. When the coupling strength is increased beyond this stable region, the synchronized state becomes unstable and the coupled systems undergo desynchronization bifurcation. We analyze this desynchronization bifurcation in coupled chaotic systems and we observe that this desynchronization bifurcation is pitchfork bifurcation of transverse manifold. We propose an integrable model which shows similar desynchronization bifurcation. In this context we propose Systems' Transverse Lyapunov Exponents (STLE) for determining the stability of individual systems in a network.

Keywords: Coupled Systems, Synchronization, Master Stability Function, Optimization, Desynchronization Bifurcation.

Contents

Chapter 1

Introduction

1.1 Motivation

The analysis of synchronization phenomena in the evolution of dynamical systems has been a subject of active investigation since the earlier days of physics. Christiaan Huygens was perhaps the first scientist who observed synchronization. He was most famous for his studies in optics and construction of telescope and pendulum clocks. In 1665, he observed that the oscillation of two pendulum clocks hanging from the same beam coincided perfectly and they always moved in opposite directions. He wrote it as *Sympathy of two clocks* [1]. In 1680, another Dutch physicist Engelbert Kaempfer observed synchronization of flashing of fireflies in south east Asia [2]. In many natural systems synchronization occurs spontaneously. There are several examples where scientist observed synchronization phenomena occurring in natural and man made systems [3].

Recently, the search for synchronization has moved to chaotic systems and is a subject of intense research[3, 4, 5, 6, 7, 8, 9, 10, 11, 12, 13, 14, 15, 16]. In chaotic systems the appearance of collective (synchronized) dynamics is, in general, non trivial. Indeed, a dynamical system is called chaotic whenever its evolution sensitively depends on the initial conditions. Two trajectories emerging from two different closeby initial conditions separate exponentially in the course of time. As a result, chaotic systems intrinsically defy synchronization, because even two identical systems starting from slightly different initial conditions would evolve in time in an unsynchronized manner (the differences in the systems' states would grow exponentially). The setting of some collective (synchronized) behavior in coupled chaotic systems has therefore of great importance and interest.

In the context of coupled chaotic systems many different types of synchronization have been studied in the past years. Chaotic identical systems when coupled in same fashion or driven by same external signal, synchronize as the coupling strength increases, and are said to be identically or completely synchronized when the variables of the systems become equal [6, 7, 8, 9, 17]. We can observe other types of synchronization, such as phase synchronization [18, 19], lag synchronization [20], generalized synchronization [21, 22, 23] etc.

For coupled identical systems the stability of the synchronized state is well analysed. Pecora and Carroll (1998) [24] introduced a master stability function (MSF) which can be calculated from a simple set of master stability equations and then applied it to the study of stability of the synchronous state of different networks. However, for coupled nonidentical systems one can not get exact synchronization, but here the synchronized state is generalized synchronization [21, 22, 23]. For this type of network the MSF introduced in [24] does not work. In this thesis work we consider this problem and we formulate a MSF for network of coupled nonidentical systems. By using the fact that the homogeneous part of a linear differential equation dominates the exponential nature of the solution we construct an MSF, which can predict the stability of the generalized synchronized state reasonably well. In this context we also consider the problem of constructing synchronized optimized network from a given random network with fixed number of nodes and links. As the second problem for this thesis we study the nature of desynchronization bifurcation in a coupled dynamical systems.An interesting situation arises when two chaotic Rössler oscillators are coupled with each other. There are two critical coupling constants, say, ε_{c1}, and ε_{c2}. When coupling strength is smaller than the first critical coupling, $\varepsilon < \varepsilon_{c1}$, the oscillators are unsynchronized. They are synchronized for $\varepsilon_{c1} < \varepsilon < \varepsilon_{c2}$ and desynchronized for $\varepsilon > \varepsilon_{c2}$. We study the nature of this desynchronization bifurcation. We introduce Systems' Transverse Lyapunov Exponents (STLE), which provide us the information about stability of each individual oscillators which are couped on a network. We give a simple two dimensional model with quadratic nonlinearity which shows similar desynchronization bifurcation and helps us to understand this bifurcation. The above mentioned two problems setup the motivation of this thesis.

1.2 Synchronization: A natural phenomena

Synchronization phenomena is very common in nature. If we carefully observe natural phenomena, we can immediately realize that synchronous behavior of interacting dynamical units is an ubiquitous phenomena and it spread throughout our daily life: from cardiac pacemaker cells to planetary motions. In human heart about 10000 cells, called sinoatrial nodes, that generate synchronized electrical rhythm and command rest of the heart to beat [25, 26]. Synchronization phenomena has been observed between cardiac and respiratory system in human [27]. One can witness spectacular sight of synchronized blinking of fireflies on the side of rivers in South-East Asia [2]. The perfect synchrony of the rotation and revolution periods of the Moon is the cause of the fact that we always observe the same face of the Moon from the Earth. Clusters of neurons in brain exhibit synchronized oscillations of neuron firing [28]. Some normal and abnormal behavior of the human brain (including some brain diseases) are the result of a sudden and abrupt synchronization in the activity of a large number of neuronal populations [29]. Synchronous neural activity in the brain give rise to a common chronic neurological disorder known as epilepsy [30]. Dynamics of extended ecological systems show synchronization [31]. Synchronization and rhythmic processes have been observed in physiology [32]. Yeast cell suspension exhibit metabolic synchronization [33, 34]. Unison chirping of crickets lead to synchronization [35].

In laboratory experiments synchronization has been observed in electrical circuits [9, 36, 37, 38], laser systems [39, 40, 41].

Synchronization phenomena have received much attention recently. Mostly, the synchronization is considered as the complete coincidence of the states of individual systems or subsystems, which is known as complete (or identical) synchronization (CS) [9] in the literature. There are other types of synchronization: phase synchronization (PS) [18], lag synchronization (LS) [20], imperfect phase synchronization

(IPS) [42], almost synchronization (AS) etc.

1.2.1 Applications of synchronization

Here we mention some applications of chaotic synchronizations.

Secure communication : to decode an encrypted signal at the receiver, chaotic synchronization is used between the sender and receiver [37, 43].

Parameter estimation: chaotic synchronization has been used to determine unknown parameters from a given time series of a system [44, 45].

1.2.2 Definition of synchronization

Synchronization can be defined as a process where two(or many) systems (equivalent or nonequivalent) adjust a given property of their motion to a common behavior, due to coupling or forcing.

1.2.3 Types of synchronization

In the context of coupled chaotic systems many different synchronization states have been studied in the past years. In many practical examples synchronization comes out as a natural phenomena. Depending on the nature of synchronization it has been divided in different types.

- Complete or identical synchronization: It is very simple and the most studied form of synchronization. When two identical systems are coupled the synchronization comes out as equality of the state variables of the coupled systems [9].

$$\begin{aligned} \dot{x} &= f(x) + \varepsilon h(x, y) \\ \dot{y} &= f(y) + \varepsilon h(y, x) \end{aligned}$$

  In the above example systems x and y are two identical system and they are coupled using a linear coupling function $h()$ and ε is the coupling strength.

Under suitable conditions the state variables of these two coupled systems asymptotically become equal, $x = y$ and complete synchronization between the coupled systems is established.

- Phase Synchronization: This type of synchronization is observed between weakly coupled chaotic systems. In this type of synchronization the phase of two coupled systems become locked, but their amplitudes remain uncorrelated. Unlike complete synchronization phase synchronization can be observed in coupled nonidentical systems [18].

$$\begin{aligned}\dot{x} &= f(x) + \varepsilon h(x, y) \\ \dot{y} &= g(y) + \varepsilon h(y, x)\end{aligned}$$

We consider the above examples of two coupled dynamical systems. Let ϕ_x and ϕ_y be the phase of systems x and y respectively. We say that the phase synchronization is established if $|\phi_x - \phi_y| <$ const.

- Generalized synchronization: This general form of synchronization is observed when nonidentical systems are coupled. The generalized synchronization is established if a functional relationship develops between the variables [21].

$$\begin{aligned}\dot{x} &= f(x) + \varepsilon h(x, y) \\ \dot{y} &= g(y) + \varepsilon h(y, x)\end{aligned}$$

The generalized synchronization is established between system x and system y when $\Psi(x, y) = 0$, where $\Psi()$ is some function of the arguments.

- Lag or anticipatory synchronization: This type of synchronization implies the boundedness of state variables of one system and state variables of other system shifted in time with a lag τ_{lag} [20].

We consider two coupled systems given as,

$$\begin{aligned}\dot{x} &= f(x) + \varepsilon h(x,y) \\ \dot{y} &= g(y) + \varepsilon h(y,x).\end{aligned}$$

In the lag synchronized state we will have $x(t) = y(t + \tau_{lag})$.

Above we have discussed some major types of synchronization. There also exist other types of synchronization such as imperfect phase synchronization [42], intermittent lag synchronization [20, 46], and almost synchronization [47]. In this thesis we will mostly consider complete synchronization and generalized synchronization.

1.3 Chaos

Chaos is a widely spread field that has become part of several subjects such as mathematics, physics, engineering, biology, economics and several more [48, 49, 50, 51, 52, 53, 54]. The term 'chaotic' means that the long term behavior can not be predicted even when there is no natural fluctuation of the system parameters or influence of a noisy environment. This unpredictability results from the internal deterministic dynamics of a system and its sensitive dependence on the initial conditions. Two completely identical chaotic systems starting from close initial points, will go away from each other in the course of time and their trajectories will become uncorrelated very soon.

Here, we give the definition of chaos from the book of R. L. Devaney [52].

Definition

We conside a set V and $f : V \to V$. f is chaotic on the set V if,

1. f has sensitive dependence on the initial conditions,i.e there exists $\delta > 0$ such that, for any $x \in V$ and any neighborhood N of x, there exists $y \in N$ and $n \geq 0$ such that $|f^n(x) - f^n(y)| > \delta$.

2. f is topologically transitive, i.e. for any pair of open sets $U, V \subset J$, there exists $k > 0$ such that $f^k(U) \cap V \neq \emptyset$.

3. periodic points are dense in V.

There are several systems which shows chaotic behavior, few of them are circuits [55, 56], lasers [57, 58], plasmas [59], fluids [60, 61], semiconductor devices [62, 63], mechanical devices [64, 65], chemistry [66, 67], acoustics [68, 69], celestial mechanics [70], atmospheric physics [71].

1.4 Measure of chaos

In this section we briefly discuss methods of quantifying chaos,i.e. we will discuss the possible measures to determine how chaotic a system's chaotic behavior is. This measure is important to determine whether a system's apparent chaotic behavior is truly chaotic or it is due to the complexity and noisy nature of the system. For detecting and quantifying chaos we consider Lyapunov characteristics exponents [72, 73, 74, 75] of the system, which is proven to be the most useful dynamical diagnostic for chaotic systems.

1.4.1 Lyapunov characteristics exponents

We have seen that chaotic systems have sensitive dependence on initial conditions. This sensitive dependence on initial conditions can be characterized using Lyapunov exponents [72]. In mathematics the Lyapunov exponent or Lyapunov characteristic exponent of a dynamical system is a quantity that characterizes the average exponential rates of divergence or convergence of nearby trajectories in different directions in phase space.

Let us now consider two trajectories $x(t)$ and $x'(t)$ start from two nearby initial conditions in the phase space $x(0)$ and $x'(0) = x(0) + \delta x(0)$ respectively. The Euclidean distance between these two trajectories is,

$$d(x(0), t) = \parallel x'(t) - x(t) \parallel = \parallel \delta x(t) \parallel . \tag{1.1}$$

where, $\parallel \ldots \parallel$ is the Euclidean norm. Then the average rate of divergence or convergence of these two nearby trajectories, defined as *Lyapunov exponent*, is given by [54, 76],

$$\lambda(x(0)) = \lim_{t\to\infty,\delta x(0)\to 0} \frac{1}{t}\log\left(\frac{d(x(0),t)}{d(x(0),0)}\right). \tag{1.2}$$

For an m-dimensional system there are m-Lyapunov exponents λ_i, $i = 1, ..., m$, and the set of m-Lyapunov exponents is known as the Lyapunov spectrum of the system. To identify whether the motion of the dynamical system is periodic or chaotic, it is sufficient to consider the largest Lyapunov exponent. For chaotic systems the largest Lyapunov exponent is positive $\lambda > 0$, for fixed points it is negative $\lambda < 0$ and for limit cycles or two-torus it is zero $\lambda = 0$.

1.4.2 Numerical calculation of Lyapunov exponents

In this section we briefly review numerical calculation of Lyapunov exponents from a set of ordinary differential equations [73, 74, 75]. The method was developed independently by Benettin et al. [74] and by Shimada and Nagashima [73].

Let us consider an m-dimensional dynamical system given by

$$\frac{dx}{dt} = F(x(t)), \tag{1.3}$$

where, $x(t) \in R^m$ is an m-dimensional state variable of the dynamical system, $x = (x_1, \ldots, x_m)$, and $F : R^m \to R^m$ is an m-dimensional vector field.

The Lyapunov exponents describe the exponential rates of divergence or convergence of nearby trajectories in the phase space, so for numerical determination of Lyapunov exponents from Eq. (1.3) we monitor long-term time evolution of an m-dimensional infinitesimal sphere in the phase space. A "fiducial" trajectory $x(t)$ (center of the sphere) is created by integrating the nonlinear equations of motion (1.3) for some post-transient initial condition. Trajectories of points on the surface of the sphere are defined by the action of the linearized equations of motion on points infinitesimally separated from the fiducial trajectory, and are obtained by linearizing Eq. (1.3) about the fiducial trajectory $x(t)$,

$$\delta\dot{x} = D_x F(x(t))\ \delta x \tag{1.4}$$

where,$\delta x \in R^m$ is the infinitesimal deviation from the fiducial trajectory and $D_x f$ is the $m \times m$ Jacobian matrix calculated at fiducial trajectory $x(t)$, $D_x f_{ij} = \partial f_i / \partial x_j$. When the fiducial trajectory $x(t)$ is constant (fixed point), we can calculate the Lyapunov exponents by evaluating the eigenvalues of the Jacobian matrix $D_x f$ [76, 77]. However, if the fiducial trajectory is chaotic this method will not work. In this case, along with the Eq. (1.3), we integrate the linearized equations of motion (1.4) for m-different initial conditions located on the surface of the m-sphere. Let, these initial conditions define an arbitrarily oriented frame of m-orthonormal vectors $(v_1^0, \ldots, v_m^0)$. The initial sphere evolve into an m-ellipsoid due the locally deforming nature of the flow and the principal axis vector of the ellipsoid diverge in magnitude. Now there are two technical problems in evaluating Lyapunov exponents by directly using Eq. (1.2) [75]. The linearized equation has at least one diverging solutions which leads to a storage problem in computer memory and the orthonormal vectors evolving in time tend to fall along the local direction of most rapid growth. Due to the finite precision of computer calculations, the collapse toward a common direction causes the tangent space orientation of all axis vectors to become indistinguishable. These two problems can be overcome by the repeated use of the Gram-Schmidt reorthonormalization (GSR) procedure on the vector frame. Let us consider that after acting on the initial frame of the orthonormal vectors the linearized equation of motion returns a set of vectors $(v_1^1, \ldots, v_m^1)$. Now, we apply GSR after dt time step which give a new set of orthonormalized vectors $v_1^2, \ldots, v_m^2$:

$$\begin{aligned}
v_1^2 &= \frac{v_1^1}{\| v_1^1 \|}, \\
v_2^2 &= \frac{v_2^1 - \langle v_2^1, v_1^2 \rangle v_1^2}{\| v_2^1 - \langle v_2^1, v_1^2 \rangle v_1^2 \|}, \\
&\vdots \\
v_m^2 &= \frac{v_m^1 - \sum_{j=1}^{m-1} \langle v_m^1, v_j^2 \rangle v_j^2}{\| v_m^1 - \sum_{j=1}^{m-1} \langle v_m^1, v_j^2 \rangle v_j^2 \|},
\end{aligned}$$

where $\langle , \rangle$ denotes the inner product. In this way the rate of growth of evolved vectors can be updated by repeated use of GSR. The after N-th stage, N large enough, the Lyapunov exponents are give by,

$$\lambda_i = \lim_{N \to \infty} \frac{1}{Ndt} \sum_{k=1}^{N} \ln \parallel v_i^k \parallel; \quad i = 1, \ldots, m. \tag{1.5}$$

For a given dynamical system, dt and N are chosen appropriately so that the convergence of Lyapunov exponents is assured. A fortran code algorithm implementing the above scheme can be found in Ref. [75].

1.5 Shadowing theorem

In the earlier sections we have seen that a chaotic system is very sensitive to the initial conditions. A very small deviation in initial conditions can give rise to a completely different trajectory. So, it is impossible to numerically calculate the exact trajectory of a chaotic system, since in the numerical calculations the true derivatives $\frac{dx}{dt}$ are replaced with finite differences $\frac{x(t+dt)-x(t)}{dt}$. This approximation will deviate the trajectory from its exact value. Also computer can store only finite precision numbers, so at every step there are rounding errors which grow exponentially with time. For this one can always ask whether a numerically generated trajectory will be of any use to study a chaotic system.

A partial answer to this problem comes from the rigorous mathematical proofs of the *shadowing property* of certain chaotic systems, which is known as *shadowing lemma*. The *shadowing lemma* sates that although a numerical trajectory diverges exponentially from the true trajectory with the same initial conditions, there exists a true (i.e. errorless) trajectory with a sightly different initial conditions that stays near (shadows) the numerical trajectory [50, 78, 79, 80, 81]. Thus there is a good reason to rely on the numerically generated trajectory to study a chaotic system.

1.6 Bifurcation theory

In this section we briefly review bifurcation theory which is an important feature of dynamical systems [82, 83]. In the bifurcation theory we study sudden qualitative changes in the nature of motion of a dynamical system when some system parameter is smoothly varied through a critical value. Typically at the critical value of the control parameter one type solution of the dynamical system loses stability and a new stable solution arises. Thus to understand the nature of the sudden qualitative changes, the stability of the solutions are studied in the neighborhood of the critical parameter value. In fact there can exists more than one critical or bifurcation value of the parameter and as the parameter is varied through these values the dynamical system undergoes transition of different types of motion and can give rise to interesting dynamical situations such as chaos. In this section we will discuss few simple bifurcations which occur in low dimensional nonlinear continuous time dynamical systems.

- Saddle node bifurcation: we consider the following one dimensional dynamical system,

  $$\frac{dx}{dt} = \mu - x^2 \tag{1.6}$$

  where, μ is some system parameter. The equilibrium points of this system are $x^* = \pm\sqrt{\mu}$. To determine the stability of these equilibrium points we consider linear stability analysis. The dynamics of a small deviation $z = x - x^*$ is given by,

  $$\frac{dz}{dt} = -2x^* z, \tag{1.7}$$

  solving which will give us, $z(t) = z(0)e^{\lambda t}$, where $\lambda = -2x^*$. When, $\mu < 0$ the system has no stable real equilibrium point. At the parameter $\mu = 0$, $x^* = 0$ becomes the unique equilibrium point. When, $\mu > 0$ the system has two equilibrium points at $x^* = \pm\sqrt{\mu}$, of which $x^* = +\sqrt{\mu}$ is stable equilibrium point and $x^* = -\sqrt{\mu}$ is unstable equilibrium. Here we can see that as the system parameter is varied the system undergo a transition of motion from no equilibrium point to one stable and one unstable equilibrium points. This type of bifurcation is known as saddle node bifurcation. In Fig. 1.1 the systems solutions are plotted as a function of system parameter. The solid line gives the stable solution and the dashed line gives the unstable solutions.

- Pitchfork bifurcation: In this type of bifurcation one stable solution of a dynamical system loses stability and two new solutions arise as the parameter

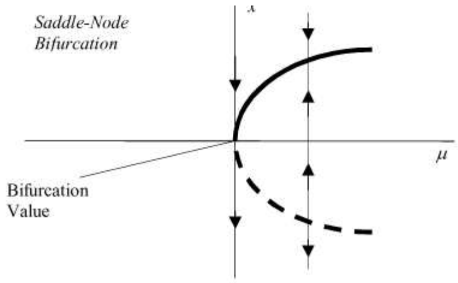

Figure 1.1: The solution of Eq. (1.6) is plotted as a function of systems parameter μ. When, $\mu < 0$ there exists no real solution, at the critical value $\mu = 0$ the system has one solution $x^* = 0$. For $\mu > 0$, there exists two solutions $x^* = \pm\sqrt{\mu}$. The stable solution $x^* = +\sqrt{\mu}$ is shown as the solid line and the unstable solution $x^* = -\sqrt{\mu}$ is shown as dashed line.

is varied through a critical value. We consider a dynamical system given by,

$$\frac{dx}{dt} = \mu x - x^3 \tag{1.8}$$

here, μ is system parameter. The systems has three solutions $x^* = 0, \pm\sqrt{\mu}$.The stability of these equilibrium points can be determined by the linear stability analysis and in this case we have $\lambda = -3x^{*^2} + \mu$, where λ gives the exponential nature of a small deviation to the solutions. For, $\mu < 0$ there exists only one stable real solution $x^* = 0$. At the critical value of the parameter $\mu = 0$, all solutions of the system collapse to $x^* = 0$. When $\mu > 0$, there exists three solutions $x^* = 0, \pm\sqrt{\mu}$, of which $x^* = 0$ is unstable solution and $x^* = \pm\sqrt{\mu}$ are the stable solutions.

Fig. 1.2 shows the nature of the solutions of Eq. (1.8) as a function of control parameter μ. The solid line gives the stable solutions and the dashed line gives the unstable solution. When $\mu < 0$ the only stable solution is $x^* = 0$ as μ is increased through the critical value 0, two new stable solutions appear $x^* = \pm\sqrt{\mu}$, while the old stable solution $x^* = 0$ becomes unstable.

- Transcritical bifurcation: In this type of bifurcation the stability of solutions of a dynamical system are exchanged. We consider a dynamical system given by,

$$\frac{dx}{dt} = -\mu x + x^2 \tag{1.9}$$

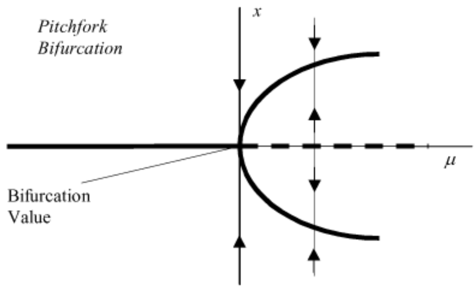

Figure 1.2: This figure shows the nature of the solutions of Eq. (1.8) as a function of the control parameter μ. The solid line gives the stable solutions and the dashed line shows the unstable solution. When $\mu < 0$ the only stable solution is $x^* = 0$ as μ is increased through the critical value 0, two new stable solutions generate $x^* = \pm\sqrt{\mu}$, while the old stable solution $x^* = 0$ becomes unstable.

The dynamical system has two equilibrium points $x^* = 0, \mu$. The stability of these equilibrium points are determined by the exponent, $\lambda = -\mu + 2x^*$. When $\mu < 0$ the equilibrium point $x^* = 0$ is unstable and $x^* = \mu$ is stable. When $\mu > 0$ the stability of the equilibrium points are exchanged and $x^* = 0$ become stable solution and $x^* = \mu$ become unstable solution. Fig. 1.3 the equilibrium points of Eq. (1.9) are plotted as function of system's parameter μ. The solid line gives the stable solution and the dashed line gives the unstable solution.

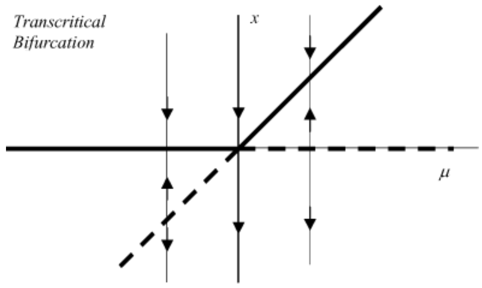

Figure 1.3: The equilibrium points of Eq. (1.9) are plotted as function of system's parameter μ. The solid line gives the stable solution and the dashed line gives the unstable solution. When $\mu < 0$ the equilibrium point $x^* = 0$ is unstable and $x^* = \mu$ is stable. When $\mu > 0$ the stability of the equilibrium points are exchanged and $x^* = 0$ become stable solution and $x^* = \mu$ become unstable solution.

1.7 Complex networks

In this section we review the topic of complex networks that is used in the thesis. Real world complex systems can be modeled as networks of interacting elements. Complex networks describe a collection of large number of systems from physical or biological or social worlds [84, 85, 86]. Below we provide some examples of complex networks.

- Cell: cell can be described as a complex network of chemicals connected by chemical reactions [87].
- Internet: the internet is a complex network of routers and computers connected by various physical or wireless links [88].
- World wide web: webpages are connected by hyperlinks [89].
- Ciruits: electrical circuits are complex networks of various electrical components such as resistors, capacitors, op-amps, etc. connected by electrical wires [90].
- Food webs: this network consist of spices linked by predator-pray relations [91].
- Neural networks: neurons are connected by axons and dendrites [92].
- Power grids: generators and transformers are connected by high voltage links [93, 94].
- Polymers: atoms are linked with bonds [95].
- Co-authorship network: in this network authors are the vertices and two authors are connected when they write a paper together [96].
- Citation network: two papers are orderly linked by the citation [97].
- Social network: fads and ideas are transported from peoples to people through social relationship [98].

- Actor network: two actors are connected when they have acted in a same movie [99].
- Disease network: disease spreads when a healthy person gets connected to an infected person [100].
- Railway network: stations are connected by rail lines [101, 102].
- Airport network: airports are linked by flights [103].

These systems represent just a few of the many examples that have recently prompted the scientific community to investigate the mechanisms that determine the topology of complex networks.

Graph theory [104] is a natural framework for the mathematical formulation of complex networks. Formally, a complex network can be represented as a graph. A graph $\mathcal{G}$ consist of two sets $\mathcal{N}$ and $\mathcal{L}$, where $\mathcal{N}$ is a nonempty set of N vertices (or nodes) $n_1, \ldots, n_N$ and $\mathcal{L}$ is a set of E edges (or links) $l_1, \ldots, l_E$ which are pairs of elements of $\mathcal{N}$. When the elements of set $\mathcal{L}$ consist of ordered pairs of elements of set $\mathcal{N}$ then the graph $\mathcal{G}$ is a directed graph. Below we briefly discuss some features of complex networks.

Adjacency matrix : It is often useful to consider a matricial representation of a graph. The adjacency matrix $A = [a_{ij}]$ of graph $\mathcal{G}$ is an $N \times N$ matrix whose ij-th entry is the number of edges from node j to node i.

Network Laplacian : The elements of the network Laplacian matrix $G = [g_{ij}]$ are defined as $g_{ij} = a_{ij} - \delta_{i,j} \sum_{k,k\neq i}^{N} a_{ik}$, where, $\delta_{i,j}$ is Kronecker delta.

Node degree and degree distribution : The number of edges incident at the nodes is called the degree. We denote degree of node i as k_i. For undirected graph degree of node i is $k_i = \sum_{j,j\neq i} a_{ij}$. Degree distribution $P(k)$; is the probability that a randomly selected node has exactly k edges.

In the case of directed graph the degree of a node has two components, in-degree $k_i^{in} = \sum_j a_{ij}$ of node i is the number of incoming links incident on node i and out-degree $k_i^{out} = \sum_j a_{ji}$ is the number of outgoing links from the node. The total degree is then defined as, $k_i = k_i^{in} + k_i^{out}$.

Connected graph : A Graph $\mathcal{G}$ is said to be connected if there is at least one path (through edges connecting a pair) between every pair of vertices in $\mathcal{G}$. Otherwise, $\mathcal{G}$ is disconnected. Size of a graph is the number of vertices in the graph.

Clustering coefficients : A common property of complex networks is formation clusters. The inherent tendency to cluster is quantified by the clustering coefficient [105]. Let us consider a node i with degree k_i. This node is connected to k_i other neighboring nodes, if any of these two neighboring nodes are connected then a triangle is formed. The clustering coefficient of node i is the ratio between the number of edges E_i that actually exist between the neighboring nodes of i and the maximum number of possible edges $k_i(k_i - 1)/2$ between them,

$$C_i = \frac{E_i}{k_i(k_i - 1)/2}$$

The clustering coefficients of the whole network is $C = 1/N \sum_i C_i$.

Shortest path lengths, diameter and characteristic path length : Shortest paths play an important role in the transport and communication within a network. Suppose one needs to send a data packet from one computer to another through the Internet: the geodesic provides an optimal path way, since one would achieve a fast transfer and save system resources [106]. The shortest path between two nodes is determined by counting the minimum numbers of edges that is needed to connect them. This is also known as the geodesic distance. The shortest path lengths of graph $\mathcal{G}$ is represented as a matrix $\mathcal{D}$ in which the entry d_{ij} is the length of the geodesic from node i to node j. The maximum value of d_{ij} is called the diameter of the graph. A measure of the typical separation between two nodes in the graph is given by the average shortest path length, also known as the characteristic path length. And it is defined as the mean of the geodesic length over all couples of the nodes,

$$L = \frac{1}{N(N-1)} \sum_{i,j,i \neq j} d_{ij}.$$

Graph spectra : The spectrum of a graph is the set of eigenvalues of its adjacency matrix A [107]. A graph $\mathcal{G}_{N,E}$ has N eigenvalues γ_i $(i = 1 \dots, N)$, and N associated eigenvectors v_i $(i = 1, \ldots, N)$. When the graph $\mathcal{G}$ is undirected then the adjacency matrix A is real and symmetric, therefore the graphs has real eigenvalues and the eigenvectors corresponding to distinct eigenvalues are orthogonal. For a directed graph the eigenvalues can be complex.

Here, we briefly review some different types of graphs which we have used for our studies,

Regular Graphs : A regular graph is a graph where each vertex has the same number of neighbors; i.e. degree of each node is same. For a directed graph the in-degree and out-degree of each vertex is same [108]. A regular graph with vertices of degree k is called a $k$regular graph. Simple cubic lattice is an example of regular graph. In a regular lattice of dimension d and size N the characteristic path length is given by $L \sim N^{1/d}$.

Complete Graphs : In a complete graph every pair of distinct vertices are connected by one unique edge. The complete graph of N vertices has $N(N-1)/2$ edges and is denoted by K_N [109]. A triangle is a complete graph with 3 nodes and it is denoted as K_3. If the edges of a complete graph have a direction then the resultant directed graph is called a tournament.

Random Graphs : Random graphs were first studied by the Hungarian mathematicians Paul Erdös and Alfréd Rényi [110, 111]. In their classic first article Erdös and Rényi define a random graph as N labeled nodes connected by E edges, these edges are selected randomly from the $N(N-1)/2$ possible edges [110]. There are a total of $C^{E}_{N(N-1)/2}$ possible different graphs that can be generated from N nodes and E edges and all configurations have equal probability. An alternative and equivalent definition of a random graph is the binomial model. Here, we start with N nodes and connect every pair of nodes with probability p. The total number of edges $E(p) = pN(N-1)/2$. In this thesis we use this alternate method to generate random graphs. In a random graph, with connection probability p, the degree distribution follows a binomial distribution,

$$P(k) = C^{k}_{N-1} p^{k} (1-p)^{N-1-k}$$

For large graphs $N \to \infty$ and small p, the degree distribution $P(k)$ follows Poisson distribution. In a random graphs both the clustering coefficient and the characteristic path length are very small. The clustering coefficient is, $C_{rand} \sim k/N$ and the characteristic path length is $L_{rand} \sim \ln(\mathrm{n})/\ln(\mathrm{k})$.

Small World Networks : Small world networks lie in between random graphs and regular networks and several of the networks consisting of natural systems are of this type. The real world networks have small characteristic path length as random graphs. This is due to the existence of shortcuts in a real network. In a regular d-dimensional lattice the characteristic path length grows with network size as $N^{1/d}$, N is the size of the network. Conversely, in most of the real networks, despite their large size, there is a relatively short path between any two nodes. This feature is known as small world property and is characterized by an average shortest path length L which grows logarithmically with the network size, $L \sim \ln\mathrm{N}$. Unlike random graphs, a small world network has larger clustering coefficient, which is a characteristic property of regular lattices. In 1998 Watts and Strogatz proposed a model to generate the small world networks [105] which have large clustering coefficients and small characteristic path lengths. In that model they consider a regular ring lattice which has N vertices and each vertex is connected to k neighboring vertices. Now each edge is rewired with a probabilty p avoiding self and duplicate connections. This rewiring helps to tune the network between a regular graph ($p = 0$) and a random graph ($p = 1$). The small world network lies in the intermediate region $0 < p < 1$. This model is quantified in terms of characteristic path length $L(p)$ and clustering coefficients $C(p)$. As $p \to 0$, the characteristic path length is $L \sim N/2k >> 1$ and, as p increases the path length scales logarithmically with the network size N, $L \sim \ln\mathrm{N}$. This is due to the generation of few long edges in the network which connect distant nodes. In addition, small world network has large clustering coefficients because of the mostly local edges [105, 112].

Scale Free Networks :

Till now we have discussed network models that start with a fixed number N of vertices that are then randomly connected or rewired, without modifying N. In contrast, most real world networks describe open systems that grow by the continuous addition of new nodes. Starting from a small number of nodes, the number of nodes increase throughout the lifetime of the network by the subsequent addition of new nodes. Network models discussed so far assume that the probability that two nodes are connected (or their connection is rewired) is independent of the nodes degree, i.e., new edges are placed randomly. Most real networks, however, exhibit preferential attachment, such that the likelihood of connecting to a node depends on the nodes degree. For example, World Wide Web, when a new web-page is created it is more likely to link with a popular web-page (which already has large degree) than a less known web-page. Thus the webpages which have larger degree are getting more connections than other webpages, or the citation network, a new paper is more likely to cite well known and thus most-cited papers than less cited papers. These two processes *growth* and *preferential attachments* generate scale-free networks [88, 113, 114, 115]. The degree distributions of nodes in a scale-free network follow power law,

$$P(k) \sim k^{-\gamma}$$

where γ is a constant with a typical value in the range $2 < \gamma < 3$.

Barabási and Albert were the first to model the scale-free networks [113]. The algorithm of Barabási and Albert model is the following,

(1). *Growth* : Consider a small network with m_0 nodes. At every time one new node with $m(< m_0)$ edges is added to already existing m nodes of the network. After t time steps total number of nodes in the network will be $N = t + m_0$.

(2). *Preferential Attachments* : The probability that the new node will be added to the existing node i depends on the degree k_i of node i. Thus the probability that a new node will be connected to node i is,

$$\pi(k_i) = \frac{k_i}{\sum_j k_j}$$

One of the most important properties of the scale-free network is that it is topologically very robust against random node failure because of few hubs (highly connected nodes). But these scale-free networks are very vulnerable to attacks on the hubs [114].

In the next sections we discuss properties of two well known chaotic systems Lorenz systems [116] and Rössler systems [117]. In this thesis most numerical calculations are done on these two systems.

1.8 Lorenz Systems

The Lorenz system is a classical example of a dynamical continuous system exhibiting chaotic behavior. This is a three dimensional system consisting of three nonlinear ordinary differential equations. In 1963 MIT meteorologist Edward Lorenz developed a simple set of three nonlinear ordinary differential equations to represent the forced dissipative hydrodynamic flow [116] and he discussed the feasibility of very-long-range weather prediction in view of this model. The Lorenz system is given as,

$$\begin{aligned} \frac{dx}{dt} &= -\sigma x + \sigma y \\ \frac{dy}{dt} &= -xz + rx - y \\ \frac{dz}{dt} &= xy - bz \end{aligned} \tag{1.10}$$

where, σ, r, b are parameters of the system; σ is related to Prandtl number. The variable $x(t)$ is proportional to the intensity of the convective motion, $y(t)$ is proportional to the temperature difference between the ascending and descending currents and $z(t)$ is proportional to the distortion of the vertical temperature profile from linearity.

The stability of the solutions $x(t)$,$y(t)$ and $z(t)$ can be investigated by considering the behavior of small superposed deviations ξ_x, ξ_y, ξ_z of the solutions. The dynamics of these deviations are given by the linearized equation,

$$\frac{d}{dt}\begin{pmatrix} \xi_x \\ \xi_y \\ \xi_z \end{pmatrix} = \begin{pmatrix} -\sigma & \sigma & 0 \\ (r-z) & -1 & -x \\ y & x & -b \end{pmatrix}\begin{pmatrix} \xi_x \\ \xi_y \\ \xi_z \end{pmatrix} \tag{1.11}$$

The Lorenz system has three equilibrium points. The equilibrium point $x^* = y^* = z^* = 0$ represents the state of no convection. The characteristic equation from Eq. (1.11) for this equilibrium point is,

$$[\lambda + b][\lambda^2 + (\sigma + 1)\lambda - \sigma(1 - r)] = 0 \tag{1.12}$$

This equation has three real roots for $r > 0$; all are negative when $r < 1$, but one is positive when $r > 1$. The equilibrium point $x^* = y^* = z^* = 0$ is stable for $r < 1$. When $r = 1$, the steady convection starts. For $r > 1$ there exists two more equilibrium points $x^* = y^* = \pm\sqrt{b(r-1)}, z^* = r - 1$. The characteristic equation for these equilibrium points is,

$$\lambda^3 + (\sigma + b + 1)\lambda^2 + (r + \sigma)b\lambda + 2\sigma b(r - 1) = 0 \tag{1.13}$$

For $r > 1$, Eq. (1.13) has two complex conjugate roots and one real negative root. The complex conjugate roots are pure imaginary when r satisfies,

$$r = \frac{\sigma(\sigma + b + 3)}{(\sigma - b - 1)}.$$

Eq. (1.10) starts showing chaotic behavior when $r > \sigma(\sigma + b + 3)/(\sigma - b - 1)$. As parameter r is increased the Lorenz system shows chaotic and periodic behavior. When $r < 1$, the Lorenz system is stable at the fixed point $x^* = y^* = z^* = 0$ and The Lyapunov exponents are $(-, -, -)$, Typical value of parameters are $\sigma = 10, r = 28, b = 8/3$. The Lorenz system is chaotic for these parameter values. Lyapunov exponents of the Lorenz system for these parameter values are $0.905, 0.000, -14.572$. For these parameter values the Lorenz attractor is shown in Fig. 1.4 where labels (1), (2), (3) show the position of three equilibrium points. In Fig. 1.5 the two largest Lyapunov exponents are plotted as a function of Loren parameter r. When the system shows fixed point behavior all Lyapunov exponents are negative, in the limit cycle region the largest Lyapunov exponent is zero others are negative and for chaotic systems the largest Lyapunov exponent is positive, second largest Lyapunov exponent is zero and the third exponent is negative.

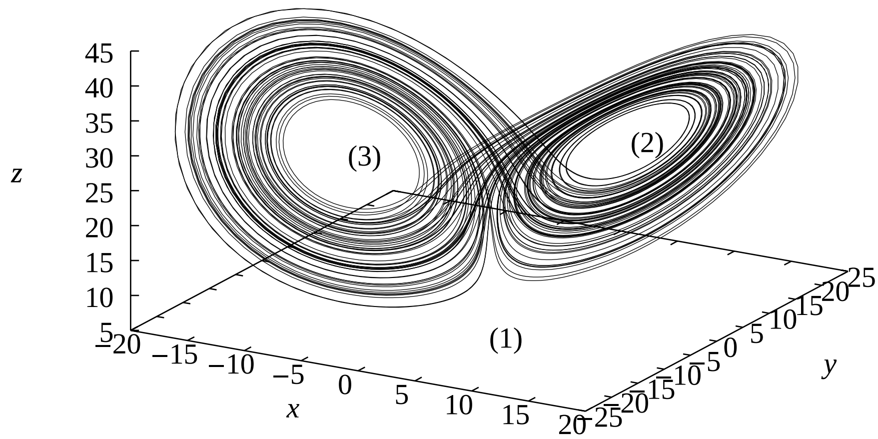

Figure 1.4: The solution of the chaotic Lorenz system is shown in the phase space. The solution remains bounded on the Lorenz attractor. The equilibrium points are shown in the figure with the labels (1) = $[x^* = y^* = z^* = 0]$, (2) = $[x^* = y^* = \sqrt{b(r-1)}, z^* = r - 1]$ and (3) = $[x^* = y^* = -\sqrt{b(r-1)}, z^* = r - 1]$. The parameters are $\sigma = 10$, $b = 8/3$ and $r = 28$.

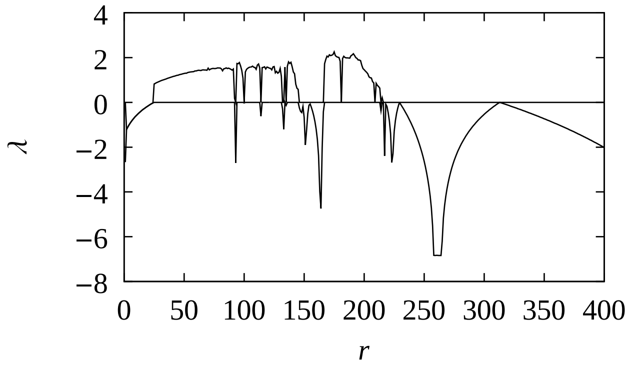

Figure 1.5: Two largest Lyapunov exponents of the Lorenz system are plotted as a function of Lorenz parameter r.

1.9 Rössler systems

In 1976 O. E. Rössler designed a continuous time dynamical system that exhibits chaotic dynamics. It was intended to behave similarly as Lorenz system, but is easier to analyze qualitatively. Rössler system is a three dimensional system represented by a set of three ordinary differential equations which has only one quadratic nonlinear term in the third equation,

$$\begin{aligned} \frac{dx}{dt} &= -\omega y - z \\ \frac{dy}{dt} &= \omega x + a_r y \qquad (1.14) \\ \frac{dz}{dt} &= b_r + z(x - c_r) \qquad (1.15) \end{aligned}$$

where, ω, a_r, b_r, c_r are Rössler parameters. Rössler studied a chaotic attractor for the parameter values $\omega = 1, a_r = 0.2, b_r = 0.2, c_r = 5.7$. The equilibrium points of the Rössler system are,

$$\begin{aligned} x^* &= \frac{c}{2} \pm \frac{1}{2}\sqrt{\omega^2 c^2 - 4ab} \\ y^* &= -\frac{\omega c}{2a} \mp \frac{\omega}{2a}\sqrt{\omega^2 c^2 - 4ab} \\ z^* &= \frac{\omega^2 c}{2a} \pm \frac{\omega^2}{2a}\sqrt{\omega^2 c^2 - 4ab} \end{aligned} \qquad (1.16)$$

Fig. 1.6 shows the Rössler attractor in the 3-dimensional x, y, z phase space for the Rössler parameter values $\omega = 1, a_r = 0.2, b_r = 0.2, c_r = 7.0$. For this parameter values Rössler system is chaotic and the three Lyapunov exponents are $0.113, 0.000, -9.773$.

In Fig. 1.7 the two largest Lyapunov exponets of the Rössler systems are plotted as a function of Rössler parameter a_r. As the parameter a_r is varied the Rössler system exhibits chaotic or periodic or intermittent behavior.

1.10 Objective and scope of the thesis

After discussing the background of the thesis we now state the objectives of this thesis. The objectives of this thesis can be divided into two general categories.

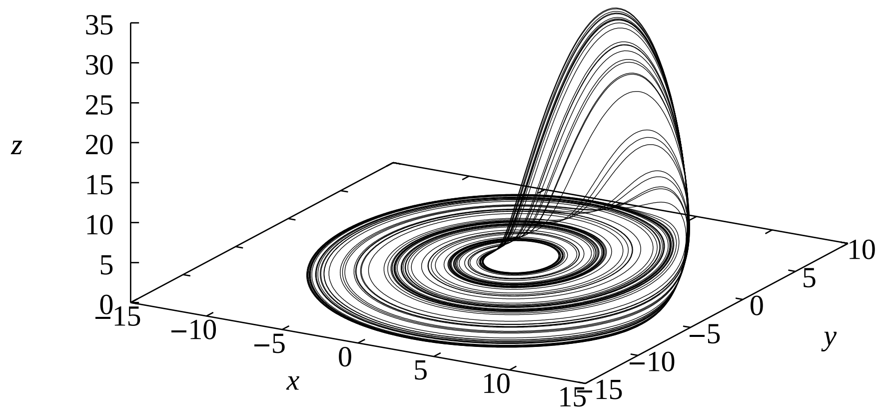

Figure 1.6: The solution of the Rössler system Eq. (1.14) is shown in the three dimentional x, y, z phase space. The solution is chaotic and remain bounded in the Rössler attractor. The Rössler parameters are $\omega = 1.0, a_r = 0.2, b_r = 0.2, c_r = 7.0$.

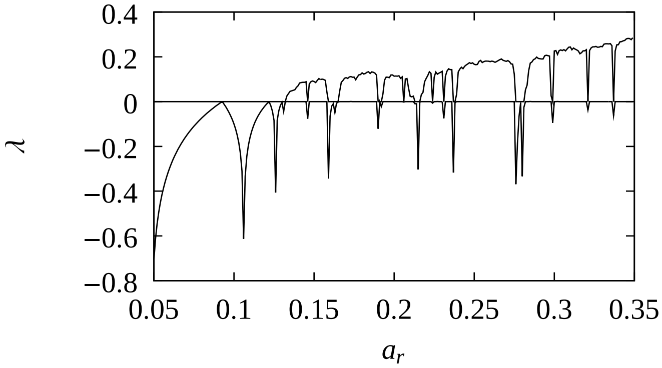

Figure 1.7: The two largest Lyapunov exponents of Rössler system are plotted as a function of parameter a_r. Rössler system is chaotic when the Largest Lyapunov exponent is positive. The other parameters of Rössler are fixed at the value $\omega = 1.0, b_r = 0.2, c_r = 7.0$.

In the first part we study the stability of synchronization for coupled nonidentical dynamical systems. In the second part we analyze the nature of desynchronization bifurcation of coupled dynamical systems. In determining stability of the synchronous state, we consider the criteria that all transverse Lyapunov exponents are negative. In the later part to understand the nature of desynchronization bifurcation of coupled dynamical systems we introduce Systems' Transverse Lyapunov Exponent (STLE). These STLEs provide information regarding stability of individual systems on a network when desynchronization bifurcation occurs. In the stable synchronized state both largest transverse Lyapunov exponents and STLEs are negative. In the desynchronized state the TLE is positive while the STLEs may have positive or negative value depending on the stability of the particular system under study. There are several methods available to calculate Lyapunov exponents of dynamical systems. Throughout our study we calculate Lyapunov exponents using standard Wolf's algorithm [75].

Synchronization of coupled nonidentical dynamical systems

When two or more identical chaotic systems are coupled then complete synchronization comes out as equality of the state variables of the coupled systems. The conditions for stability of complete synchronized states are well analyzed using Master Stability Function[24, 118]. This study only supports to find the stability condition for a network of identical systems, but in practical life it is impossible to find a network of exactly identical systems. In our study we make progress to analyze the stability condition of synchronous state for nonidentical dynamical systems using perturbation theory. We provide a Master Stability Function (MSF) that can predict the stability of generalized synchronous state reasonably well. Later we use this MSF to find the best synchronization optimized network from any random network with fixed number of nodes and edges.

Desynchronization bifurcation of coupled dynamical systems

In the later part of this thesis we study desynchronization bifurcation of coupled dynamical systems. For some specific dynamical systems an interesting phenomenon is observed when they are coupled and coupling strength is increased smoothly. As the coupling strength is increased, one can find synchronization between the systems when coupling strength crosses some critical value (say it is ε_{c1},

ε is scalar coupling strength). This synchronization is complete synchronization as we are considering identical systems. When coupling strength is increased further the systems remain synchronized for some time and the synchronous state is stable. As coupling strength is increased beyond a second critical value (ε_{c2}) the systems undergo a desynchronization bifurcation. We analyze this desynchronization bifurcation in coupled chaotic systems and we observe that this desynchronization bifurcation is pitchfork bifurcation of transverse manifold. We propose an integrable model which shows similar desynchronization bifurcation and this model can be treated as normal form for this type of bifurcation.

1.11 Outline of the thesis

The thesis is organized as follows. In chapter 2, we briefly review the synchronization of coupled identical dynamical systems and we discuss the stability of synchronization by using master stability function. In chapter 3 we study synchronization for coupled nonidentical dynamical systems and we extend the idea of master stability function for analyzing the generalized synchronization. In chapter 4 we consider the problem of constructing synchronized optimized network from any random network that has fixed number of nodes and links. In chapter 5 we study the nature of desynchronization bifurcation of coupled dynamical systems. Summary and future directions are given in chapter 6.

Chapter 2

Synchronization of coupled identical systems

2.1 Introduction

We have seen in chapter 1 that chaotic systems are highly sensitive to the initial conditions.Two identical chaotic systems starting from nearly same initial points in phase space will evolve with time in a very uncorrelated manner. So, by definitions chaotic systems appear to defy synchronization. So, setup of synchronization between coupled chaotic systems is of great interest and important.

It has been shown that it is possible to synchronize chaotic systems, by introducing coupling between separate systems or forcing them together with a common signal [4, 5, 6, 7, 8, 9, 17]. In this chapter we briefly review synchronization of coupled identical systems. When two or many identical systems are coupled synchronization comes out as the equality of the state variables of the coupled systems which is known as complete or identical synchronization [9]. To determine the stability of the complete synchronization we consider the criteria that the largest transverse Lyapunov exponents are negative. In this chapter we review the master stability approach to the synchronization of coupled identical dynamical systems. The master stability equation allows us to calculate the stability of synchronization for a particular choice of system (e.g., Rössler, Lorenz, etc.) and a particular choice of component coupling (e.g., x, etc.).

This chapter is organized as follows. In section 2.2 we introduce the model of coupled identical dynamical systems and in section 2.3 we determine stability of synchronized state and establish the criteria for analysing stability of synchronized state by determining Master Stability Function (MSF), if MSF in negative for all eigenvalues of the coupling matrix the synchronized state is stable. We consider a network of coupled chaotic systems in section 2.4 and investigate the stable synchronization state by determining the MSF. We summarize the chapter in section 2.5.

2.2 Model for coupled identical systems

The time evolution of any dynamical system can be represented by the equation of motion or the dynamical euqation of that systems. Let us consider the dynamics of an m dimensional system is given by,

$$\dot{x} = f(x) \tag{2.1}$$

where, $x \in R^m$ is m dimensional state variable of the system and $f : R^m \to R^m$ provides the dynamics of the systems.

To study synchronization between identical chaotic systems we consider N coupled identical systems,

$$\dot{x}^i = f(x^i) + \varepsilon \sum_{j=1}^{N} g_{ij} h(x^j) \tag{2.2}$$

where, ε is the coupling strength that can be tuned to establish synchronization between the coupled systems, $G = [g_{ij}]$ is the coupling matrix. If node i interacts with node j then $g_{ij} = 1$ otherwise zero. And the diagonal elements of the coupling matrix G are $g_{ii} = -\sum_{j,j \neq i} g_{ij}$, i.e. the coupling matrix is related to the network Laplacian. $h : R^m \to R^m$ is the coupling function.

For some suitable value of coupling strength ε in Eq. (2.2) the complete or identical synchronization is established between the coupled systems. At this the state variables of the coupled systems will be equal, $x^1 = x^2 = \ldots = x^N = s(t)$, where s is solution of an isolated systems $\dot{s} = f(s)$. This equality of the state variable provides a hyperplane of dimension m which is known as synchronization manifold $\mathcal{M}$. On the synchronization manifold the contribution from the coupling term of Eq. (2.2) will be zero since the coupling matrix G satisfies, $\sum_j g_{ij} = 0$. The coupling matrix G has one eigenvalue $\mu_1 = 0$, since it satisfies the condition $\sum_j g_{ij} = 0$. The eigenvector of G corresponding the eigenvalue $\mu_1 = 0$ is $e_1 = (1, \ldots, 1)^T$. This eigenmode is parallel to the synchronization manifold $\mathcal{M}$. Other eigenmodes corresponding to the nonzero eigenvalues of G define the manifold which is transverse to the synchronization manifold $\mathcal{M}$.

2.3 Stability of synchronization: Master Stability Function (MSF)

In this section we review the stability analysis of the identical synchronization [9, 10, 11, 24, 119]. To determine the stability the criteria is that the largest transverse Lyapunov exponent is negative for stable synchronization.

For analysing the stability of the synchronization we put a small deviation to the synchronized solution. Let, z^i be the deviation of x^i from the synchronized solution s.

$$z^i = x^i - s \tag{2.3}$$

The synchronization is stable when all deviations which are transverse to the synchronization manifold go to zero as the systems evolves with time. From Eq. (2.2) and Eq. (2.3) we can write the dynamics of the deviation, i.e. the linearized equation as,

$$\dot{z}^i = D_x f \ z^i + \varepsilon \sum_{j=1}^{N} g_{ij} D_x h \ z^j \tag{2.4}$$

where, $D_x f$ and $D_x h$ are partial derivatives of f and h respectively and these quantities are calculated at the synchronized solution s. Eq. (2.4) can be written in a matrix form by consider a $m \times N$ deviation matrix Z,

$$Z = (z^1 \ z^2 \ \dots \ z^N) \tag{2.5}$$

In matrix form Eq. (2.4) is,

$$\dot{Z} = D_x f \ Z + \varepsilon D_x h \ Z \ G^T \tag{2.6}$$

where, G^T is transpose of connectivity matrix G. Let, e_k be eigenvector of G^T corresponding to the eigenvalue μ_k,

$$G^T e_k = \mu_k e_k.$$

Now we multiply Eq. (2.6) by e_k from right and writing $Ze_k = \eta_k$ we get the dynamics of deviation along k-th eigenmode of coupling matrix G^T,

$$\dot{\eta}_k = D_x f \ \eta_k + \varepsilon \mu_k D_x h \ \eta_k. \tag{2.7}$$

We have seen before that matrix G has one eigenvalue $\mu_1 = 0$ and the corresponding eigenvector $e_1 = (1 \dots 1)^T$. For this eigenvector Eq. (2.7) will give the dynamics of deviations which are parallel to the synchronization manifold $\mathcal{M}$ and hence, will not affect the stability of the synchronization and the rest of the eigenvectors of G are the transverse eigenvectors. These will provide the dynamics of deviations which are transverse to the synchronization manifold.

Eq. (2.7) can be written in a generic form for $\forall k$,

$$\dot{\phi} = [D_x f + \alpha D_x h]\phi \tag{2.8}$$

where, $\alpha = \varepsilon \mu_k$ and $\phi \in R^m$ is an m dimensional vector. Eq. (2.8) is known as master stability equation and from this master stability equation we calculate the maximum Lyapunov exponent as a function of α. This is know in the literature as Master Stability Function (MSF) λ_{max}. The synchronized state is stable when the MSF is negative for all nonzero eigenvalue of G.

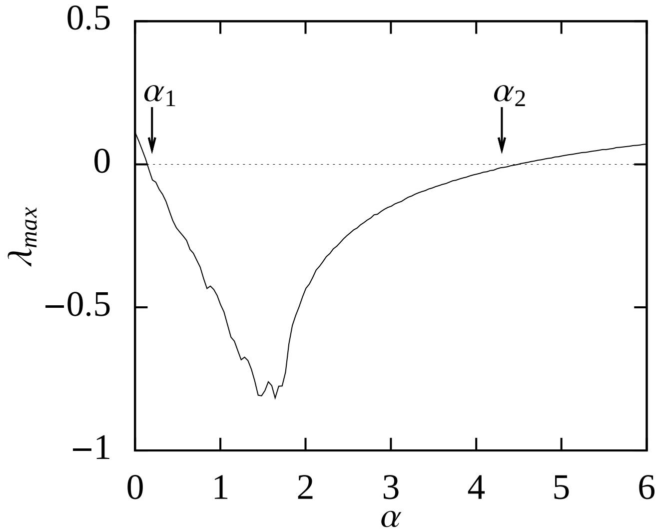

Figure 2.1: The MSF λ_{max} is plotted as a function of α for a network of chaotic Rössler systems. The Rössler parameters are $a_r = 0.2, b_r = 0.2, c_r = 7.0$. The synchronized state is stable in the region $\alpha_1 < \alpha < \alpha_2$.

2.4 Coupled chaotic systems

For numerical experiments we consider that the dynamics of an isolated system in Eq. (2.2) is given by chaotic Rössler systems [117],

$$\begin{aligned} \dot{x} &= -\omega y - z \\ \dot{y} &= \omega x + a_r y \\ \dot{z} &= b_r + z(x - c_r) \end{aligned} \tag{2.9}$$

where, ω, a_r, b_r, c_r are Rössler parameters. These Rössler systems are coupled in the x-component, i.e. the coupling function is

$$h(x) = \begin{pmatrix} x & 0 & 0 \\ 0 & 0 & 0 \\ 0 & 0 & 0 \end{pmatrix}$$

In Fig. 2.1 the MSF λ_{max} is plotted as a function of α for x-component coupled chaotic Rössler systems. The synchronized state is stable in region where the MSF λ_{max} is negative for all transverse eigenvalues of G. In this figure the stable range is provided by $\alpha_1 < \alpha < \alpha_2$.

In a more general case the coupling matrix G can be an asymmetric matrix and it may have non-zero complex eigenvalues. And thus the parameter α can be a complex quantity. In Fig. 2.2 the MSF λ_{max} is plotted on the surface of $(Re\alpha, Im\alpha)$ for x-component coupled Rössler systems. The synchronized state is stable where the MSF λ_{max} is negative for all transverse eigenvalues of G. In Fig. 2.2 the synchronization is stable under the region bounded by 0-curve.

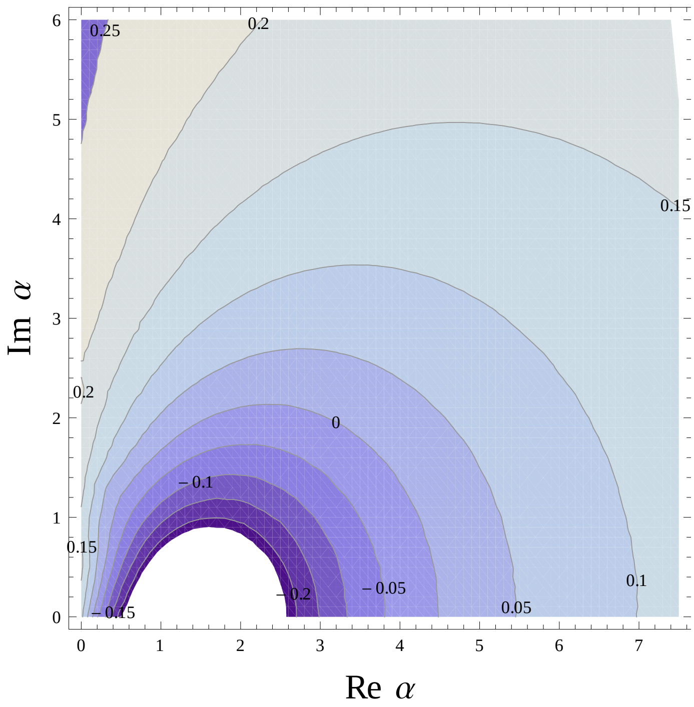

Figure 2.2: The MSF for coupled Rössler systems is plotted as a function of $(Re\alpha, Im\alpha)$. The region below the 0 line give the stable region. This plot is symmetric about the real axis. The Rössler parameters are $a_r = 0.2, b_r = 0.2, c_r = 7.0$.

Now, for a given network and given value coupling strength ε, we can locate the point $\alpha = \varepsilon\mu_k$ on the complex surface in Fig. 2.2. The sign of λ_{max} on that point determine the stability of the k-th eigenmode of coupling matrix. When all transverse eigenmodes of the coupling matrix is stable the the synchronized state is stable for that coupling strength.

2.5 Summary

In this chapter we have introduced the model of coupled dynamical systems to study synchronization between coupled identical systems. For coupled identical systems the synchronization is complete synchronization for suitable coupling strength. We review the stability analysis of complete synchronization by using Master Stability Function. For a given network and coupling strength, we can determine the stability of synchronization from the sign of the Master Stability Function. If the MSF is negative for all non-zero eigenvalues of the coupling matrix then the synchronized state is stable.

Chapter 3

Synchronization of coupled nonidentical systems

3.1 Introduction

In this chapter we analyse stability of synchronous state for coupled nonidentical systems. For coupled nonidentical systems it is not possible to achieve complete or identical synchronization as discussed in chapter 2. Instead of exact synchronization one will get generalized synchronization where the state variables of coupled systems are related with some functional relationship [21, 22]. In this work we consider that the non-identity between the coupled systems is introduced through some parameter mismatch. This parameter mismatch between the coupled systems can lead to desynchronization bursts which is known as bubbling transition [120, 121, 122, 123]. This desynchronization bursts are observed when a periodic orbit of the dynamical system leaves the invariant synchronized manifold. The orbit eventually returns back to its original vicinity after the desynchronization bursts. The system returns to the synchronized state. Here we are interested in the long term stability of the synchronization manifold. To determine stability of synchronized state we use the criteria that the largest transverse Lyapunov exponent is negative in stable synchronized state.

There are some earlier works motivated by the problem of determining master stability function of generalized synchronization for coupled nonidentical systems [124, 125]. In these works instead of determining stability of the coupled nonidentical systems the authors find the deviation of trajectories of the coupled nonidentical systems from the average trajectory as a function of parameter mismatch. Thus these works fails to provide good stability condition of generalized synchronization for coupled nonidentical systems. Also Sorrentino et. al. [125] found that the parameter mismatch does not affect the stability of the synchronized state.

Here, we extend the concept of master stability function, originally introduced by Pecora ans Carroll [24], for coupled nonidentical systems. By considering the fact that the exponential behavior of solutions of a linear differential equation are dominated by the homogeneous terms we find the Master Stability Function (MSF) for synchronized state of coupled nonidentical systems. The stability of the generalized synchronization is provided by negative MSF.

This chapter is organized as following. In section 3.2 we introduce the model of coupled nonidentical systems and in section 3.3 we analyse the stability of the generalized synchronized state and we extend the concept of Master Stability Function (MSF) [24] to analyze synchronization of coupled nonidentical systems. We compare between the actual Lyapunov exponents of coupled systems and their estimated values using our method in section 3.4, and we show that our MSF can determine stability of generalized synchronized state reasonably well.

3.2 Model for coupled nonidentical systems

We consider a network of N coupled nonidentical systems. The dynamics of system i is given by,$i = 1, \ldots, N$

$$\dot{x}^i = f(x^i, r_i) + \varepsilon \sum_{j=1}^{N} g_{ij} h(x^j) \tag{3.1}$$

where, $x \in R^m$ is an m dimensional state variable of system i and $f : R^m \to R^m$ provides the dynamics of the isolated systems. ε is scalar coupling strength. $G = [g_{ij}]$ is coupling matrix; if systems i and system j are connected then $g_{ij} = 1, i \neq j$, otherwise $g_{ij} = 0$ and the diagonal elements of G are $g_{ii} = -\sum_{j=1;j\neq i}^{N} g_{ij}$. The elements of G satisfy $\sum_j g_{ij} = 0.h : R^m \rightarrow R^m$ is a linear coupling function. r_i is some parameter of the dynamical system i. Let, $r_i = \tilde{r} + \delta r_i$, where $\tilde{r}$ is typical value of parameter r and δr_i is small parameter mismatch. In this case the synchronization between the coupled dynamical systems will be of generalized type, i.e. $\phi(x^i, x^j) = 0$.

3.3 Stability analysis of the generalized synchronization

For coupled nonidentical systems one will get generalized type of synchronization where the state variable of the coupled systems are correlated by some function. In most of the cases it is difficult to determine the functional relationship between the system variables. In this section we consider first order perturbation theory along with the observation that the exponential behavior of solutions of a linear differential equations are determined by the homogeneous terms to determine the stability of the generalized synchronized state. We show that this method can be used for stability analysis of coupled nonidentical systems.

To determine stability of the generalized synchronized state we do linear stability analysis. We consider the fact that the exponential nature of solution of a linear differential equation is dominated by the homogeneous term of that differential equation. The effect of the parameter mismatch appears first in the homogeneous part from the quadratic terms in Taylor's series expansion of the function $f(x^i, r_i)$ about the solution of a typical trajectory $\tilde{x}$. Hence, we retains terms upto second order in $z^i = x^i - s$ and δr_i. The dynamics of deviations is given by,

$$
\begin{aligned}
\dot{z}^i &= D_x f(\tilde{x}, \tilde{r}) z^i + \varepsilon \sum_{j=1}^{N} g_{ij} D_x h(\tilde{x}) z^j + D_r f(\tilde{x}, \tilde{r}) \delta r_i + \frac{1}{2} + D_x^2 f(\tilde{x}, \tilde{r}) (z^i)^2 \\
&\quad + D_r D_x f(\tilde{x}, \tilde{r}) + \frac{1}{2} D_r^2 f(\tilde{x}, \tilde{r}) \delta r_i^2 + \ldots \qquad (3.2)
\end{aligned}
$$

where, $\tilde{x}$ is the solution of a system with typical parameter value $\tilde{r}$. As we are interested in the solution $z^i = 0$ the term containing higher order in z^i can be dropped from Eq. (3.2).

In matrix form we can write Eq. (3.2) as,

$$\dot{Z} \;=\; D_x f\ Z + \varepsilon D_x h\ Z\ G^T + D_r f\ R + D_r D_x f\ Z\ R + \frac{1}{2} D_r^2 f\ R^2 + \dots \tag{3.3}$$

where,Z is $m \times N$ matrix $Z = (z^1, \dots, z^N)$, G^T is the transpose of connectivity matrix G and $R = \mathrm{diag}[\delta \mathrm{r}_1, \dots, \delta \mathrm{r}_\mathrm{N}]$ is $n \times N$ diagonal matrix whose diagonal entries are the parameter mismatch.

As an equation for z^i, the RHS of Eq. (3.3) contains both homogeneous and inhomogeneous terms. The inhomogeneity won't affect the Lyapunov exponents or the exponential rate of convergence to the synchronous solutions though it can shift the solution. To see this we consider a general linear equation,

$$Du = p(t) \tag{3.4}$$

where D is a differential operator and $p(t)$ is the inhomogeneous part. The solution of Eq. (3.4) is,

$$u = u_h + g(t) \tag{3.5}$$

where, $u_h = \sum_i A_i h_i(t) exp(k_i t)$ is the solution of the homogeneous equation $Du = 0$. If $p(t)$ does not have any exponential dependence, then $g(t)$ cannot contain any additional exponential other than already in u_h, since the derivative of an exponential is also an exponential with the same exponent. For example, we consider a simple linear equation,

$$\dot{u} = -ku + p, \tag{3.6}$$

the solution of Eq. (3.6) for constant p is,

$$u(t) = [u(0) - \frac{p}{k}] e^{-kt} + \frac{p}{k}. \tag{3.7}$$

The inhomogeneity shifts the asymptotic solution but does not change the exponential. Hence, to calculate Lyapunov exponent from Eq. (3.3) we consider the homogeneous equation obtained from Eq. (3.3),

$$\dot{Z} \;=\; D_x f\ Z + \varepsilon D_x h\ Z\ G^T + D_r D_x f\ Z\ R. \tag{3.8}$$

We can see from Eq. (3.8) that it is necessary to include the quadratic terms in $z^i = x^i - s$ and δr_i in the Taylor series expansion as the effect of the parameter mismatch is not seen in the linear terms.

Let μ_k, e_k^R, $k = 2, \ldots, N$ be the nonzero eigenvalues and right eigenvectors of G^T. Acting Eq. (3.8) on e_k^R and using the m dimensional vectors $\eta_k = Ze_k^R$, we get

$$\dot{\eta}_k \;=\; [D_x f + \varepsilon\gamma_k D_x u]\eta_k + D_r D_x f\ Z\ R\ e_k^R. \tag{3.9}$$

In general, e_k^R are not eigenvectors of R and hence Eq. (3.9) is not easy to treat. To solve Eq. (3.9) we use first order perturbation theory [126] and write Eq. (3.9) as

$$\dot{\eta}_k \;=\; [D_x f + \varepsilon\gamma_k D_x u + \nu_k D_r D_x f]\eta_k \tag{3.10}$$

where $\nu_k = (e_k^L)^T R e_k^R$ is the first order correction and e_k^R and e_k^L are the right and the left eigenvector of G^T corresponding to the eigenvalue μ_k.

Since both μ_k and ν_k can be complex, treating them as complex parameters $\alpha = \varepsilon\mu_k$ and $\Delta = \nu_k$ respectively, we can construct the master stability equation as

$$\dot{\eta} = [D_x f + \alpha D_x h + \Delta D_r D_x f]\eta. \tag{3.11}$$

here, α contains information from the coupling strength ε and the eigenvalue μ_k of the connectivity matrix G and Δ contains information about the mismatch of the coupled systems.

For the coupled identical systems, the above equation reduces to the master stability equation given by Pecora and Carroll [24]. We can determine the MSF or λ_{max}, which is the largest Lyapunov exponent for Eq. (3.11), as a surface in the complex space defined by α and Δ. The synchronized state is stable if the MSF is negative at each of the eigenvalues $\mu_k = \alpha/\varepsilon$ and $\nu_k = \Delta$ ($k \neq 1$). This

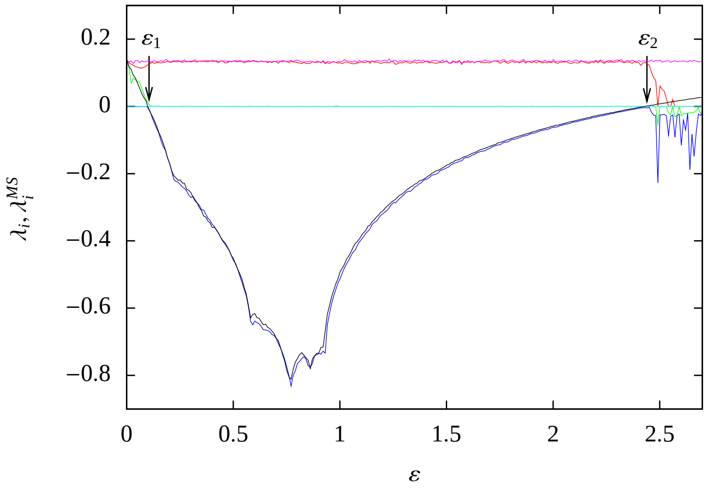

Figure 3.1: The figure shows the three largest Lyapunov exponents $\lambda_i, i = 1, 2, 3$ (red, green and blue) and their estimated values λ_i^{MS} obtained from the master stability equation (Eq. (3.11)) (pink, cyan and black) as a function of ε for two coupled Rössler systems with frequencies $\omega_1 = 1.05$ and $\omega_2 = 1.07$. Taking $\tilde{\omega} = 1.0$ we get $\Delta_1 = \Delta_2 = 0.06$ which are used in Eq. (3.11). Rössler parameters are $a_r = b_r = 0.2, c_r = 7.0$. The synchronous state is stable in the region given by $\varepsilon_1 < \varepsilon < \varepsilon_2$ indicated by the arrows.

ensures that all the transverse Lyapunov exponents are negative. This MSF λ_{max} can estimate the stability of synchronization reasonably well. In the next section we give some numerical results showing how well this MSF can approximate the actual value of Lyapunov exponents.

3.4 Numerical Comparison

3.4.1 Rössler system

We consider a network of N coupled nonidentical Rössler systems give by,

$$\begin{aligned} \dot{x}^i &= -\omega_i y^i - z^i + \varepsilon \sum_{j=1}^{N} a_{ij}(x^j - x^i) \\ \dot{y}^i &= \omega_i x^i + a_r y^i \\ \dot{z}^i &= b_r + z^i(x^i - c_r) \end{aligned} \tag{3.12}$$

where a_r, b_r, c_r and ω are Rössler parameters. We consider that the parameter ω has mismatch. $A = [a_{ij}]$ is the adjacency matrix of the network.

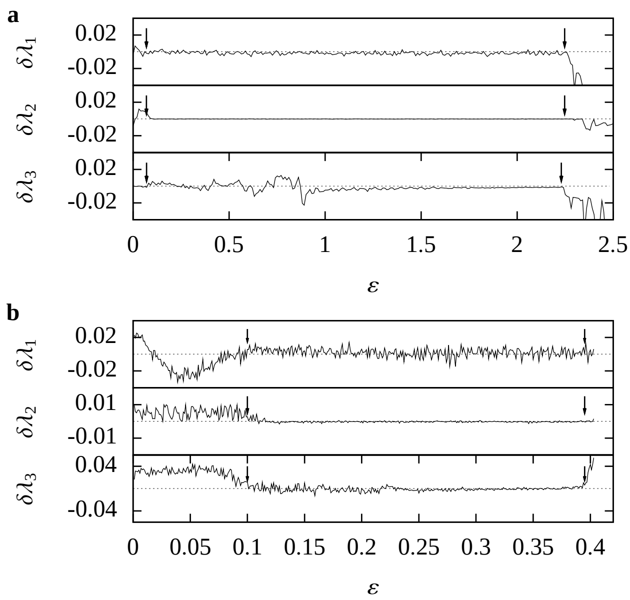

Figure 3.2: **a**. The figure shows the difference $\delta\lambda_i = \lambda_i - \lambda_i^{MS}$ for the three largest Lyapunov exponents as a function of the coupling constant ε for two coupled Rössler systems with parameters as in Fig 1. **b**. The figure shows the difference $\delta\lambda_i$ for the three largest Lyapunov exponents as a function of ε for sixteen randomly coupled Rössler systems having different internal frequencies ω_i. We find that the differences are small in the synchronization region.

We consider the simplest case of two coupled Rössler systems to examine how well Eq. (3.11) allows the estimation of Lyapunov exponents. The frequencies of these two coupled Rössler oscillators are $\omega_1 = 1.05$ and $\omega_2 = 1.07$. We consider the typical value of the frequencies as $\tilde{\omega} = 1.00$ and this gives first order correction in Eq. (3.11) $\Delta_1 = \Delta_2 = 0.06$. We calculate the Lyapunov exponents for the coupled Rössler systems and also their estimated values from Eq. (3.11) and compare them. Fig. 3.1 shows the three largest Lyapunov exponents $\lambda_i, i = 1, 2, 3$ (red, green and blue) and their estimated values λ_i^{MS} obtained from the master stability equation (Eq. (3.11)) (pink, cyan and black) as a function of coupling strength ε for these two coupled Rössler systems. The synchronized state is stable in the region $\varepsilon_1 < \varepsilon < \varepsilon_2$. In this region the third largest Lyapunov exponent and the master stability function both are negative. From this figure we can observe that in the synchronized state the Lyapunov exponents λ_i calculated by actually integrating two Rössler systems and their estimated value λ_I^{MS} calculated from Eq. (3.11) have good matching.

To see the difference between the Lypunov exponent and their estimated values we consider the error between them $\delta\lambda_i = \lambda_i - \lambda_i^{MS}$. In Fig. (3.2)**a** this error

$\delta\lambda_i$ is plotted as a function of coupling strength for the largest three Lyapunov exponents of two coupled Rössler systems. The stable synchronized state is the region indicated by arrows. From this figure we find that this difference $\delta\lambda_i$ is small in the synchronization region and close to it. In Fig. 3.2b we plot the difference $\delta\lambda_i$ as a function of ε for the three largest Lyapunov exponents and their estimated values for a random network of sixteen Rössler systems. Here also we observe the differences are small in the synchronization region. So, we can conclude that the master stability function calculated from Eq. (3.11) can estimate the stability of the synchronized state reasonably well.

3.4.2 Lorenz system

Now we consider coupled nonidentical Lorenz systems given by,

$$\begin{aligned} \dot{x}^i &= \sigma_i(y^i - x^i) + \varepsilon \sum_{j=1}^{N} a_{ij}(x^j - x^i) \\ \dot{y}^i &= x^i(r - z^i) - y^i \\ \dot{z}^i &= xy - bz \end{aligned} \tag{3.13}$$

where, σ_i, r, b are Lorenz parameters, ε coupling strength, a_{ij} is adjacency matrix. The parameter σ_i is considered to introduce mismatch between the coupled systems. We consider the mismatch is small so that $\sigma_i = \tilde{\sigma} + \delta\sigma_i$, where $\delta\sigma_i$ is small. To see how good Eq. (3.11) can determine the stability of synchronized state we calculate the Lyapunov exponents of this network and determine their estimated values from Eq. (3.11).

Fig. 3.3(a) shows three largest Lyapunov exponents λ_i (red, green and blue) for two coupled nonidentical Lorenz systems and their estimated values λ_i^{MS} (pink, cyan and black) as a function of coupling strength ε. The synchronized state is stable when the third largest Lyapunov exponent become negative. In Fig. 3.3(a) The onset of stable synchronization is shown by an arrow for $\varepsilon = \varepsilon_c$. The Lorenz systems have mismatch in parameter σ. We take $\sigma_1 = 11$ and $\sigma_2 = 9.5$ and the typical value of the parameter as $\tilde{\sigma} = 10$. Considering this the value of correction in Eq. (3.11) is $\Delta = 0.5$ and we calculate the MSF λ_i^{MS}. In Fig. 3.3(a) we observe

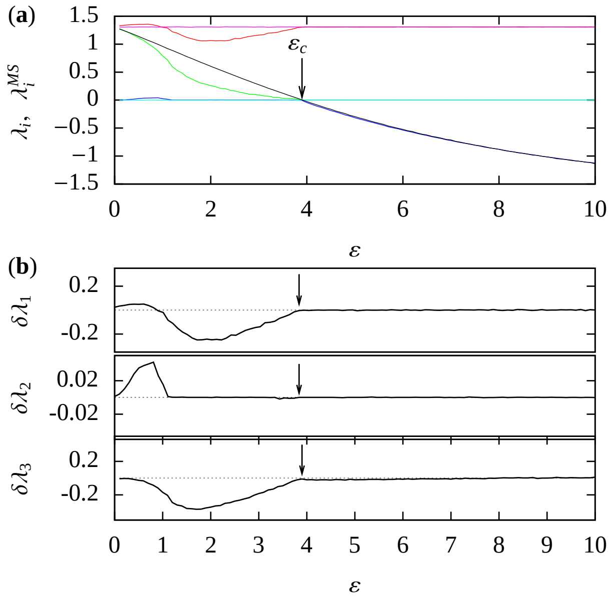

Figure 3.3: (a) The three largest Lyapunov exponents $\lambda_i; i = 1, 2, 3$ (red,green,blue) and their estimated values $\lambda_i^{MS}, i = 1, 2, 3$(pink,cyan,black) from master stability equation (Eq. (3.11)) of two coupled Lorenz systems are plotted as a function of coupling ε. Lorenz parameters $\sigma_1 = 11.0$ and $\sigma_2 = 9.5$. Other parameters are same for all systems and their values are $r = 28, b = 8/3$. The coupled systems are synchronized when $\varepsilon > \varepsilon_c$. (b) The difference between the Lyapunov exponents λ_i and their estimated values λ_i^{MS}, $\delta\lambda_i = \lambda_i - \lambda_i^{MS}$ are plotted as a function of ε.

a good match between these two exponents when the coupled systems are synchronized. The errors between the Lyapunov exponents and their estimated values are better quanties to compare the results. So in Fig. 3.3(b) this difference between the Lyapunov exponents and their estimated values $\delta\lambda_i = \lambda_i - \lambda_i^{MS}$ is plotted as a function of coupling constant ε. The difference become negligibly small in the synchronized state. The onset of stable synchronization is shown in the figure with arrows.

3.5 MSF of Rössler systems

In this section we determine MSF for nonidentical Rössler systems. The mismatch between the coupled systems are very small and all systems are chaotic. This allows us to calculated the mismatch parameter Δ in Eq. (3.11) using perturbation theory.

Here, the dynamics of an isolated node is given by,

$$\begin{aligned} \dot{x} &= -\omega y - z \\ \dot{y} &= \omega x + a_r y \\ \dot{z} &= b_r + z(x - c_r) \end{aligned} \tag{3.14}$$

where, ω, a_r, b_r, c_r are Rössler parameters. And these systems are coupled in the x-component, i.e. the coupling function is,

$$h(x) = \begin{pmatrix} x & 0 & 0 \\ 0 & 0 & 0 \\ 0 & 0 & 0 \end{pmatrix}.$$

3.5.1 Mismatch in one parameter

We have observed that the master stability equation Eq. (3.11) can approximate the stability of synchronized state reasonably well. Now, we consider that the non-identity between the Rössler systems in introduced through the parameter ω and the other parameters are fixed at the values $a_r = 0.2, b_r = 0.2, c_r = 7.0$ and the typical parameter value is $\tilde{\omega} = 1$. We can calculate the MSF, λ_{max}, using Eq. (3.11) as a function of α and Δ_ω, where Δ_ω is the correction term due the parameter mismatch in Rössler parameter ω. In Fig. 3.4 we plot λ_{max} in the parameter plane (α, Δ_ω) as a contour plot for Rössler system. The stability region is given by the "V" shape region bordered by the 0 curve from both sides. From the figure we can see that the stability region increases with the mismatch parameter Δ_ω.

Next, we consider another case where the parameter mismatch is in the Rössler parameter a_r and other parameters have constant values $\omega = 1, b_r = 0.2, c_r = 7.0$ and the typical parameter value is $\tilde{a_r} = 0.2$. Fig. 3.5 shows the master stability function λ_{max} for this case as a function of (α, Δ_a), where Δ_a is the correction term due to mismatch in Rössler parameter a_r. In this case the stable synchronization region is given by the inverted "V" shaped region bounded by the 0 curve from both sides. The stability region decreases with increase in the correction term Δ_a.

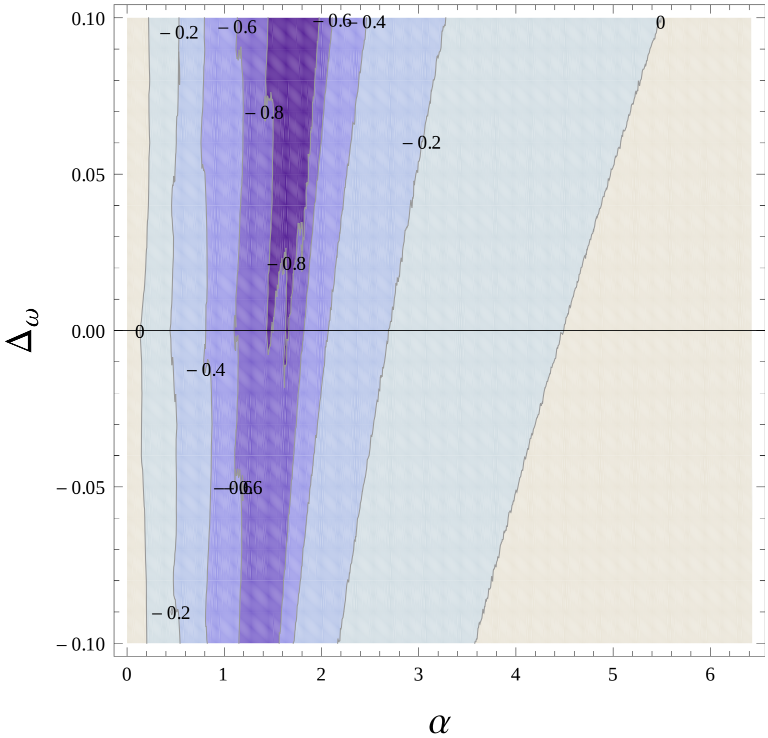

Figure 3.4: The master stability function λ_{max} of coupled Rössler systems is plotted as a function of α, Δ_ω. Here the mismatch is in parameter ω. The stability region given by the "V" shape region bordered by the 0 curve from both sides. The stability region increases with the correction term Δ_ω. The Rössler parameters are $a_r = 0.2, b_r = 0.2, c_r = 7.0$ and the typical parameter value $\tilde{\omega} = 1$.

We have also studied the other two cases where the mismatch is in Rössler parameters b_r and c_r respectively. For both of these cases the stability of the generalized synchronization is not affected due to parameter mismatch. In Fig. 3.6(a) we plot λ_{max} as a function of (α, Δ_b) for the case where mismatch is in Rössler parameter b_r and Δ_b is the correction due to the mismatch. The solid line gives the zero MSF curve, the dashed line is the contour line for $\lambda_{max} = .05$ and the dotted line is the contour line for $\lambda_{max} = -.2$. In Fig. 3.6(b) the MSF λ_{max} is plotted as a function of (α, Δ_c) where Δ_c is the correction due to the mismatch in Rössler parameter c_r. The solid line gives the zero MSF curve, the dashed line is the contour line for $\lambda_{max} = .05$ and the dotted line is the contour line for $\lambda_{max} = -.2$. In both of these figures we can see that the zero MSF contour curve is almost vertical.

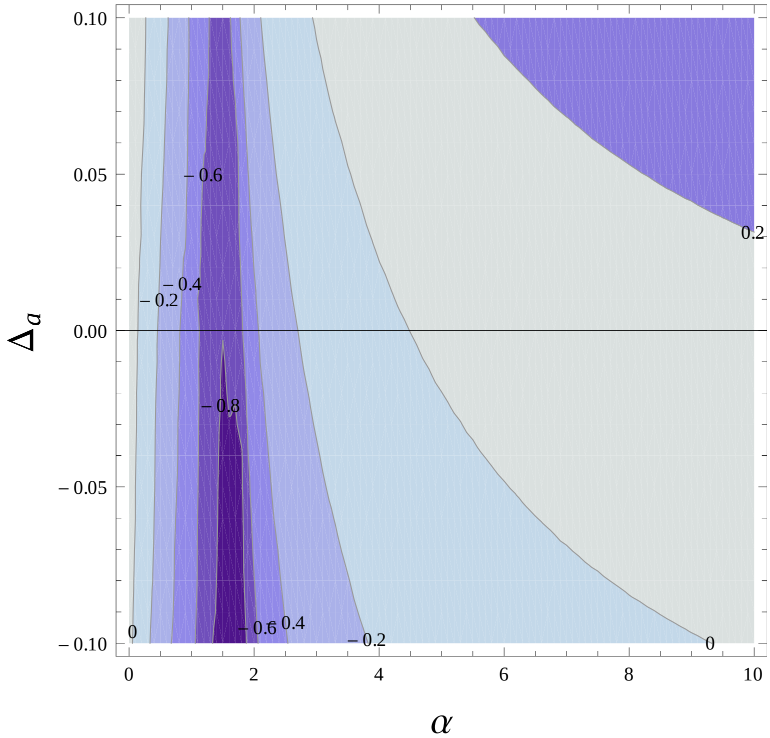

Figure 3.5: The master stability function λ_{max} of coupled Rössler systems is plotted as a function of α, Δ_a. The Rössler systems have mismatch in the parameter a_r. The stability region given by inverted "V" shape region bordered by the 0 curve from both sides. The stability region decreases with the increase in correction term Δ_a. The Rössler parameters are $\omega = 1, b_r = 0.2, c_r = 7.0$ and the typical parameter value is $\tilde{a_r} = 0.2$.

3.5.2 Mismatch in two parameters

Here we consider a more general case where the coupled nonidentical systems have mismatch in two parameters. We take the example of Rössler systems Eq. (2.10) and consider that mismatch is present in both of the parameters ω and a_r. For this case we can determine the master stability function λ_{max} from Eq. (3.11) as a function of $(\alpha, \Delta_\omega, \Delta_a)$, where Δ_ω and Δ_a are the corrections due to mismatch in ω and a_r respectively. The other Rössler parameters are kept constant at $b_r = 0.2, c_r = 7.0$ and the typical values of the parameters ω and a_r are $\tilde{\omega} = 1.0$ and $\tilde{a_r} = 0.2$ respectively. In Fig. 3.7 we have plotted the zero master stability surface, $\lambda_{max} = 0$, in phase space defined by $(\alpha, \Delta_\omega, \Delta_a)$. The master stability function λ_{max} is negative inside the region covered by these two surfaces and the generalized synchronization is stable in that region. From Fig. 3.7 we can see how the stability of the generalized synchronization is affected by the combined effect due to the

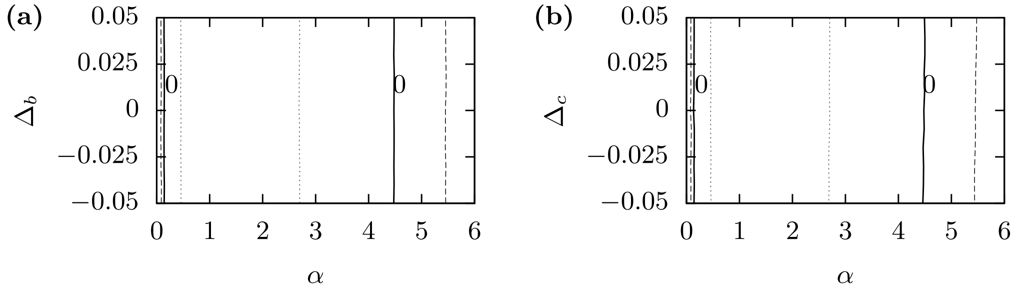

Figure 3.6: (a) The master stability function λ_{max} of coupled Rössler systems is plotted as a function of α, Δ_b. The Rössler systems have mismatch in the parameter b_r. The solid line gives the zero MSF line, the dashed line and the dotted line give the contour line for $\lambda_{max} = .05$ and $\lambda_{max} = -.2$ respectively. The stability region is bounded by the 0 MSF curve from both sides and these curves are almost vertical. The Rössler parameters are $\omega = 1, a_r = 0.2, c_r = 7.0$ and the typical parameter value is $\tilde{b_r} = 0.2$. (b) The MSF λ_{max} of coupled Rössler systems is plotted as a function of α, Δ_c. The Rössler systems have mismatch in the parameter c_r. The solid line gives the zero MSF line, the dashed line and the dotted line give the contour line for $\lambda_{max} = .05$ and $\lambda_{max} = -.2$ respectively. The stability region is bounded by the 0 MSF curve from both sides and these curves are almost vertical. The Rössler parameters are $\omega = 1, a_r = 0.2, b_r = 0.2$ and the typical parameter value is $\tilde{c_r} = 0.2$.

mismatch in parameters ω and a_r.

We have discussed the master stabiilty analysis for determining stability of generalized synchronization considering coupled nonidentical Rössler systems. Now for a given network of coupled nonidentical Rössler systems, if we have the information about parameter mismatch, typical parameter value and the coupling strength ε, then we can determine the value of α and the correction Δ which together give us a point in the (α, Δ) phase space. Then the stability of the given network can be determined by determining the sign of master stability function λ_{max} at that point. If the master stability function is negative for all transverse eigenmodes of the coupling matrix, then the network is in stable generalized synchronization.

We have similar studies with other chaotic systems like Lorenz system [116]. In the next section we briefly discuss our study with Lorenz system.

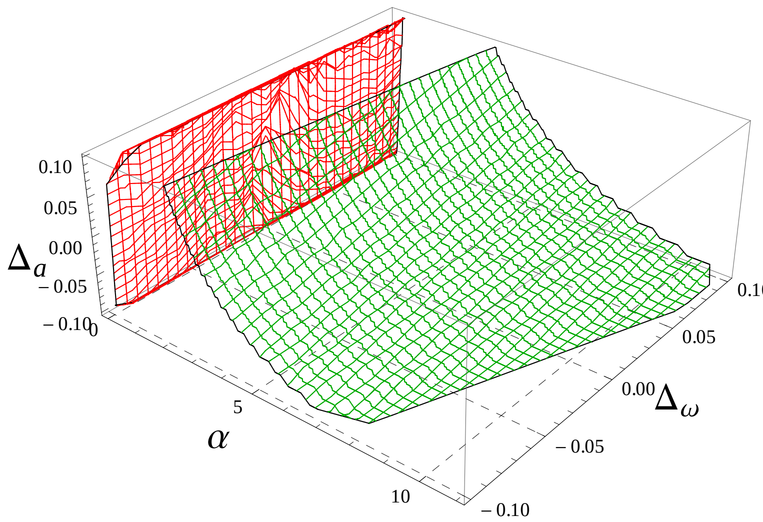

Figure 3.7: In this figure we plot the zero master stability surface, $\lambda_{max} = 0$, in phase space defined by $(\alpha, \Delta_\omega, \Delta_a)$. The inside region which is bounded by these two surfaces, (where $\lambda_{max} < 0$,) gives the stable generalized synchronization. The typical values of the parameters ω and a_r are $\tilde{\omega} = 1$ and $\tilde{a_r} = 0.2$ respectively, and other Rössler parameters are $b_r = 0.2, c_r = 7.0$.

3.6 MSF of Lorenz system

Here, the dynamics of an isolated system is given by the Lorenz system [116],

$$\begin{aligned} \dot{x} &= \sigma(y - x) \\ \dot{y} &= x(r - z) - y \\ \dot{z} &= xy - bz. \end{aligned} \tag{3.15}$$

where, σ, r, b are the Lorenz parameters. We consider that the Lorenz systems are coupled in the x-component by the coupling function,

$$h(x) = \begin{pmatrix} x & 0 & 0 \\ 0 & 0 & 0 \\ 0 & 0 & 0 \end{pmatrix}.$$

Let, the parameter mismatch be present in the Lorenz parameter σ and all other parameters are fixed at $b = 8/3, r = 28.0$. For this case we can determine the MSF λ_{max} from Eq. (3.11) as a function of α and Δ. In Fig. 3.8 the MSF

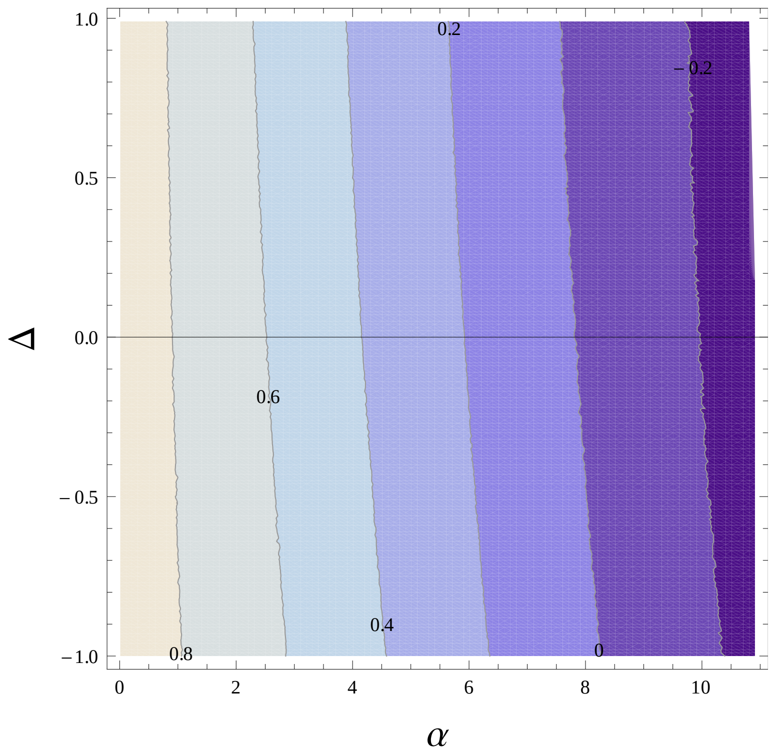

Figure 3.8: The MSF λ_{max} for coupled Lorenz systems Eq. (3.13) is plotted as a function of (α, Δ). From this figure we can see that the coupled systems can be synchronized for smaller value of α as Δ is increased. The Lorenz parameters are $\tilde{\sigma} = 10, r = 28, b = 8/3$.

λ_{max} of coupled Lorenz systems is plotted as a function of (α, Δ). We can see from Fig. 3.8, that as the mismatch parameter Δ is increased, the coupled systems show stable synchronization for smaller value of α.

3.7 Determining typical value $\tilde{r}$

In this section we discuss how to determine the typical parameter value $\tilde{r}$ of Eq. (3.11), so that the error between Lyapunov exponents and their estimated values will be least. Eq. (3.1) provides the model for coupled nonidentical systems, where r_i is the parameter of system i and $r_i = \tilde{r} + \delta r_i$; for small δr_i. $\tilde{r}$ provides the typical value of parameter r. To calculate the largest Lyapunov exponent from Eq. (3.11) the Jacobians $D_x f$, $D_x h$ and $D_r D_x f$ are evaluated at the typical value of parameter $\tilde{r}$. The typical value should satisfy the following conditions,

(1.) the nature of the coupled dynamical systems should not change at the typical

value; i.e. if all coupled systems are chaotic then the system should be chaotic at parameter $\tilde{r}$.
(2.) the deviations of the parameter δr_i should be small.

Analytically, it is not possible to determine $\tilde{r}$ which can best predict the stability of the synchronized state. So, we follow the numerical method to determine best value of $\tilde{r}$. Consider two coupled nonidentical Rössler systems with mismatch in parameter ω given by,

$$\begin{aligned}
\dot{x}^{1,2} &= -\omega_{1,2}y^{1,2} - z^{1,2} + \varepsilon(x^{2,1} - x^{1,2}) \\
\dot{y}^{1,2} &= \omega_{1,2}x^{1,2} + a_r y^{1,2} \\
\dot{z}^{1,2} &= b_r + z^{1,2}(x^{1,2} - c_r)
\end{aligned} \tag{3.16}$$

where, $\omega_{1,2}, a_r, b_r, c_r$ are Rössler parameters. We choose $\omega_1 = 0.985$ and $\omega_2 = 1.015$. Other parameter are fixed and their values are $a_r = 0.2, b_r = 0.2, c_2 = 7.0$. For these parameter values the coupled Rössler systems are chaotic. For this coupled systems we determine the Lyapunov exponents and compare the third largest Lyapunov exponent with its estimated value from Eq. (3.11) for different typical parameter values $\tilde{r}$. We determine the difference between the third largest Lyapunov exponent λ_3 and the MSF λ_{max} as $\delta\lambda_3 = \lambda_3 - \lambda_{max}$. The left hand column of Fig. 3.9 shows the three largest Lyapunov exponents $\lambda_i; i = 1, 2, 3$ (red,green,blue) and the master stability function λ_{max} (pink). The stable synchronized state is the bounded region bordered with arrows at both ends. The right part of Fig. 3.9 shows the difference $\delta\lambda_3$ as a function of coupling strength ε. The typical values of the parameter $\tilde{\omega}$ are (a) $\tilde{\omega} = 0.985$, (b) $\tilde{\omega} = 0.990$, (c) $\tilde{\omega} = 0.995$, (d) $\tilde{\omega} = 1.000$, (e) $\tilde{\omega} = 1.005$, (f) $\tilde{\omega} = 1.010$ and (g) $\tilde{\omega} = 1.015$.
Figure 3.9: Continued. The typical parameter values are (e) $\tilde{\omega} = 1.005$, (f) $\tilde{\omega} = 1.010$, (g) $\tilde{\omega} = 1.015$.

From the figures Fig. 3.9 we can see that the difference $\delta\lambda_3$ is minimum in Fig. 3.9(d), in which the typical parameter value $\tilde{\omega} = 1.000$ which is the average value of $\omega_1(= 0.985)$ and $\omega_2(= 1.015)$. We find that in general the average value gives good results in all the cases that we studied. There are other values of the

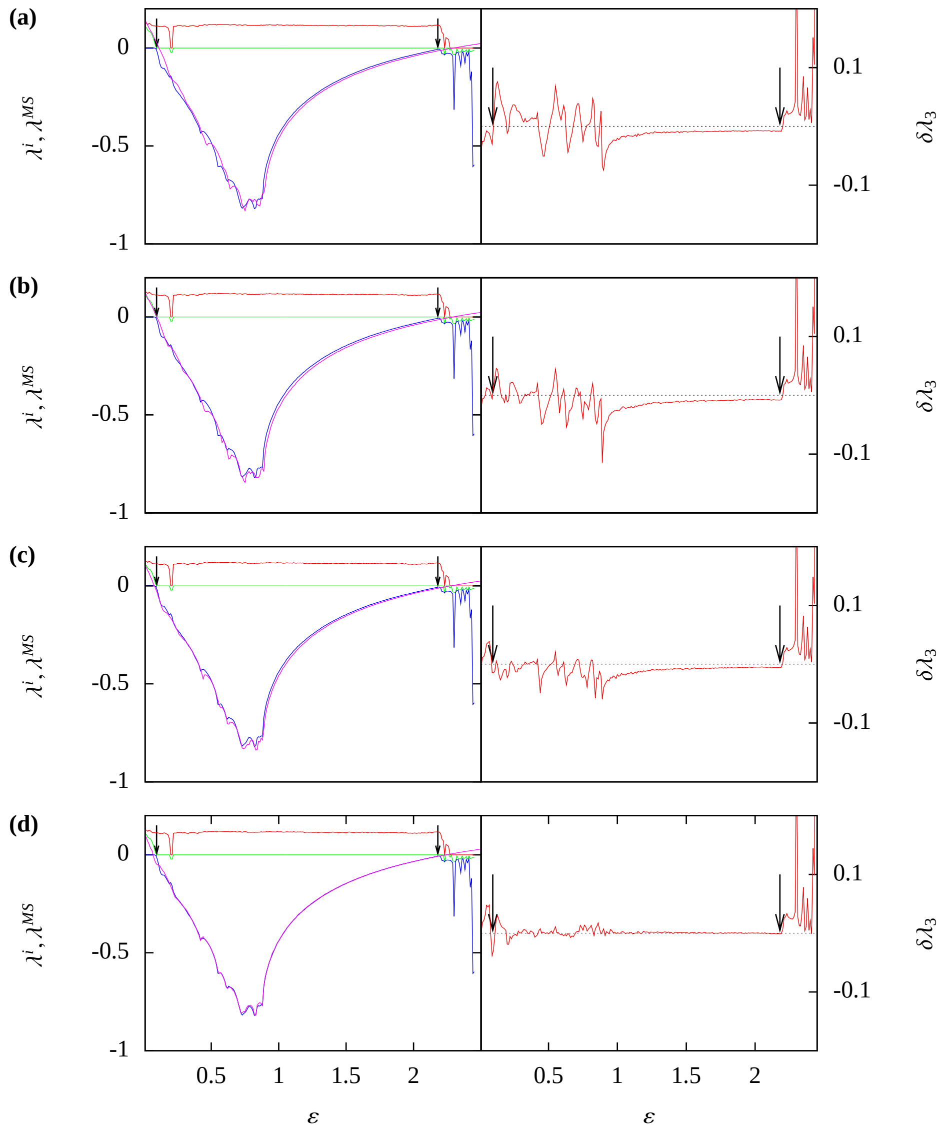

Figure 3.9: In the left column three largest Lyapunov exponents of Eq. (3.16) and the MSF λ_{max} is plotted as a function of coupling strength ε. In the right column the difference between the third largest Lyapunov exponent λ_3 and the MSF λ_{max} with different typical parameter values $\tilde{\omega}$ are plotted as a function of coupling strength. The stable synchronized state is bounded with arrows from both ends. The typical parameter values are (a) $\tilde{\omega} = 0.985$, (b) $\tilde{\omega} = 0.990$, (c) $\tilde{\omega} = 0.995$, (d) $\tilde{\omega} = 1.000$.

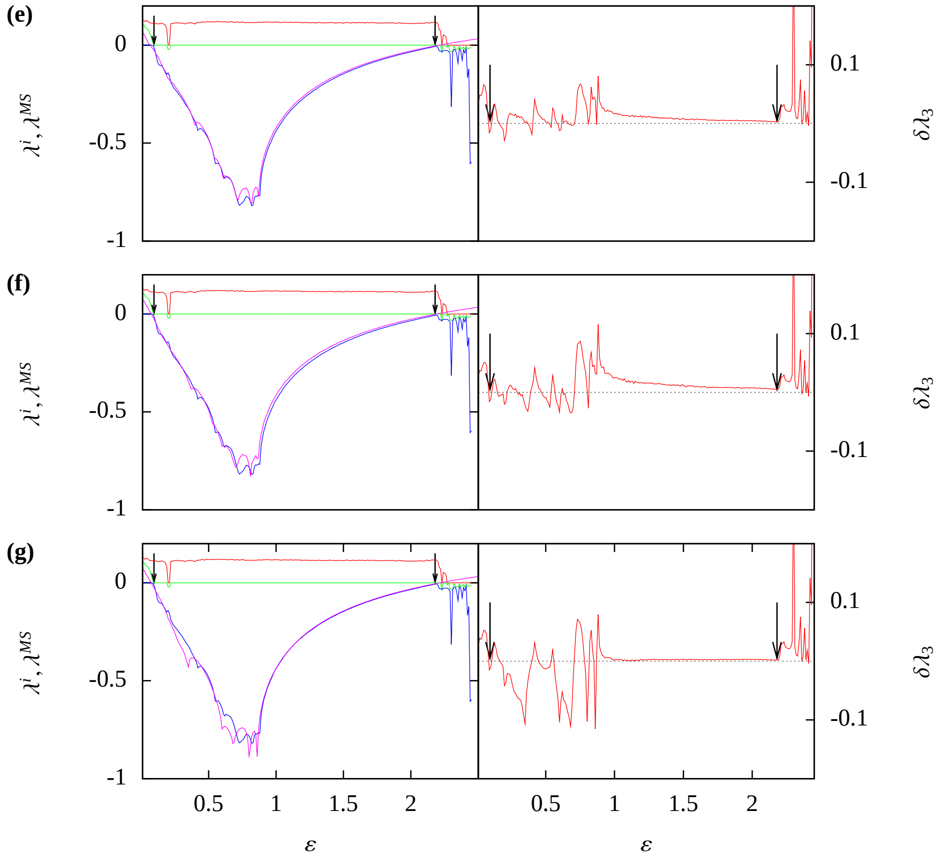

typical parameter which also reasonable results. But we could not obtain any systematic procedure to determine such values.

3.8 Practical region of δr

In section 3.3 we have developed a theory for determining the master stability function of coupled nonidentical systems. In this section we present numerical evidence to support our above derivation leading to Eq. (3.11) and also we discuss the valid range of parameter where this theory is applicable. Let us first consider the expansion (3.2) around some typical value of the parameter ($\tilde{r}$) and the solution of system ($\tilde{x}$) with typical parameter. For coupled identical systems one expands around the synchronized solution which corresponds to the solution of uncoupled dynamics, i.e. the dynamics without the coupling term. Taking hint from this, for nearly identical systems, we consider the properties of synchronized dynamics by omitting the coupling term. Consider N coupled chaotic Rössler systems,

$$\begin{aligned} \dot{x}^i &= -\omega_i y^i - z^i + \varepsilon \sum_{j=1}^{N} a_{ij}(x^j - x^i) \\ \dot{y}^i &= \omega_i x_i + a y^i \\ \dot{z}^i &= b + z^i(x^i - c) \end{aligned} \tag{3.17}$$

where ω_i is the parameter of the i-th oscillator and $a_{ij} = 1$ if the nodes i and j are connected and zero otherwise. We choose the couplings a_{ij} randomly. The different parameters ω_i are chosen randomly in an interval $(\bar{\omega} - \delta\omega/2, \bar{\omega} + \delta\omega/2)$. Now, we evolve the coupled Rössler systems. To see how the attractors of different systems are related to each other, we define subsystem Lyapunov exponents as the exponents calculated by the following procedure. We evolve the Rössler equations as above with the coupling term, and then using the variables from this evolution, we calculate subsystem Lyapunov exponents by the usual procedure of calculating Lyapunov exponents with the coupling term omitted. Thus for each system i we get three subsystem Lyapunov exponents, say $\lambda^s_{im},\ i = 1, \ldots, N,\ m = 1, 2, 3$. For coupled identical systems these subsystem Lyapunov exponents will be the same for all the systems, i.e. they will be independent of i.

Fig. 3.10(a) shows the subsystem Lyapunov exponents λ^s_{i1}, λ^s_{i2} and λ^s_{i3} as a function of the parameter ω for a system of 32 coupled Rössler systems in the synchronized state, with the parameters ω chosen randomly in the range $(0.999, 1.001)$. We see that the three Lyaponov exponents for the subsystems vary linearly with $\delta\omega_i$. The linear variation is in agreement with Eq. (3.3) omitting the coupling term. We find that the subsystem Lyapunov exponents calculated from Eq. (3.3) match with those shown in Fig. 3.10. The linear variation of the subsystem Lyapunov exponents for different systems, supports the conjecture that the different attractors are not significantly deformed in the synchronized state.

To see the range of ω values for which the linear variation holds, in Fig. 3.10(b) we plot the subsystem Lyapunov exponents λ^s_{i1}, λ^s_{i2} and λ^s_{i3} as a function of the frequency ω for a system of 32 coupled nearly identical Rössler oscillators in the synchronized state, with frequencies chosen randomly in a wider range $(0.98, 1.02)$.

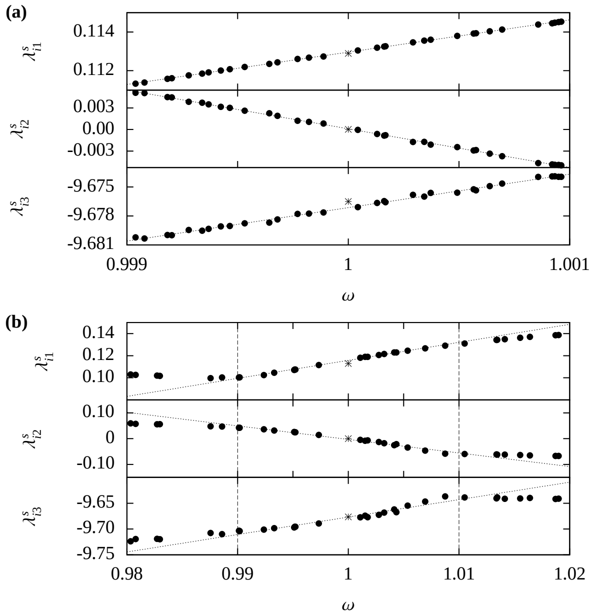

Figure 3.10: (a) The figure shows the subsystem Lyapunov exponents, λ^s_{i1}, λ^s_{i2} and λ^s_{i3}, for a system of 32 coupled Rössler oscillators as a function of the parameter ω in the synchronized state (solid circles). The parameters ω are chosen randomly in the interval $(0.999, 1.001)$. We see that the three subsystem Lyaponov exponents vary linearly with ω. The three stars show the Lyapunov exponents, $\tilde{\lambda}_m$, for a system with the average value of the parameter $\bar{\omega} = 1$. (b) The same plot as in (a), except that the parameters are now chosen randomly in the interval $(0.98, 1.02)$. We see that the subsystem Lyapunov exponents vary almost linearly in the interval $(0.99, 1.01)$. Nonlinearity can be seen outside this interval.

We see a linear variation in the range $(0.99, 1.01)$ while nonlinearity can be seen outside this range. The linear region defines the range of validity of our theory.

We now consider the choice of the typical value of the parameter $\tilde{\omega}$. One choice is the average value $\tilde{\omega} = \bar{\omega} = 1$ and in section 3.7 we numerically demonstrate that the average parameter value gives good estimation of Lyapunov exponents. Here, we make some more investigation to determine the good value of the typical parameter considering subsystem Lyapunov exponents. The three Lyapunov ex-

	$j=1$	$j=2$	$j=3$
$\lambda^s_{\bar{\omega}j}$	0.1130	0.0001	-9.6771
$\tilde{\lambda}_j$	0.1130	0.0000	-9.6765

Table 3.1: The table shows the three subsystem Lyapunov exponents $\lambda^s_{\bar{\omega}j}$, $j = 1, 2, 3$ for the coupled Rössler system Eq. (3.17) obtained for $\omega = \bar{\omega} = 1$ from linear fits in Fig. 3.10 and the corresponding values of the Lyapunov exponents λ^a_j, $j = 1, 2, 3$ for the attractor for the average parameter $\bar{\omega}$.

ponents for the uncoupled trajectory for $\bar{\omega}$, say $\tilde{\lambda}_j$, are shown in Fig. 3.10 by stars and they lie almost on the three lines. In Table 3.1 we give the three values $\tilde{\lambda}_j$ and also the three values $\lambda^s_{\bar{\omega}j}$ for $\bar{\omega}$ obtained from the linear fits in Fig. 3.10. There is a good agreement between the two sets of Lyapunov exponents. Thus we conclude that the average value of the parameter $\bar{\omega}$ is one good choice for the typical value $\tilde{\omega}$.

3.9 Summary

In this chapter we analyse stability of generalized synchronization of coupled non-identical systems by considering the master stability function (MSF). We use the fact the the exponential nature of solutions of a linear differential equation will be dominated by the homogeneous part of a linear differential equation. We consider the synchronous solution of coupled identical systems and treat the parameter mismatch in first order perturbation theory. This allows us to construct a master stability equation. The largest transverse Lyapunov exponent is calculated from the master stability equation. The master stability function (MSF) is defined by the largest transverse Lyapunov exponent as a function of coupling strength. The synchronized state is stable when the largest transverse Lyapunov exponent is negative. We have also shown that this MSF can well approximate the stability of synchronous state by comparing them with the Lyapunov exponents of coupled systems.

Chapter 4

Construction of synchronization optimized networks

4.1 Introduction

In this chapter we consider the problem of constructing synchronization optimized network by rewiring the links of a given network that has fixed number of links and nodes and we search for networks which shows best synchronizability property. By best synchronizability property we mean the largest stable interval of the coupling constant ε which shows synchronization. We consider a network of coupled non-identical systems. To construct the synchronization optimized network we adapt Monte Carlo optimization method [127, 128, 129] and we use the stability criteria provided by the Master Stability Function (MSF) in chapter 3.

For a network of coupled identical systems it has been shown that a small-world network has best synchronizability properties [130]. As we consider a network of coupled nonidentical systems, there are other questions like which nodes are chosen as hubs and which links are more preferable in the optimized network. We investigate these questions here.

This chapter is divided in the following sections. In section 4.2 we briefly review the Monte Carlo optimization method. In section 4.3 we construct synchronized optimized networks from a given undirected network. In this section we consider two cases, first we consider the case when the parameter mismatch is present in one parameter of coupled systems and for the second case we consider the mismatch in two parameters of the coupled systems. In section 4.4 we consider a more general network with directed links. We summarize the chapter in section 4.5.

4.2 Monte-Carlo optimization

The method of *simulated annealing* [131] is a technique that has attracted significant attention as suitable for optimization problems of large scales, particularly where a desired global extremum is hidden among many, poorer, local extrema. Back in 1953, Metropolis et. al. [127] first provided a numerical method which shows simulation of stimulated annealing of a liquid. This numerical method is based on Gibbs sampling of states from a large ensemble. When a system is at thermal equilibrium at temperature t, the number of states with energy E is given by Maxwell-Boltzmann distribution, $Prob(E) \sim e^{-E/kt}$, where, k is Boltzmann constant. Such a thermodynamic system changes its configuration from energy E_1 to energy E_2 with probability $p = exp[-(E_2 - E_1)/kt]$. When $E_2 < E_1$ then, $p > 1$, in such a case the probability is arbitrarily assigned with probability $p = 1$ and the state is chosen. Otherwise the state is chosen with probability $p = exp[-(E_2 - E_1)/kt]$ by comparing p with a random number between $0 < x < 1$; if $p > x$ the state is accepted and rejected when $p < x$. This general scheme, of mostly taking a downhill step while sometimes taking uphill steps is known as Metropolis algorithm. Here we apply this algorithm to construct synchronized optimized network from any given network of coupled nonidentical systems.

4.3 Optimization of undirected graph

In this section we consider symmetric coupling matrix. All the links of the network are undirected. All the eigenvalues of the coupling matrix are real. This simplifies the problem of constructing synchronized optimized network.

4.3.1 The Optimization Method:

We start with a connected random network with total N nodes and E randomly chose links. We consider the links as undirected. We rewire the links of this random network to construct a network that shows best synchronizability. We remove a randomly selected existing link of the network and create a new link in a link vacancy between a randomly selected pair of nodes. After doing this we confirm that the network does not become disconnected. In the following section we discuss the details of Metropolis algorithm for constructing synchronization optimized networks.

4.3.2 Mismatch in one parameter

First we consider the simplest case where the coupled systems on a network have mismatch in only one parameter. In section 3.5.1 of chapter 3 we have developed the master stability function λ_{max} to analyse stability of generalized synchronization for x-component coupled nonidentical Rössler systems having mismatch in one parameter. The generalized synchronization is stable when the master stability function λ_{max} is negative for all transverse eigenmode of the coupling matrix G.

Let us consider a network of N coupled Rössler systems as in Chapter 3,

$$\begin{aligned}
\dot{x}^i &= -\omega_i y^i - z^i + \varepsilon \sum_{j=1}^{N} g_{ij} x^j \\
\dot{y}^i &= \omega_i x^i + a_r y^i, \\
\dot{z}^i &= b_r + z^i (x^i - c_r)
\end{aligned} \tag{4.1}$$

where a_r, b_r, c_r and ω are Rössler parameters. We consider parameter ω has mismatch. $G = [g_{ij}]$ is the Laplacian of the network. We rewire this network keeping the total number of links constant and searche for the optimal network showing best synchronizability.

In Fig. 4.1 we plot the zero contour lines of the master stability function $\lambda_{max} = 0$ in the parametric space (α, Δ) for coupled Rössler systems with mismatch in parameter ω. In the "V" shaped region bounded by these two contour

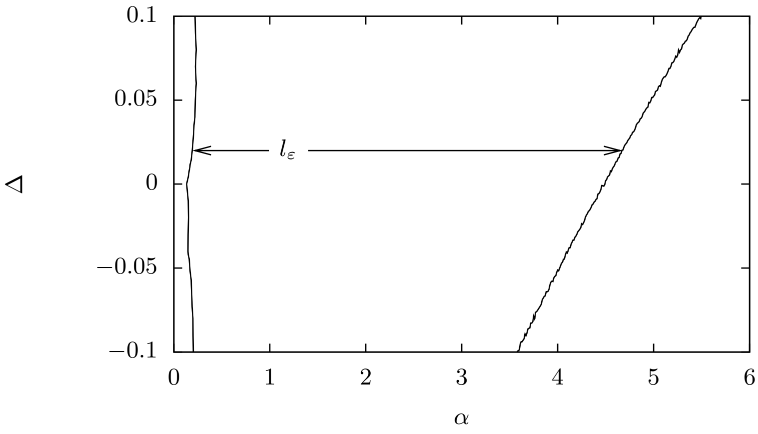

Figure 4.1: The zero master stability function $\lambda_{max} = 0$ is plotted as a function of (α, Δ) for coupled Rössler systems with mismatch in parameter ω. The stable region is the "V" shaped region bounded by these two curves. The other Rössler parameters are $a_r = 0.2, b_r = 0.2, c_r = 7.2$ and the typical value of parameter ω is $\tilde{\omega} = 1$.

lines the master stability function λ_{max} is negative and thus provides the stability generalized synchronization. We denote this stable interval of coupling constant by l_ε. In this case the stability region increases with the parameter Δ.

Metropolis algorithm for constructing synchronization optimized networks

Let us start with a random network of N coupled nonidentical Rössler systems which are connected by total E edges and the coupling matrix of this initial random network is G^i in Eq. (4.1). From the information of parameter mismatch of the coupled Rössler systems we can find the value of the first order correction term Δ. Now from Fig. 4.1 we can determine the stable interval of the coupling constant ε by calculating the difference between the two critical values of coupling constant ε_1 and ε_2. These two critical values of the coupling constant can be obtained from the two contour lines $\lambda_{max} = 0$ which give the two ends of the stable generalized synchronization. Let, $l_\varepsilon^i = (\varepsilon_2^i - \varepsilon_1^i)$ be the initial stable interval for the coupling matrix G^i. Now in this network we randomly delete an existing link and create a new link at a link vacancy. Let, the coupling matrix of the resultant network be G^f and l_ε^f be the new stable interval of the resultant network. We reject the resultant network if it is disconnected. When $l_\varepsilon^f > l_\varepsilon^i$ we accept the network, else we

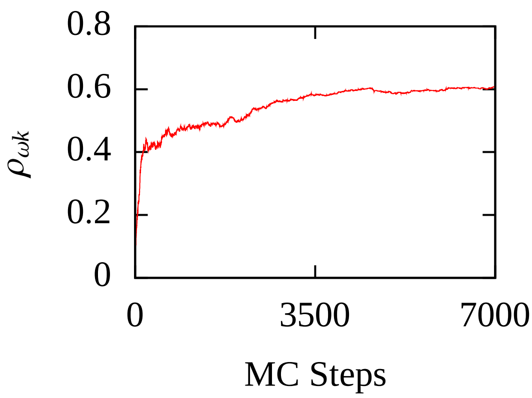

Figure 4.2: The figure plots the correlation coefficient $\rho_{\omega k}$ as a function of the Monte Carlo steps of optimization for 32 coupled Rössler systems. We see that $\rho_{\omega k}$ increase and saturate to positive values.

accept it with a probability $e^{(l_\varepsilon^f - l_\varepsilon^i)\beta}$, where $\beta = 1/T$, where T is a temperature-like parameter. This rewiring procedure which defines a Monte Carlo step, is repeated several times. We start with a high value of T $(= 1)$. T is kept fixed for 1000 Monte Carlo steps or 10 accepted ones, whichever occurs first. Then T is decresed by a certain factor ($T_{factor} < 1$) so that stimulated annealing or slow cooling occurs [128, 132, 133]. We keep on repeating this process until there are no more changes during five successive temperature steps, assuming in this case that the optimal network topology has been found.

Properties of the optimal networks

Now, in the optimized network we searched for the nodes which have more connections than other nodes, i.e. which nodes are selected as hubs. To find this we define the correlation coefficient between the node parameter and the node degree as,

$$\rho_{\omega k} = \frac{< (k_i - < k_i >)(\omega_i - < \omega_i >) >}{\sqrt{< (k_i - < k_i >)^2 >< (\omega_i - < \omega_i >)^2 >}} \tag{4.2}$$

where, $k_i = -g_{ii}$ is the degree of node i.

Fig. 4.2 shows $\rho_{\omega k}$ as a function of Monte Carlo steps. For the random network $\rho_{\omega k} = 0$. We find that $\rho_{\omega k}$ increases and saturates to a positive value. Thus, in the synchronized optimized network the nodes which have larger frequencies have more connections and are preferred as hubs. The reason for this is the “V” shape

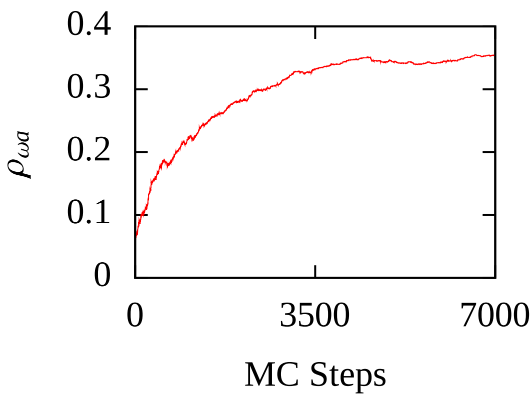

Figure 4.3: The figure plots the correlation coefficient $\rho_{\omega a}$ as a function of the Monte Carlo steps of optimization for 32 coupled Rössler systems. We see that $\rho_{\omega k}$ increases and saturates to positive value.

of the stability region in Fig. 3.4, i.e. the stability range increases as Δ increases.

To investigate the question of which edges are preferred, we define the correlation coefficient between the absolute parameter differences between two nodes and the edges as,

$$\rho_{\omega a} = \frac{< (A_{ij} - < A_{ij} >)(|\omega_i - \omega_j| - < |\omega_i - \omega_j| >) >}{\sqrt{< (A_{ij} - < A_{ij} >)^2 >< (|\omega_i - \omega_j| - < |\omega_i - \omega_j| >)^2 >}} \tag{4.3}$$

where, $A_{ij} = 1$ if nodes i and j are connected and 0 otherwise. For a random network $\rho_{\omega a}$ will be zero. When the nodes with larger parameter difference $|\omega_i - \omega_j|$ are chosen to create a link, then $\rho_{\omega a}$ increases.

Fig. 4.3 shows $\rho_{\omega a}$ as a function of Monte Carlo steps. We find that $\rho_{\omega a}$ increases from 0 (the value for the random network) and saturates. Thus, in the synchronized optimized network the pair of nodes which have a larger relative frequency mismatch are preferred as edges for the optimized network. Again, the reason for this preference of edges is probably the conical shape of the stability region in Fig. 3.4. The edges are to be chosen so that the parameter Δ increases and the stability region increases.

Next, we consider a different case where the coupled Rössler systems have mismatch in parameter a_r instead of ω. The other Rössler parameters are fixed at $\omega = 1, b_r = 0.2, c_r = 0.2$ and the typical value of the parameter a_r is $\tilde{a_r}$. The master stability function of such a network is calculated as a function of network

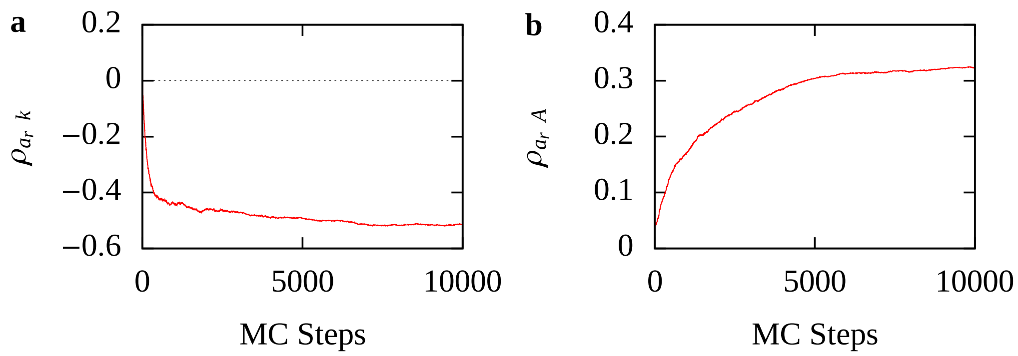

Figure 4.4: **a** The figure plots the correlation coefficient $\rho_{a_r k}$ as a function of the Monte Carlo steps of optimization for 32 coupled Rössler systems. We see that $\rho_{a_r k}$ decreases and saturates to negative value. **b** The figure plots the correlation coefficient $\rho_{a_r A}$ as a function of the Monte Carlo steps of optimization for 32 coupled Rössler systems. We see that $\rho_{a_r A}$ increases and saturates to positive value.

parameter α and mismatch parameter Δ. Fig. 3.5 in Chapter 3 shows the nature of MSF λ_{max} as a function of (α, Δ). The stability region is provided by the inverted "V" shaped region bounded by the 0 curve from both sides. From the figure we can see that the stability region decreases with increase in mismatch parameter Δ.

We consider the above mentioned Monte Carlo method to construct a synchronization optimized network from a random network of 32 coupled Rössler systems. To find the nodes which are selected as hubs in the optimized network we consider the correlation between node parameter and degree $\rho_{a_r k}$ given by Eq. (4.2). In Fig.4.4a we plot $\rho_{a_r k}$ for such a network as a function of Monte Carlo steps. We find that $\rho_{a_r k}$ decreases from 0 and saturates to a negative value. Thus, in the synchronized optimized network the nodes which have smaller value of a_r have more connections and are preferred as hubs. The correlation coefficient between the absolute parameter differences between two nodes $\rho_{a_r A}$ and the edges given by Eq. (4.3) will give the information about which edges are more preferable in the optimized network. Fig. 4.4b shows the nature of $\rho_{a_r A}$ as a function of Monte Carlo steps. We find that $\rho_{a_r A}$ increases from zero and saturates to a positive value, indicating the pair of nodes which have larger parameter mismatch are selected to create edges in the optimized network.

4.3.3 Mismatch in two parameters

In this section we consider that the coupled Rössler systems have mismatch in two parameters, ω ans a_r. Other Rössler parameters are fixed at the values $b_r = 0.2, c_r = 7.0$ and the typical values of the parameters ω and a_r are $\tilde{\omega} = 1$ and $\tilde{a_r} = 0.2$. Fig. 3.7 of Chapter 3 shows the MSF for generalized synchronization in the three dimensional space defined by $(\alpha, \Delta_a, \Delta_\omega)$. We use Monte Carlo optimization method to construct synchronization optimized networks. Now, in this optimal network we investigate which nodes are selected as hubs and which pair of node are selected to create links in the optimized network. We calculate two correlations, one between node degree k_i and parameter ω_i, and the other between the node degree k_i and parameter $(a_r)_i$. In Fig. 4.5a we plot these two correlation coefficients as a function of Monte Carlo steps. The red line in Fig. 4.5a is the correlation coefficients between node degree k_i and parameter ω_i, and we can see that the correlation increases from zero and saturates to a positive value and the blue line of Fig. 4.5a is the correlation coefficient between the node degree k_i and the node parameter $(a_r)_i$ and this curve start from zero and decreases and saturates to a negative value. Thus, in the optimized network the nodes which have larger value in parameter ω_i and smaller value in parameter $(a_r)_i$ are selected as hubs.

To find which links are more preferable we consider two correlation coefficients, first the correlation between the absolute parameter differences between two nodes $|\omega_i - \omega_j|$ and the edges A_{ij} and the correlation between the absolute parameter differences between two nodes $|(a_r)_i - (a_r)_j|$ and the edges A_{ij}, from Eq. (4.3). In Fig. 4.5**b** the red and blue lines show these two correlation coefficients as a function of Monte Carlo steps. We can see from Fig. 4.5b that both of these correlation coefficients increase from zero and saturate to a positive value. Thus, the pair of nodes which have larger parameter mismatch both in parameter ω and parameter a_r are selected to construct the links in the optimized network.

In Fig. 4.6 the node degree is plotted as a function of node parameter ω and a_r for the optimal network. The color code represents the node degree. From the figure we can see that the nodes which have larger value in parameter ω and smaller value in parameter a_r have larger degree and are chosen as hubs in the optimized

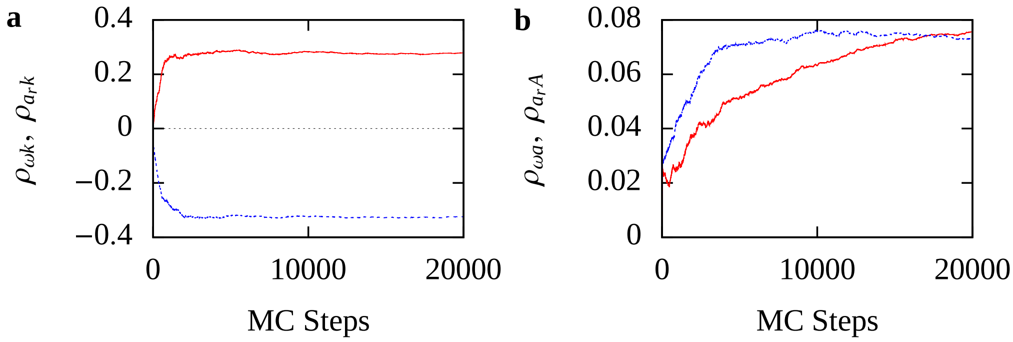

Figure 4.5: **a** The red line shows the correlation coefficient between node degree k_i and parameter ω_i and the blue line shows the correlation coefficients between node degree k_i and parameter $(a_r)_i$ as a function of Monte Carlo steps. We can see the correlation between node degree k_i and parameter ω_i increases from zero and saturates to a positive value, while the correlation between the node degree k_i and node parameter $(a_r)_i$ decreases from zero and saturates to a negative value. **b** The red line shows the the correlation coefficient between the absolute parameter differences between two nodes $|\omega_i - \omega_j|$ and the edges A_{ij}, and the blue line shows the the correlation coefficient between the absolute parameter differences between two nodes $|(a_r)_i - (a_r)_j|$ and the edges A_{ij}. We can see both of these correlation coefficients increase from zero and saturate to a positive value.

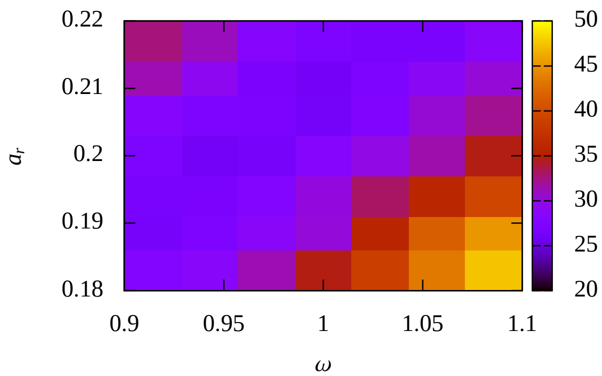

Figure 4.6: In this figure the node degree is plotted as a function of node parameter ω and a_r for the optimal network. The color code represents the node degree. From the figure we can see that the nodes which have larger value in parameter ω and smaller value in parameter a_r have larger degree and are chosen as hubs in the optimized network.

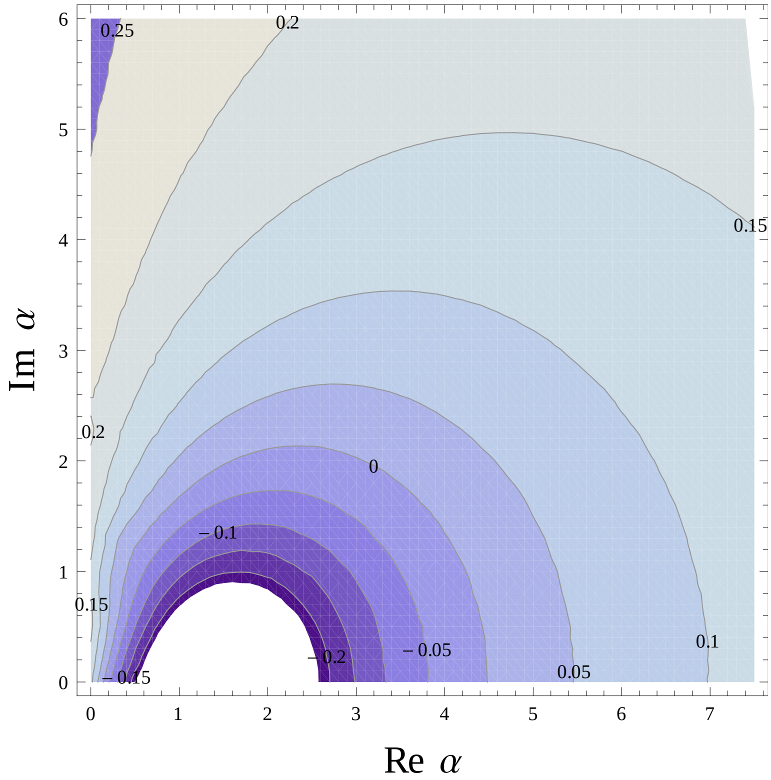

Figure 4.7: This figure plots the MSF λ_{max} on a plane of complex α for a network of coupled identical Rössler systems. The stable synchronized state is given by the region under the 0 curve.

network.

4.4 Optimization in directed networks

In the previous sections we considered networks where the links are undirected; i.e. the coupling matrix is symmetric. In this section we consider a more general case where the coupled systems have directed links between them and so the coupling matrix is asymmetric. For a directed graph both α and Δ can be complex quantities. In Fig. 4.7, the MSF is plotted on the complex plane of α for a directed network of coupled identical Rössler systems, $\Delta = 0$. The stable synchronized state is given by $\lambda_{max} < 0$.

4.4.1 The optimization method

We consider a network of N coupled nonidentical Rössler systems,

$$\begin{aligned}
\dot{x}^i &= -\omega_i y^i - z^i + \varepsilon \sum_{j=1}^{N} g_{ij} x^j \\
\dot{y}^i &= \omega_i x^i + a_r y^i \\
\dot{z}^i &= b_r + z^i (x^i - c_r)
\end{aligned} \tag{4.4}$$

here, if there is a directed link from node j to node i, then $g_{ij} = 1$, otherwise $g_{ij} = 0$. The diagonal elements $g_{ii} = -\sum_j g_{ij}; j \neq i$. The eigenvalue and eigenvectors of the coupling matrix $G = [g_{ij}]$ can be complex for directed networks. There will be one eigenvalue $\mu_1 = 0$ of the matrix G and the corresponding eigenvector is $e_1 = (1, \ldots, 1)^T$. This eigenmode defines the synchronization manifold. The other eigenmodes corresponds to the transverse manifold. The rest of eigenvalues of G are $\mu_2 < \ldots < \mu_N$.

We consider that the Rössler parameter ω is different from system to system, while other parameters a_r, b_r, c_r are same for all systems. For such a network the MSF can be calculated (Eq. 3.11 of Chapter 3) as a function of the complex parameter α and Δ. The typical value of the Rössler parameter ω in the given network (Eq. (4.4)) is $\tilde{\omega} = 1$. For such a random network with 10% mismatch in the parameter ω the typical range of the first order correction, i.e. the mismatch parameter Δ is $0.00 < \Delta < 0.05$.

We have calculated the MSF for some discrete values of complex mismatch parameter Δ. In Fig. 4.8 the MSF $\lambda_{max} = 0$ curve is plotted as a function of α. The stability range l_ε^{old} of any random network given by Eq. (4.4) can be interpolated from Fig. 4.8. Now, we rewire the random network by deleting any randomly chosen directed link and creating a new directed link in a link vacancy. After doing this, the new stability range l_ε^{new} of the new network is determined. If $l_\varepsilon^{new} > l_\varepsilon^{old}$ then we accept the new network, otherwise the new network is accepted with probability $e^{\beta(l_\varepsilon^{new} - l_\varepsilon^{old})}$, where β is inverse temperature. The temperature is reduced after certain Monte Carlo steps. In Fig. 4.9 the stability range l_ε is plotted as a function of Monte Carlo steps. From Fig. 4.9 we can observe that after initial

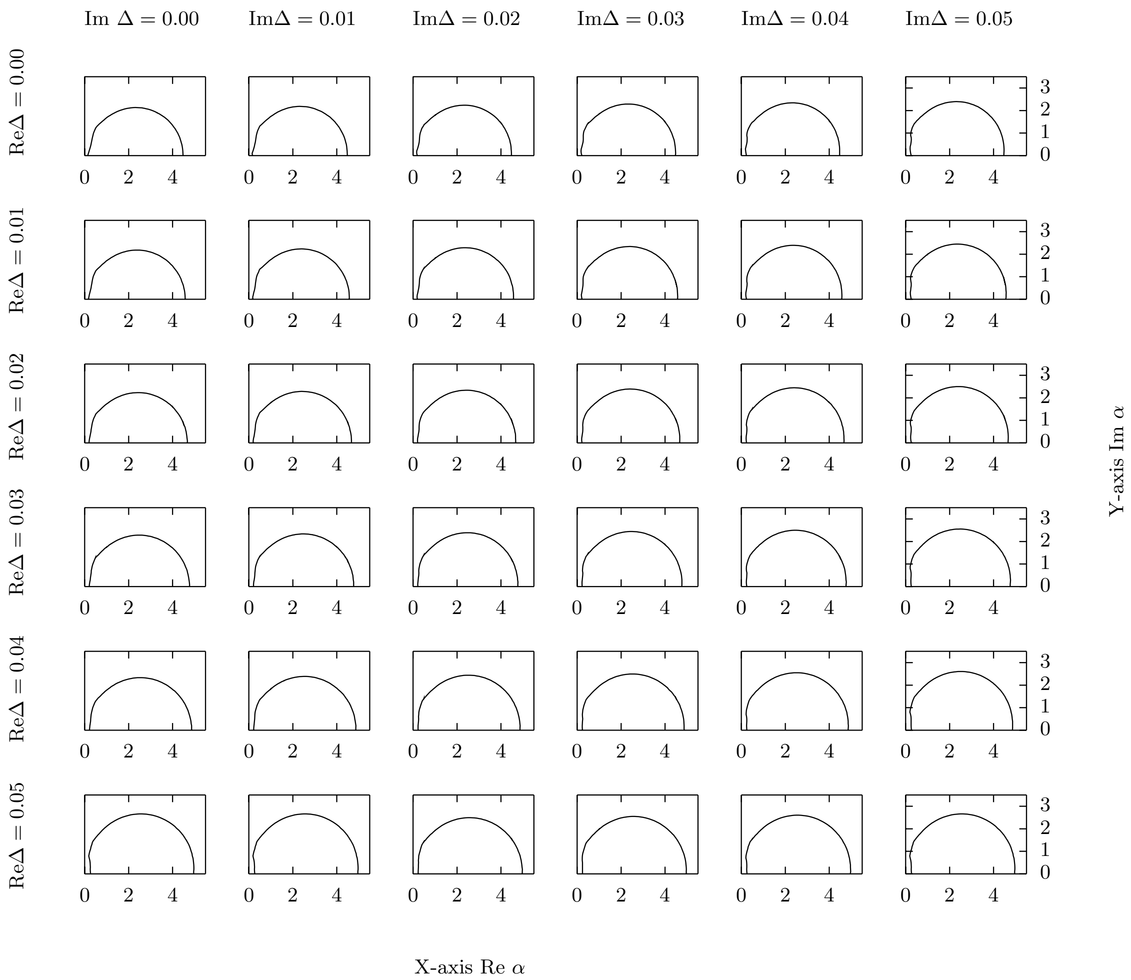

Figure 4.8: The MSF is plotted at some discrete values of ReΔ and ImΔ as a function of the complex parameter α. The black curve is for the zero MSF ($\lambda_{max} = 0$) and below this curve the MSF is negative and the synchronized state is stable.

increase the stability range saturates.

Now, we calculate the correlation $\rho_{\omega k^{in}}$ between the in-degree k^{in} and parameter ω following Eq. (4.2) and the correlation $\rho_{\omega k^{out}}$ between the out-degree k^{out} and parameter ω. In Fig. 4.10 the red line shows $\rho_{\omega k^{in}}$ as a function of Monte Carlo steps and the blue line shows the correlation $\rho_{\omega k^{out}}$ as a function of Monte Carlo steps. The correlation $\rho_{\omega k^{in}}$ increases and saturates to a positive value. Thus, the nodes with larger value of parameter ω are prone to having more incoming links in the optimized network. While, the correlation with the out-degree $\rho_{\omega k^{out}}$ (blue line) remains nearly zero and we do not see any correlation between node out-degree and node parameter.

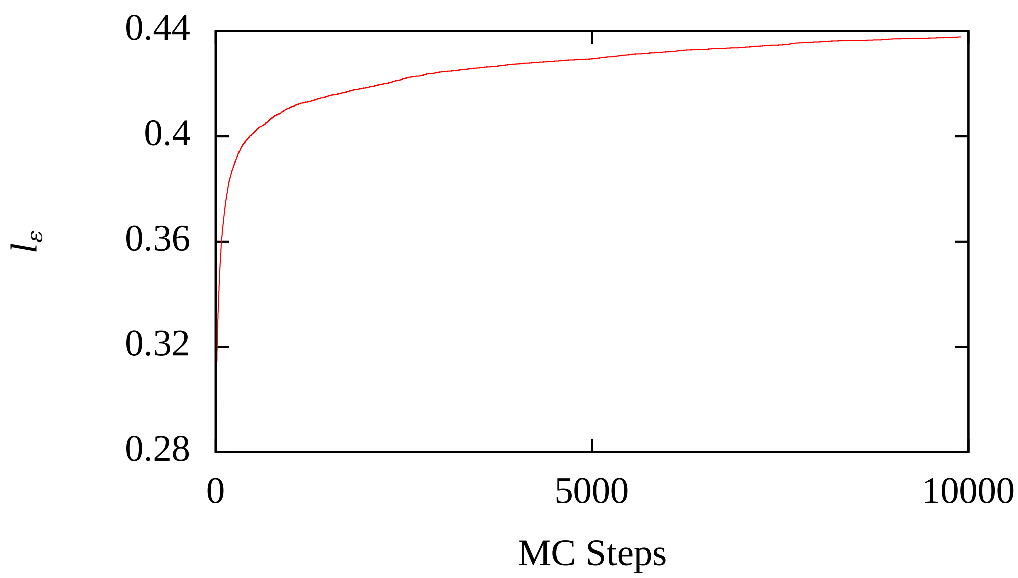

Figure 4.9: The stability range l_ε is plotted as a function of Monte Carlo steps. For the initial Monte Carlo steps the stability range l_ε increases sharply then it comes to saturation.

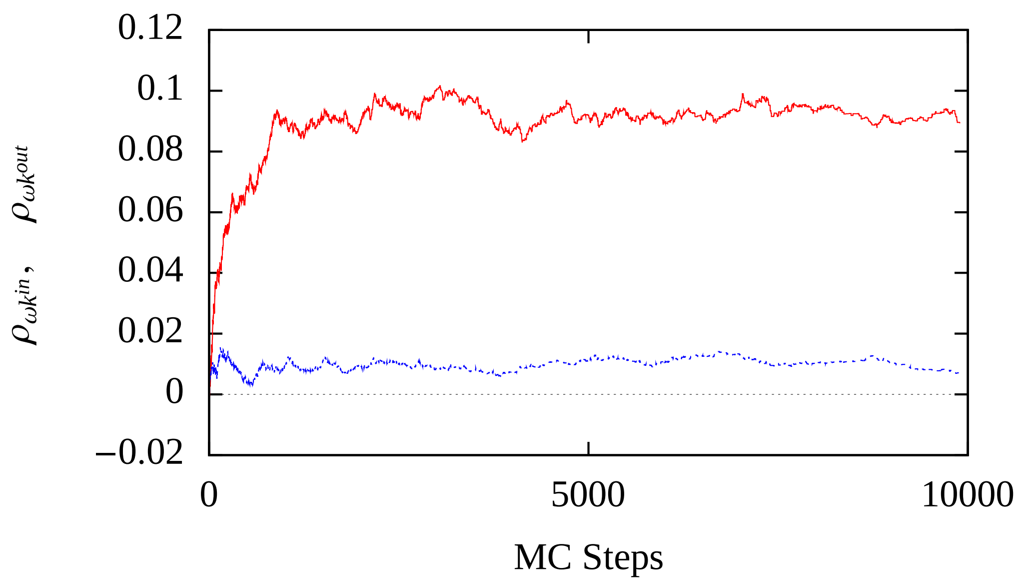

Figure 4.10: The correlation coefficients $\rho_{\omega k^{in}}$ (red line) and $\rho_{\omega k^{out}}$ (blue line) are plotted as a function of Monte Carlo steps. $\rho_{\omega k^{in}}$ increase from zero and saturates to a positive value, but $\rho_{\omega k^{out}}$ remains near th zero line.

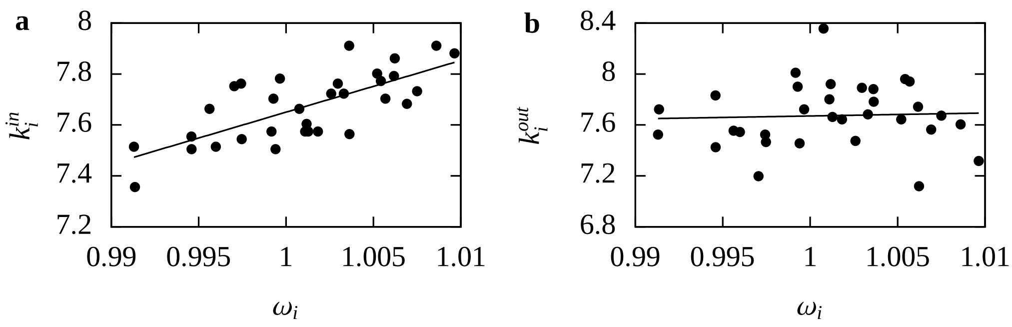

Figure 4.11: **a** The in-degree k^{in} is plotted as a function of node parameter ω. We can see that the nodes with larger value of parameter ω have more in-degree. **b** The out-degree k^{out} of a node is plotted with node parameter ω. Here, we can see there is no correlation between the node parameter and node out-degree.

This conclusion is further supported by Fig. 4.11. In Fig. 4.11a the in-degree k^{in} of the nodes is plotted as a function of parameter ω in the optimized network. The nodes with larger value of parameter ω have more in-degree. In Fig. 4.11b the out-degree k^{in} of the nodes is plotted as a function of parameter ω in the optimized network. In this case there is no correlation between out-degree and parameter value of a node.

4.5 Summary

In this chapter we have constructed a synchronized optimized network from any given network with fixed number of nodes and links. We rewire the links of a random network by deleting an existing link and creating a new link in a link vacancy. It has been observed in an undirected graph that the nodes with parameter values at one extreme ends are selected as hubs in the optimized network and the pair of nodes with larger parameter mismatch are selected to construct links in the optimized network. For directed graphs the we have seen that the systems with larger value of the parameter ω tends to have more incomining links. But we could not find any correlation between the out-degree of a node and its parameter value.

Chapter 5

Desynchronization bifurcation of coupled dynamical systems

5.1 Introduction

In this chapter we study the nature of desynchronization bifurcation in coupled nonlinear systems. In the earlier chapters we studied stability of synchronization of coupled dynamical systems. To determine stability of synchronized state we use the criteria that the largest transverse Lyapunov exponent (TLE) is negative. For a large number of chaotic oscillators it has been observed that the synchronized state is stable in an interval of the coupling strength ($\varepsilon_{c1} < \varepsilon < \varepsilon_{c2}$) [24, 119, 134, 135], where ε is the coupling strength. We consider a network of such coupled systems. As we increase the coupling strength ε, we observe establishment of synchronization between the coupled systems when coupling strength ε crosses the first critical coupling ε_{c1} and the largest TLE becomes negative. When the coupling strength is further increased the synchronized state remains stable for some time and as the couping strength increases beyond second critical value ε_{c2}, the synchronicity is lost, i.e. the systems undergo desynchronization bifurcation.

We consider a simple numerical experiment on two identical chaotic Rössler oscillators which are coupled in the first component. When the coupling strength ε is very small the Rössler systems will evolve with time in unsynchronized manner. When coupling strength, ε, is increased beyond the first critical coupling, ε_{c1}, the oscillators synchronize and remain synchronized for $\varepsilon_{c1} < \varepsilon < \varepsilon_{c2}$. In this range the largest transverse Lyapunov exponent (TLE) is negative. When the coupling strength exceeds the second critical value, ε_{c2}, the oscillators desynchronize. At this point the largest TLE becomes positive.

To understand the desynchronization bifurcation, we define system transverse Lyapunov exponents (STLE) which are specific to each system. In the synchronized state the STLE and TLE have the same values and all are negative. But in the desynchronized state one of the STLEs is positive and another is negative which implies that the perturbation grows about one system while it dies out about the other system, i.e. one system is trying to fly away while the other is holding it. We present a simple integrable general model of two coupled systems with quadratic nonlinearity which shows similar phenomena and the nature of this desynchronization can be explored in more details with the help of this model. This simple model shows that the desynchronization bifurcation is a pitchfork bifurcation of the transverse manifold and one STLE is positive while the other is negative after the desynchronization bifurcation. We also study the cubic nonlinearity which also shows a pitchfork bifurcation of the transverse manifold. However, in this case both the STLEs are negative in the desynchronized state. The quadratic nonlinearity gives the result corresponding to the desynchronization bifurcation in Rössler system.We find that for $\varepsilon > \varepsilon_{c2}$, the attractors of the two coupled systems split and start drifting away from each other and the rate of drift is proportional to $\sqrt{\varepsilon - \varepsilon_{c2}}$.

This chapter is organized as follows. In section 5.2.1 we study linear stability analysis of two n dimensional systems. In section 5.2.2 we define system transverse Lyapunov exponents and develop an algorithm to calculate STLE. In section 5.2.3 we present numerical results on Rössler oscillators. We propose a simple integrable model in section 5.3 which shows similar behavior to this desynchronization bifurcation.

5.2 Desynchronization bifurcation

We first consider the linear stability analysis of the synchronized state of two coupled dynamical systems. Next, we introduce system transverse Lyapunov exponents. Then, these are used to study the desynchronization bifurcation in the coupled Rössler systems. The condition for identical synchronization, or for simplicity synchronization, can be obtained by linear stability analysis. The phase space of the coupled system can be split into two manifolds, the synchronization manifold and the transverse manifold. The synchronization takes place when all the transverse Lyapunov exponents (TLEs) become negative [119, 134].

5.2.1 Linear stability analysis of synchronized state

Consider an n-dimensional autonomous dynamical system,

$$\dot{x} = f(x), \tag{5.1}$$

and couple this system with an identical dynamical system y,

$$\begin{aligned} \dot{x} &= f(x) + \varepsilon_1 \Gamma(y - x) \\ \dot{y} &= f(y) + \varepsilon_2 \Gamma(x - y) \end{aligned} \tag{5.2}$$

where, ε_1 and ε_2 are scalar coupling parameters. Γ is known as the diffusive coupling matrix. In general, $\Gamma = \mathrm{diag}(\gamma_0, \gamma_1, ..., \gamma_{n-1})$, and defines the components of x and y which are coupled. The synchronization manifold is defined by $x = y = s$, where s satisfies Eq. (5.1). Let, ξ_x and ξ_y be the deviations of x and y from the synchronized solution s. We have

$$\begin{aligned} \dot{\xi}_x &= \nabla f(s)\xi_x + \varepsilon_1 \Gamma(\xi_y - \xi_x) \\ \dot{\xi}_y &= \nabla f(s)\xi_y + \varepsilon_2 \Gamma(\xi_x - \xi_y) \end{aligned} \tag{5.3}$$

where, $\nabla f(s)$ is the Jacobian matrix at the synchronized solution. These two equations can be also be written as [118],

$$\dot{\xi} = \nabla f(s)\xi + \Gamma \xi G^T \tag{5.4}$$

where, $\xi = (\xi_x, \xi_y)$ and G is the coupling matrix. In this case

$$G = \left(\begin{smallmatrix} -\varepsilon_1 & \varepsilon_1 \\ \varepsilon_2 & -\varepsilon_2 \end{smallmatrix}\right).$$

Let, P_k be an eigenvector of G^T with eigenvalue μ_k; $G^T P_k = \mu_k P_k$. Operating Eq. (5.4) on μ_k and defining $\zeta_k = \xi P_k$ and we can write an equation for ζ_k as [118],

$$\dot{\zeta}_k = \left[\nabla f(s) + \mu_k \Gamma\right] \zeta_k. \tag{5.5}$$

Here, the matrix G has two eigenvalues $\mu_0 = 0$ and $\mu_1 = -(\varepsilon_1 + \varepsilon_2)$. Thus, Eq. (5.5) gives the two equations,

$$\dot{\zeta}_0 = \nabla f(s)\zeta_0 \tag{5.6}$$

$$\dot{\zeta}_1 = \left[\nabla f(s) - \mu_1 \Gamma\right] \zeta_1. \tag{5.7}$$

Here Eqs. (5.6) and (5.7) define motion of small perturbations on the synchronization and transverse manifolds respectively and these can be used to obtain the Lyapunov exponents for the two manifolds. The synchronized state will be stable when all the transverse perturbations die with time, i.e. when all the transverse Lyapunov exponents are negative.

5.2.2 System Transverse Lyapunov Exponents

We now introduce transverse Lyapunov exponents which are specific to the individual systems x and y.

The dynamics of the difference vector $z = x - y$, is

$$\dot{z} = f(x) - f(y) - (\varepsilon_1 + \varepsilon_2)\Gamma z \tag{5.8}$$

In Eq. (5.8) we can expand $f(y)$ in Taylor's series about the coordinate of the first system x or $f(x)$ about the second system y. This gives us the following two equations.

$$\dot{z} = (z \cdot \nabla) f(x) - (\varepsilon_1 + \varepsilon_2)\Gamma z \tag{5.9a}$$

$$\dot{z} = (z \cdot \nabla) f(y) - (\varepsilon_1 + \varepsilon_2)\Gamma z \tag{5.9b}$$

where we neglect the higher order terms. In the synchronized state, Eqs. (5.9a) and (5.9b) are identical and give the transverse Lyapunov exponents. In the desynchronized state, Eqs. (5.9a) and (5.9b) in general give different exponents and we refer to them as system transverse Lyapunov exponents (STLEs) since they are specific to each system and denote the largest of them as λ_x and λ_y respectively. For the synchronized state $\lambda_x = \lambda_y$ and they are negative. For the desynchronized state λ_x may not be equal to λ_y and tell us about how the difference vector z behaves in the neighborhood of the two systems. Note that for the synchronized state these STLEs belong to the actual spectrum of Lyapunov exponents of the coupled systems, but not for the desynchronized state.

We describe in short the method to calculate STLE from Eqs. (5.9a) and (5.9b). Eq. (5.9a) can be written in the matrix form as,

$$\dot{z} = D_x.z, \tag{5.10}$$

where, $D_x = \nabla_x f(x) + (\varepsilon_1 + \varepsilon_2)\Gamma$ is the Jacobian. When the system trajectories are constant (solutions are fixed points) then the stability analysis can be made by evaluating the eigenvalues (or the Floquet multipliers) of the matrix D_x [5, 76, 77]. We only need to calculate the largest transverse exponent λ_x which is the largest real part of the eigenvalues. Similar calculation can be done to obtain λ_y by replacing x by y in Eq. (5.10). When the system trajectories are periodic or chaotic then one has to take a time average of the eigenvalues to find the system transverse Lyapunov exponents. In this case, we use the algorithm of Ref. [75] for the numerical calculation of $\lambda_{x,y}$.

5.2.3 Two coupled Rössler systems

We now take the specific example of two coupled Rössler oscillators [117]. Denoting the variables of the two systems by x and y the coupled equations are,

$$\begin{aligned}\dot{x}_1 &= -x_2 - x_3 + \varepsilon(y_1 - x_1),\\ \dot{x}_2 &= x_1 + a_r x_2,\\ \dot{x}_3 &= b_r + x_3(x_1 - c_r),\end{aligned} \tag{5.11}$$

and a similar set of equations for the other system y given by,

$$\begin{aligned}\dot{y}_1 &= -y_2 - y_3 + \varepsilon(x_1 - y_1),\\ \dot{y}_2 &= y_1 + a_r y_2,\\ \dot{y}_3 &= b_r + y_3(y_1 - c_r).\end{aligned} \tag{5.12}$$

Here, we have coupled the first component, i.e. $\Gamma = \text{diag}(1, 0, 0)$ and we take symmetric coupling, $\varepsilon = \varepsilon_1 = \varepsilon_2$.

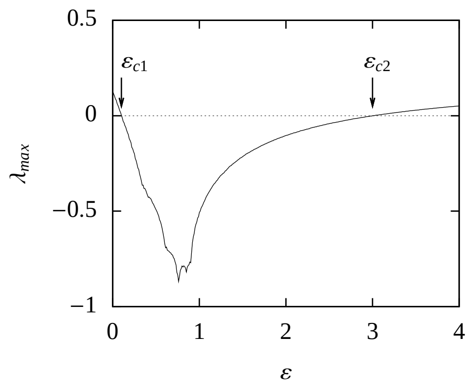

Figure 5.1: The largest transverse Lyapunov exponent, λ_{max}, of the two coupled chaotic identical Rössler oscillators is plotted with the coupling parameter ε. There are two critical couplings $\varepsilon_{c1}(\sim 0.1)$ and $\varepsilon_{c2}(\sim 3.0)$. In the range $\varepsilon_{c1} < \varepsilon < \varepsilon_{c2}$ the synchronized state is stable. The desynchronization bifurcation takes place when $\varepsilon = \varepsilon_{c2}$. The λ_{max} is calculated from Eq. 5.7. Rössler parameters are $a_r = 0.15$, $b_r = 0.2$ and $c_r = 10.0$. Note that for very large couplings the coupled system become unstable.

Fig. 5.1 shows the variation of the largest transverse Lyapunov exponent (λ_{max}) with coupling strength for two mutually coupled identical Rössler oscillators. As discussed in the introduction there are two critical coupling constants ε_{c1} and ε_{c2}. The synchronized state is stable when $\varepsilon_{c1} < \varepsilon < \varepsilon_{c2}$. At $\varepsilon = \varepsilon_{c2}$ the system undergoes a desynchronization bifurcation. As we see in Fig 5.1, λ_{max} is positive when $\varepsilon > \varepsilon_{c2}$, which implies that the synchronous state is unstable. To understand this phenomena in detail we calculate the system transverse Lyapunov exponents (λ_x and λ_y) introduced in the previous subsection using Eq. (5.10). The Jacobian D_x is given by

$$D_x = \begin{pmatrix} -2\varepsilon & -1 & -1 \\ 1 & a_r & 0 \\ x_3 & 0 & x_1 - c_r \end{pmatrix} \tag{5.13}$$

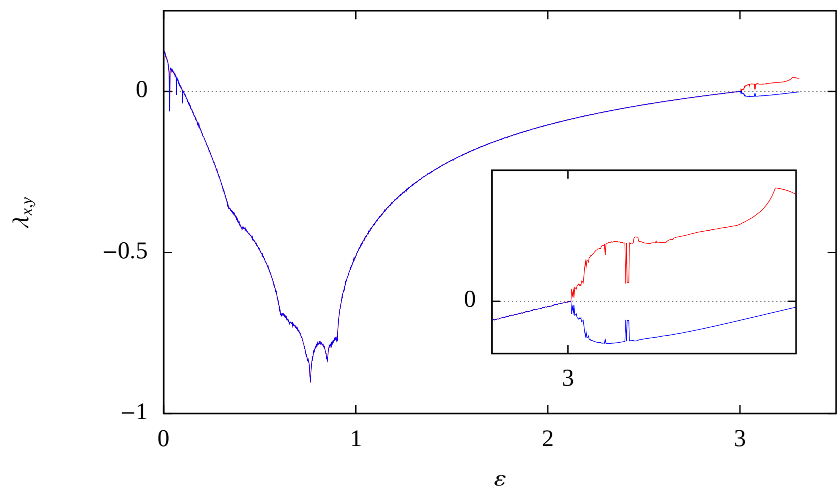

Figure 5.2: The largest system transverse Lyapunov exponents, $\lambda_{x,y}$, of the two coupled chaotic identical Rössler oscillators are plotted with the coupling parameter ε. The desynchronization bifurcation is observed for large coupling (here at $\varepsilon \sim 3$). The inset shows a blowup of λ_x and λ_y just after the desynchronization takes place. Rössler parameters are $a_r = 0.15$, $b_r = 0.2$ and $c_r = 10.0$.

In Fig. 5.2, the two largest system transverse Lyapunov exponents, λ_x and λ_y are plotted as a function of the coupling strength ε. As noted before, there are two critical coupling constants, ε_{c1} and ε_{c2}. At both the critical points $\lambda_x = \lambda_y = 0$. For $0 < \varepsilon < \varepsilon_{c1}$, the coupled oscillators are desynchronized. The attractors of the two systems overlap and are similar in nature. In this region, $\lambda_x \simeq \lambda_y$ and both are mostly positive. For, $\varepsilon_{c1} < \varepsilon < \varepsilon_{c2}$, the two Rössler oscillators are synchronized. Here, $\lambda_x = \lambda_y$ and both are negative. For $\varepsilon > \varepsilon_{c2}$, the oscillators become desynchronized. Here, the largest STLEs show an interesting behavior. One of STLEs becomes positive but the other becomes negative. Note that for very large values of ε the coupled system becomes unstable.

To understand the result that one STLE is positive and the other is negative, let us first look at the phase space plots of the attractors of the two coupled oscillators in Fig. 5.3a. The two attractors are identical and overlap at $\varepsilon = \varepsilon_{c2}$. As ε increases the two attractors split and start moving away from each other as shown in Fig. 5.3a. We also look at the frequency and the phase difference between the two oscillators after the desynchronization bifurcation. The frequency of both the oscillators does not change after the bifurcation. The phase difference remains constant, i.e. the two oscillators remain phase synchronized though they do not show complete synchronization.

Figure 5.3b shows the distance D, between the centers of the two attractors as a function of ε. For $\varepsilon > \varepsilon_{c2}$, the distance D shows a power law behavior,

$$D = \gamma(\varepsilon - \varepsilon_{c2})^{\nu}, \tag{5.14}$$

The fit is shown in Fig. 5.3b and the exponent is $\nu = 0.474 \pm 0.054 \sim 0.5$ and the other parameters are $\gamma = 67.38 \pm 15.75, \varepsilon_{c2} = 3.002 \pm 0.000004$. The power law behavior is a characteristic feature of a second order phase transition.

Let us now come back to the result of Fig. 5.2, that for $\varepsilon > \varepsilon_{c2}$ one of the STLE is positive and the other is negative. These STLEs tell us about the behavior of the distance between the attractors as viewed from each of them in the linear approximation. Thus, we can say that in the linear approximation one of the attractors is trying to fly away while the other one is trying to hold them together. The stability of the coupled system implies that the negative STLE wins the battle. It appears that as ε increases, the hold of the negative STLE decreases and hence the two attractors start drifting away from each other and for large values of ε the system becomes unstable.

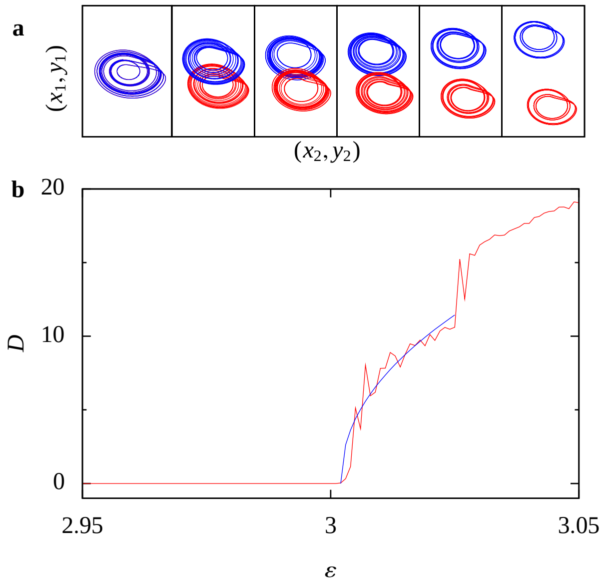

Figure 5.3: **a**. The projection of the attractors of the two Rössler oscillators (red and blue lines) on $(x_1 - x_2)$ and $(y_1 - y_2)$ planes respectively plotted on the same graph for $\varepsilon = 3.000, 3.025, 3.050, 3.100, 3.150, 3.200$. Note that Eqs. (5.11) obey the $x \Leftrightarrow y$ exchange symmetry and hence the attractor obtained by the exchange $x \Leftrightarrow y$, is also a solution. **b**. The distance D, between the centers of the attractors of the two Rössler oscillators is plotted as a function of the coupling strength ε. The continuous curve (blue) is a power law fit (Eq. (5.14)) with the exponent $\nu = 0.5$. Note that the distance D is also proportional to the distance between the two solutions obtained by the $x \Leftrightarrow y$ exchange symmetry.

5.3 Model system

Since Rössler oscillators are chaotic it is not easy to decipher the behavior of the desynchronization bifurcation. Hence, we now propose a simple model of coupled integrable systems showing a similar desynchronization bifurcation. For coupled one dimensional systems the synchronized state will become stronger when coupling strength is increased. We want the systems to desynchronize when coupling strength is increased above some critical value. It is only possible when there exists atleast one uncoupled component of the systems which will pull out the systems from synchronized state. This is not possible for a one dimensional system and hence the minimum dimension is two. The proposed model is

$$\begin{aligned}
\dot{x_1} &= ax_1 + bx_2 + \varepsilon(y_1 - x_1) \\
\dot{x_2} &= cx_1 + dx_2 + g(x_1, x_2) \\
\dot{y_1} &= ay_1 + by_2 + \varepsilon(x_1 - y_1) \\
\dot{y_2} &= cy_1 + dy_2 + g(y_1, y_2),
\end{aligned} \tag{5.15}$$

Here, $a, b, c, d, \alpha, \beta$ are the parameters of the systems and g is a nonlinear function of its arguments. As in the case of Rössler systems we couple the x_1 component. The model system is chosen so that the synchronized state corresponds to the fixed point $x^* = y^* = (0,0)$ for small values of ε and we observe a desynchronization transition as ε increases. For this to happen the parameters of the system must obey the conditions; $a + d < 0,\ d > 0,\ (ad - bc) > 0$. Under these conditions, the fixed point $(0,0)$ becomes unstable at the critical coupling constant $\varepsilon_c = \varepsilon_{c2} = \frac{1}{2}(a - \frac{bc}{d})$.

5.3.1 Quadratic nonlinearity

We first consider a general form of quadratic nonlinearity,

$$g(u_1, u_2) = \alpha(u_1^2 + \beta u_1 u_2 + u_2^2) \tag{5.16}$$

With quadratic nonlinearity, the model system has three fixed points. One is $(0,0,0,0)$ which is also a fixed point $(0,0)$ of the uncoupled systems. The other two fixed points are given by

$$\begin{aligned}
x_1^* &= \frac{A}{2} \pm \sqrt{B}, \\
x_2^* &= -\frac{a-\varepsilon}{b}x_1^* - \frac{\varepsilon}{b}y_1^*, \\
y_1^* &= A - x_1^*, \\
y_2^* &= -\frac{a-\varepsilon}{b}y_1^* - \frac{\varepsilon}{b}x_1^*
\end{aligned} \tag{5.17}$$

where $A = -\frac{b(2d\varepsilon - ad + bc)}{\alpha(b^2 - \beta b(a-\varepsilon) + a(a-2\varepsilon))}$, $B(\varepsilon) = \frac{A^2}{4} - \frac{\varepsilon^2 A^2}{W} - \frac{bd\varepsilon A}{\alpha W}$, $W = a^2 + b^2 + 4\varepsilon^2 - 4a\varepsilon - \beta b(a - 2\varepsilon)$.

For $\varepsilon < \varepsilon_c$, the fixed point $(0, 0)$ is stable and it becomes unstable at the critical coupling constant $\varepsilon_c = \varepsilon_{c2}$. For $\varepsilon > \varepsilon_c$ the coupled system has two stable fixed points given by Eqs. (5.17).

To determine the STLE of the synchronized state we use the transverse component $z = x - y$ and Eq. (5.10). The Jacobian matrix D_x is,

$$D_x = \begin{pmatrix} (a - 2\varepsilon) & b \\ (c + P_1) & (d + P_2) \end{pmatrix} \tag{5.18}$$

where, $P_1 = (2\alpha p_1^* + \alpha\beta p_2^*)$ and $P_2 = (\alpha\beta p_1^* + 2\alpha p_2^*)$, with $p_1^* = x_1^*, p_2^* = x_2^*$ for calculating STLE λ_x about system x and $p_1^* = y_1^*, p_2^* = y_2^*$ for calculating STLE λ_y about system y. In the desynchronized state, we use the stable fixed points (Eq. (5.17)) in Eq. (5.18) and we find that the largest STLEs by calculating the eigenvalue of D_x having largest real part. The STLEs are given by,

$$\lambda_{x,y} \approx \pm C\sqrt{\varepsilon - \varepsilon_c} + O(\varepsilon - \varepsilon_c), \tag{5.19}$$

where $C = \frac{\frac{2\alpha}{b}(a^2+b^2+4\varepsilon_c^2-4a\varepsilon_c+2\beta b\varepsilon_c-\beta ad)}{(a+d-2\varepsilon_c)+\frac{\alpha(2a-\beta b)}{2b}A+\frac{\alpha}{2}(\beta b-2a+4\varepsilon_c)\sqrt{B}}\sqrt{F}$,, $F = \frac{4b^2 d^4(ad-bc)}{\alpha^2 GH}$, $G = d(a^2 + b^2 - \beta ab) + (ad - bc)(\beta b - 2a)$ and $H = d^2(a^2 + b^2 - \beta ab) - (ad - bc)(ad + bc - 2\beta bd)$. Figure 5.4a shows the largest STLE $\lambda_{x,y}$ as a function of the coupling constant ε. For $\varepsilon < \varepsilon_c$, $\lambda_{x,y}$ are negative and equal. At $\varepsilon = \varepsilon_c$, they are zero and for $\varepsilon > \varepsilon_c$, one of the STLE is positive while the other is negative. This behavior of $\lambda_{x,y}$ is similar to that of the desynchronization transition in the coupled Rössler system seen in Fig. 5.2.

The distance between the attractors of the two systems, i.e. between (x_1^*, x_2^*) and (y_1^*, y_2^*), is given by,

$$D = \frac{\sqrt{(b^2 + (2\varepsilon_c - a)^2)F}}{b}\sqrt{\varepsilon - \varepsilon_c} + O(\varepsilon - \varepsilon_c) \tag{5.20}$$

Figure 5.4b plots the distance D as a function of the coupling constant ε. Thus, for $\varepsilon > \varepsilon_c$, $D \propto \sqrt{\varepsilon - \varepsilon_c}$.

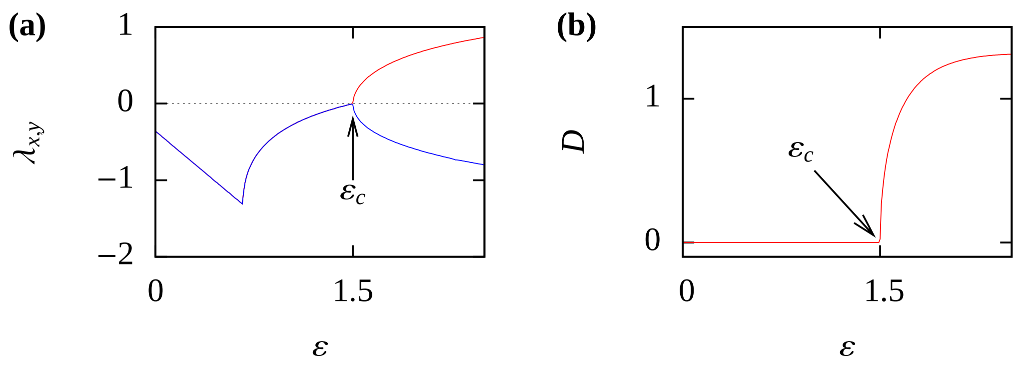

Figure 5.4: **(a)**. Two largest system transverse Lyapunov exponents, $\lambda_{x,y}$ of the model, Eq. (5.15) with quadratic nonlinearity, Eq. (5.16), are shown as a function of the coupling parameter ε. Other parameters are $a = -1.00, b = -2.00, c = 1.00, d = 0.50, \alpha = -1.00, \beta = 2.00$. **(b)**. The distance D between the fixed points of the two systems (Eq. (5.17)) as a function of the coupling constant ε.

At the desynchronization bifurcation in the model system the fixed point $(0, 0)$ becomes unstable and two new stable fixed points emerge. The distance between the stable fixed points grows proportional to $\sqrt{\varepsilon - \varepsilon_c}$. These are the characteristic features of the supercritical pitchfork bifurcation [82, 83]. This bifurcation takes place in the transverse manifold. This can be seen by noting that the three fixed points of the the model system, can also be obtained from the equation satisfied by the transverse component z_1^* as

$$z_1^*(B(\varepsilon) - (z_1^*)^2) = 0 \tag{5.21}$$

This is a cubic equation and $B(\varepsilon) \propto (\varepsilon - \varepsilon_c)$ with $B(\varepsilon_c) = 0$. This equation is exactly the normal form of a pitchfork bifurcation [82, 83]. Similar equation can be written for z_2^*.

The proposed model with quadratic nonlinearity shows supercritical pitchfork bifurcation when $\beta >= \frac{(ad-bc)(a^2+b^2)-2\varepsilon(a^2d-b^2d-2abc)}{a(ad-bc)+2bc\varepsilon}$. Otherwise it undergoes subcritical pitchfork bifurcation.

5.3.2 Cubic nonlinearity

We now consider cubic nonlinearity

$$g(u_1, u_2) = \alpha_1(u_1^3 + \beta_1 u_1^2 u_2 + \beta_2 u_1 u_2^2 + x_2^3) \tag{5.22}$$

In Fig. 5.5 the largest transverse Lyapunov exponent (λ_{max}) of this system is plotted with the coupling strength. As ε crosses the critical coupling strength (ε_c) the largest transverse Lyapunov exponent become positive and the synchronized state become unstable.

In Fig. 5.6 **(a)** we plot the two largest systems' transverse Lyapunov exponents (λ_x and λ_y) of the model system given by Eq. 5.15 with cubic nonlinearity as a function of the coupling strength ε. Here we can find that the exponents have same value for all coupling strengths and everywhere they are negative, except at the critical coupling strength, ε_c where both of them are zero.

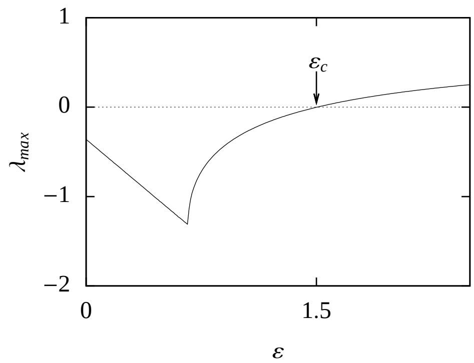

Figure 5.5: The largest transverse Lyapunov exponent, λ_{max} is plotted with the coupling strength ε for the model, Eq. (5.15) with cubic nonlinearity (Eq. 5.22). The critical coupling strength is $\varepsilon_c = 1.5$. When $\varepsilon > \varepsilon_c$ the λ_{max} is positive and synchronous state become unstable. The system parameters are $a = -1.00, b = -2.00, c = 1.00, d = 0.50, \alpha_1 = -1.00, \beta_1 = 3.00, \beta_2 = 3.00$.

In the desynchronized state one can calculate the stable solutions analytically for the cubic nonlinearity (Eqs. (5.15) and (5.22)). The fixed points are given by,

$$\begin{aligned} x_1^* &= \pm\frac{b\sqrt{2d(\varepsilon-\varepsilon_c)}}{\sqrt{F'}} \\ x_2^* &= -\frac{(a-2\varepsilon)}{b}x_1^* \\ y_1^* &= -x_1^* \\ y_2^* &= -x_2^*, \end{aligned} \tag{5.23}$$

where $\varepsilon_c = \frac{1}{2}(a-\frac{bc}{d})$ and $F' = \alpha_1\{(a-2\varepsilon)^3 - \beta_2 b(a-2\varepsilon)^2 + \beta_1 b^2(a-2\varepsilon) - b^3\}$. In the synchronized state the systems synchronize in the $(0,0)$ solution. When the coupling strength ε crosses the critical value ε_c the systems undergo desynchronizaion

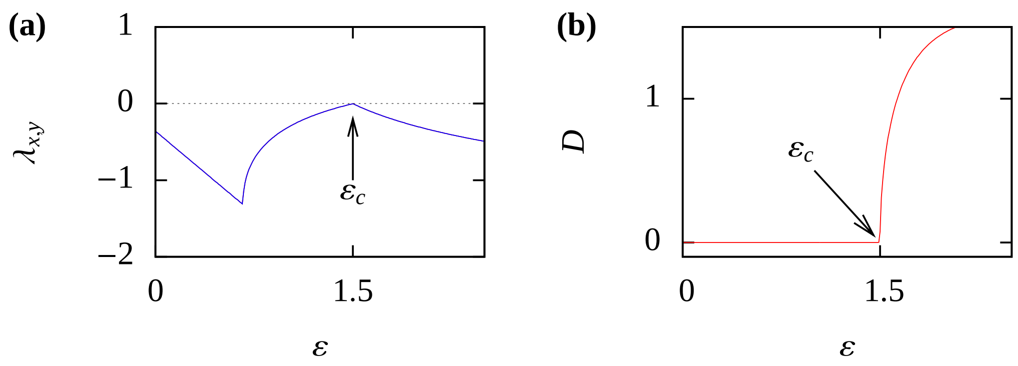

Figure 5.6: **(a)**. Two largest system transverse Lyapunov exponents, $\lambda_{x,y}$ of the model, Eq. (5.15) with cubic nonlinearity, Eq. (5.22), are shown as a function of the coupling parameter ε. Other parameters are $a = -1.00, b = -2.00, c = 1.00, d = 0.50, \alpha_1 = -1.00, \beta_1 = 3.00, \beta_2 = 3.00$. **(b)**. The distance D between the fixed points of the two systems for cubic nonlinearity as a function of the coupling constant ε.

bifurcation as depicted in Fig. 5.5, but all STLEs are negative (Fig. 5.6**(a)**). So, the individual systems are stable. The distance between the two fixed points is proportional to $\sqrt{\varepsilon - \varepsilon_c}$ and is shown in Fig. 5.6b.

We can calculate the STLEs for cubic nonlinearity by considering the transverse component $z = x - y$, The STLEs of this coupled systems are calculated by considering the transverse component $z = x - y$ and for this model the Jacobian matrix of Eq. (5.10) is,

$$D_x = \begin{pmatrix} (a-2\varepsilon) & b \\ (c+3\alpha(p_1^*)^2) & (d+3\alpha(p_2^*)^2) \end{pmatrix} \tag{5.24}$$

From Eq. (5.24) we calculate the STLE λ_x about system x by replacing $p_1^* = x_1^*, p_2^* = x_2*$ and determining the eigenvalue of D_x with largest real part. Similarly we find λ_y.

The STLEs are give by,

$$\lambda_{x,y} \approx \frac{2F'd\{F' - (a-2\varepsilon)G' - bH'\}}{\{(a+d-2\varepsilon)F' + (\varepsilon - \varepsilon_c)G'\}}(\varepsilon - \varepsilon_c) + \text{higher order} \tag{5.25}$$

where, $G' = 3(a-2\varepsilon)^2 + \beta_1 b^2 - 2\beta_2 b(a-2\varepsilon)$ and
$H' = 3b^2 + \beta_2(a-2\varepsilon)^2 - 2\beta_1 b(a-2\varepsilon)$. The STLEs for cubic nonlinearity (5.22) have linear dependence on the parameter after the desynchronization bifurcation

takes place and both are negative.

5.3.3 Comparison with coupled Rössler systems

We now compare the results for the model system with that of two coupled Rössler systems. Comparing Figures 5.3b, 5.4b and 5.6b, we see that for both the model and the coupled Rössler systems, for $\varepsilon > \varepsilon_c$, $D \propto \sqrt{\varepsilon - \varepsilon_c}$.We note that D may be taken as the distance between the attractors of the two systems or the distance between the two solutions obtained by the $x \rightleftarrows y$ exchange symmetry. For the coupled Rössler systems these solutions are chaotic while for the model system they are fixed points. The nature of these solutions depends on the synchronization manifold. However, the desynchronization bifurcation takes place in the transverse manifold were both the coupled Rössler systems and our model show a very similar behavior.

For the coupled Rössler systems we can carry out an approximate analysis. We write equations for the difference and sum of the variables of the two systems, $z = u^{(1)} - u^{(2)}$ and $s = u^{(1)} + u^{(2)}$, and then treat z and s as constants near the desynchronization bifurcation. This gives a cubic equation for the transverse components as $z_2(\mathcal{B} - z_2^2)$ where $\mathcal{B}$ depends on the parameters. The condition $\mathcal{B} = 0$ gives $\varepsilon_{c2} \sim 3.33\ldots$ which is somewhat larger than the observed value of 3.002 of the desynchronization bifurcation.

Thus both the transitions in the coupled Rössler systems and our model can be identified as supercritical pitch-fork bifurcations of the transverse manifold.

The nature of the nonlinearity can be identified using STLEs defined by us. Comparing the behavior of STLEs for $\varepsilon > \varepsilon_c$ in Figs. 5.2, 5.4a and 5.6a, we see that the behavior of STLEs for the coupled Rössler systems matches with that of our model with quadratic nonlinearity, but not with the cubic nonlinearity.

We find that the form used in Eq. (5.15) with quadratic (Eq. (5.16)) or cubic (Eq. (5.22)) nonlinearity, is the simplest form we could get for the desynchronization bifurcation of the transverse manifold. The model also gives the standard normal form (Eq. (5.21)), of the pitchfork bifurcation for the transverse component. We note that the coupled Rössler systems and the model with quadratic nonlinearity have similar properties. Hence, we can say that our model of Eq. (5.15) with quadratic nonlinearity (Eq.(5.16)) is the simplest model for the desynchronization bifurcation of the coupled Rössler systems.

5.4 Discussion

From the discussion above, we conclude that the desynchronization bifurcation of the coupled model system, Eq. (5.15) as well as the coupled Rössler systems, Eq. (5.11), are supercritical pitchfork bifurcations of the transverse manifold. The synchronization manifold decides the nature of the attractor which is chaotic for the coupled Rössler systems while it is periodic (fixed points) for our model system.

We have presented the analysis for symmetric coupling with $\varepsilon = \varepsilon_1 = \varepsilon_2$. If instead we take asymmetric coupling $\varepsilon_1 \neq \varepsilon_2$, the nature of the desynchronization bifurcation does not change. This is because this bifurcation takes place in the transverse manifold defined by the difference vector z and in the equation for z, (Eq. (5.8)), we only have the sum $\varepsilon_1 + \varepsilon_2$. We also note that for $\varepsilon_1 \neq \varepsilon_2$, the $x \Leftrightarrow y$ exchange symmetry exists in the transverse component though not in the longitudinal component.

We find that the form used in Eq. (5.15) to be the simplest form we could get for the desynchronization bifurcation and also, we get the standard normal form (Eq. (5.21)), of the pitchfork bifurcation for the transverse component. The model is a simple form for the desynchronization bifurcation. We can further simplify the model by choosing $a = -1$, $c = 1$, $\alpha = \pm 1$. We note that the coupled Rössler systems and the model have similar properties. Hence, Eq. (5.15) with the quadratic nonlinearity (Eq.(5.16)) is a simple model for the desynchronization bifurcation of the coupled Rössler systems.

We can covert our model of Eq. (5.15) to a normal form by making a transformation to the central manifold [53]. This involves transforming to the coordinates of the eigenspace so that the linear terms are diagonal. This systematic transformation and reduction will lead to the normal form of the bifurcation. However, after this transformation the simple picture of a system of two coupled dynamical systems showing desynchronization bifurcation is lost. Hence, we do not make this transformation and retain our model equations in the present form.

Let us now consider the coupled Rössler systems on a network. Consider n coupled Rössler oscillators. Denoting the variables by $u^{(j)}$, $j = 1, 2, \ldots, N$, the equations can be written as

$$\dot{u}^{(j)} = f(u^{(j)}) + \varepsilon \sum_k J_{jk} \Gamma(u^{(k)} - u^{(j)}), \tag{5.26}$$

where J is the coupling matrix. The analysis of Pecora and Carrol [24] shows that the equations for the transverse manifold can be cast into a general form of a master equation and is the same as that for the two coupled systems. Thus, the present analysis should be applicable for the desynchronization transition for coupled systems on a network. How do the attractors of the different systems split for $\varepsilon > \varepsilon_{c2}$? Consider three mutually coupled Rössler systems. We observe an interesting phenomena of symmetry breaking. In this case at the desynchronization bifurcation we still get splitting of the attractors into two as in Fig. 5.3a, with two oscillators on one side and the remaining oscillator on the other side. The two oscillators on the same side remain synchronized We find that the distance between the center of these oscillators varies with the coupling in the same fashion as in Eq. (5.14). When four oscillators are coupled in a rectangle then this desynchronization bifurcation takes place between two pairs of oscillators. The oscillators in the same pair remain synchronized.

5.5 Summary

To conclude, we have analyzed the desynchronization bifurcation in the coupled Rössler systems. We give a simple model of coupled integrable systems which shows similar phenomena. The model may be treated as the simplest form showing the desynchronization bifurcation in coupled systems. After the desynchronization bifurcation the attractors of the coupled systems split into two and start moving away from each other. We define system transverse Lyapunov exponents corresponding to the difference vector of the variables of the systems. For $\varepsilon > \varepsilon_c$ and quadratic nonlinearity, the STLE for one system becomes positive while that for the other system becomes negative. While for $\varepsilon > \varepsilon_c$ and cubic nonlinearity, the STLEs of both systems are negative. From the analysis of the distance between the two attractors which is proportional to $\sqrt{\varepsilon - \varepsilon_c}$, the behavior of STLEs and the cubic form for the transverse components, we conclude that the desynchronization bifurcation in the coupled Rössler systems is a pitchfork bifurcation of the transverse manifold and is represented by our model with quadratic nonlinearity.

Chapter 6

Summary

In conclusion, this thesis addresses two different problems. First we extend the concept of master stability function to determine synchronization of coupled nonidentical systems. For coupled nonidentical systems, one will have generalized type of synchronization. In practical life it is impossible to imagine a network of completely identical systems. So, it is very relevant to formulate a master stability function to analyze generalized synchronization for coupled nonidentical systems. By considering the fact that the exponential nature of solution of a linear differential equation is determined by the homogeneous part we formulate master stability function for coupled nonidentical systems and this master stability function can predict the stability of synchronization reasonably well.

Next, we consider the problem of constructing synchronized optimized network from a given network which has fixed number of nodes and links. To understand the structure of the optimized network we search for the nodes that are preferable as hubs and links that are more preferable in the optimized network. For undirected network the nodes whose parameter values lies at one of the extreme ends are getting more connections and preferred as hubs and the pair of nodes which have larger parameter mismatch are selected to create links. In a directed network we observe that the nodes with extreme parameter values are prone to having more incoming links than other nodes.

In the second problem we study the nature of desynchronization bifurcation of coupled nonlinear dynamical systems. In this context we introduce Systems'

Transverse Lyapunov Exponents (STLEs) to study stability of individual systems on a network. We give a simple model of coupled integrable systems which shows similar phenomena. After the desynchronization bifurcation the attractors of the coupled systems split into two and start moving away from each other. In the desynchronized state the STLE of one system is positive and another system is negative indicating that one systems is trying to fly away from the synchronized state while the other is trying to hold the synchronized state. Also we observe that the distance between the attractors has a square root dependence on the parameter value. This desynchronization bifurcation is a pitchfork bifurcation of the transverse manifold and it can be represented by the proposed simple model.

Bibliography

[1] C. Huygens. Horologium oscillatorium. *Apud F. Muguet*, 1673.

[2] J. Buck and E. Buck. Mechanism of rhythmic synchronous flashing of fireflies. *Science*, 159:1319, 1968.

[3] S. Strogatz. *Sync: The Emerging Science of Spontaneous Order*. Penguin Books, Limited (UK), 2008.

[4] A. Pikovsky, M. Rosenblum, and J. Kurths. *Synchronization: a universal concept in nonlinear sciences*. Cambridge University Press, 2001.

[5] S. Boccaletti, J. Kurths, G. Osipov, D.L. Valladares, and C.S. Zhou. The synchronization of chaotic systems. *Physics Reports*, 366(1-2):1 – 101, 2002.

[6] Hirokazu Fujisaka and Tomoji Yamada. Stability theory of synchronized motion in coupled-oscillator systems. *Progress of Theoretical Physics*, 69(1):32–47, 1983.

[7] Tomoji Yamada and Hirokazu Fujisaka. Stability theory of synchronized motion in coupled-oscillator systems. ii. *Progress of Theoretical Physics*, 70(5):1240–1248, 1983.

[8] V. S. Afraimovich, N. N. Verichev, and M. I. Rabinovich. Stochastic synchronization of oscillations in dissipative systems. *Izvestiya Vysshikh Uchebnykh Zavedenii Radiofizika*, 29:795, 1986.

[9] Louis M. Pecora and Thomas L. Carroll. Synchronization in chaotic systems. *Phys. Rev. Lett.*, 64(8):821–824, 1990.

[10] J. F. Heagy, T. L. Carroll, and L. M. Pecora. Synchronous chaos in coupled oscillator systems. *Phys. Rev. E*, 50(3):1874–1885, 1994.

[11] Louis M. Pecora, Thomas L. Carroll, Gregg A. Johnson, Douglas J. Mar, and James F. Heagy. Fundamentals of synchronization in chaotic systems, concepts, and applications. *Chaos*, 7(4):520–543, 1997.

[12] R. E. Amritkar and Neelima Gupte. Synchronization of chaotic orbits: The effect of a finite time step. *Phys. Rev. E*, 47:3889–3895, 1993.

[13] Neelima Gupte and R. E. Amritkar. Synchronization of chaotic orbits: The influence of unstable periodic orbits. *Phys. Rev. E*, 48:R1620–R1623, 1993.

[14] Sarika Jalan and R. E. Amritkar. Self-organized and driven phase synchronization in coupled maps. *Phys. Rev. Lett.*, 90:014101, 2003.

[15] Sarika Jalan, R. E. Amritkar, and Chin-Kun Hu. Synchronized clusters in coupled map networks. i. numerical studies. *Phys. Rev. E*, 72:016211, 2005.

[16] R. E. Amritkar, Sarika Jalan, and Chin-Kun Hu. Synchronized clusters in coupled map networks. ii. stability analysis. *Phys. Rev. E*, 72:016212, 2005.

[17] A. R. Volkovskii and N. F. Rul'kov. Experimental study of bifurcations on the threshold for stochastic locking. *Sov. Tech. Phys. Lett.*, 15:249, 1989.

[18] Michael G. Rosenblum, Arkady S. Pikovsky, and Jürgen Kurths. Phase synchronization of chaotic oscillators. *Phys. Rev. Lett.*, 76(11):1804–1807, 1996.

[19] Epaminondas Rosa, Edward Ott, and Mark H. Hess. Transition to phase synchronization of chaos. *Phys. Rev. Lett.*, 80(8):1642–1645, 1998.

[20] Michael G. Rosenblum, Arkady S. Pikovsky, and Jürgen Kurths. From phase to lag synchronization in coupled chaotic oscillators. *Phys. Rev. Lett.*, 78(22):4193–4196, 1997.

[21] Nikolai F. Rulkov, Mikhail M. Sushchik, Lev S. Tsimring, and Henry D. I. Abarbanel. Generalized synchronization of chaos in directionally coupled chaotic systems. *Phys. Rev. E*, 51(2):980–994, 1995.

[22] Henry D. I. Abarbanel, Nikolai F. Rulkov, and Mikhail M. Sushchik. Generalized synchronization of chaos: The auxiliary system approach. *Phys. Rev. E*, 53:4528–4535, 1996.

[23] L. Kocarev and U. Parlitz. Generalized synchronization, predictability, and equivalence of unidirectionally coupled dynamical systems. *Phys. Rev. Lett.*, 76(11):1816–1819, 1996.

[24] Louis M. Pecora and Thomas L. Carroll. Master stability functions for synchronized coupled systems. *Phys. Rev. Lett.*, 80(10):2109–2112, 1998.

[25] DC Michaels, EP Matyas, and J Jalife. Dynamic interactions and mutual synchronization of sinoatrial node pacemaker cells. a mathematical model. *Circulation Research*, 58(5):706–720, 1986.

[26] C. S. Peskin. *Mathematical Aspects of Heart Physiology.* Courant Institute of Mathematical Science Publication, New York, 1975.

[27] Carsten Schafer, Michael G. Rosenblum, Jurgen Kurths, and Hans-Henning Abel. Heartbeat synchronized with ventilation. *Nature*, 392:239, 1998.

[28] P. A. Robinson, J. J. Wright, and C. J. Rennie. Synchronous oscillations in the cerebral cortex. *Phys. Rev. E*, 57:4578–4588, 1998.

[29] Jane H. Sheeba, V. K. Chandrasekar, and M. Lakshmanan. Event-related desynchronization in diffusively coupled oscillator models. *Phys. Rev. Lett.*, 103:074101, 2009.

[30] Bethany Percha, Rhonda Dzakpasu, Michał Żochowski, and Jack Parent. Transition from local to global phase synchrony in small world neural network and its possible implications for epilepsy. *Phys. Rev. E*, 72:031909, 2005.

[31] B. Blasius, A. Huppert, and L. Stone. Complex dynamics and phase synchronization in spatially extended ecological systems. *Nature*, 399:354, 1999.

[32] L. Glass. Synchronization and rhythmic processes in physiology. *Nature*, 410:277, 2001.

[33] J. Aldridge and E. K. Pye. Cell density dependence of oscillatory metabolism. *Nature*, 259:670–671, 1976.

[34] M. A. Aon, S. Cortassa, H. V. Westerhoff, and K. V. Dam. Synchrony and mutual stimulation of yeast cells during fast glycolytic oscillations. *Journal of General Microbiology*, 138(10):2219–2227, 1992.

[35] T. J. Walker. Acoustic synchrony: Two mechanisms in the snowy tree cricket. *Science*, 166:891–894, 1969.

[36] Louis M. Pecora and Thomas L. Carroll. Driving systems with chaotic signals. *Phys. Rev. A*, 44(4):2374–2383, 1991.

[37] Kevin M. Cuomo and Alan V. Oppenheim. Circuit implementation of synchronized chaos with applications to communications. *Phys. Rev. Lett.*, 71:65–68, 1993.

[38] D. V. Senthilkumar, K. Srinivasan, K. Murali, M. Lakshmanan, and J. Kurths. Experimental confirmation of chaotic phase synchronization in coupled time-delayed electronic circuits. *Phys. Rev. E*, 82:065201, 2010.

[39] Rajarshi Roy and K. Scott Thornburg. Experimental synchronization of chaotic lasers. *Phys. Rev. Lett.*, 72:2009–2012, 1994.

[40] Toshiki Sugawara, Maki Tachikawa, Takayuki Tsukamoto, and Tadao Shimizu. Observation of synchronization in laser chaos. *Phys. Rev. Lett.*, 72:3502–3505, 1994.

[41] Kenju Otsuka, Ryoji Kawai, Siao-Lung Hwong, Jing-Yuan Ko, and Jyh-Long Chern. Synchronization of mutually coupled self-mixing modulated lasers. *Phys. Rev. Lett.*, 84:3049–3052, 2000.

[42] Michael A. Zaks, Eun-Hyoung Park, Michael G. Rosenblum, and Jürgen Kurths. Alternating locking ratios in imperfect phase synchronization. *Phys. Rev. Lett.*, 82:4228–4231, 1999.

[43] L. Kocarev and U. Parlitz. General approach for chaotic synchronization with applications to communication. *Phys. Rev. Lett.*, 74:5028–5031, 1995.

[44] U. Parlitz, L. Junge, and L. Kocarev. Synchronization-based parameter estimation from time series. *Phys. Rev. E*, 54:6253–6259, 1996.

[45] Anil Maybhate and R. E. Amritkar. Use of synchronization and adaptive control in parameter estimation from a time series. *Phys. Rev. E*, 59:284–293, 1999.

[46] S. Boccaletti and D. L. Valladares. Characterization of intermittent lag synchronization. *Phys. Rev. E*, 62:7497–7500, 2000.

[47] Ricardo Femat and Gualberto Sols-Perales. On the chaos synchronization phenomena. *Physics Letters A*, 262(1):50 – 60, 1999.

[48] Robert C. Hilborn. *Chaos and Nonlinear Dynamics*. Oxford University Press, 1994.

[49] M. Lakshmanan and S. Rajasekar. *Nonlinear Dynamics*. Springer, 2003.

[50] E. Ott. *Chaos in Dynamical Systems*. Cambridge University Press, 1993.

[51] K. T. Alligood, T. D. Sauer, and J. A. Yorke. *Chaos: An Introduction to Dynamical Systems*. Springer, 1996.

[52] R. L. Devaney. *An Introduction to Chaotic Dynamical Systems*. Westview Press, 2003,.

[53] John Guckenheimer and Philip Holmes. *Nonlinear Oscillations, Dynamical Systems, and Bifurcations of Vector Fields*. Springer-Verlag, 1983.

[54] Allan J. Lichtenberg and Michael A. Lieberman. *Regular and chaotic dynamics*. Springer, 1991.

[55] Paul S. Linsay. Period doubling and chaotic behavior in a driven anharmonic oscillator. *Phys. Rev. Lett.*, 47:1349–1352, 1981.

[56] R. W. Rollins and E. R. Hunt. Intermittent transient chaos at interior crises in the diode resonator. *Phys. Rev. A*, 29:3327–3334, 1984.

[57] F. T. Arecchi, R. Meucci, G. Puccioni, and J. Tredicce. Experimental evidence of subharmonic bifurcations, multistability, and turbulence in a q-switched gas laser. *Phys. Rev. Lett.*, 49:1217–1220, 1982.

[58] J. Mørk, J. Mark, and B. Tromborg. Route to chaos and competition between relaxation oscillations for a semiconductor laser with optical feedback. *Phys. Rev. Lett.*, 65:1999–2002, 1990.

[59] Xiaodong Chen and P.A. Lindsay. Oscillations and chaos in plasma-filled diodes. *IEEE Transactions on Plasma Science*, 24:1005 – 1014, 1996.

[60] J. P. Gollub and S. V. Benson. Many routes to turbulent convection. *J . Fluid Mech.*, 100:449–470, 1980.

[61] A. Brandstater and Harry L. Swinney. Strange attractors in weakly turbulent couette-taylor flow. *Phys. Rev. A*, 35:2207–2220, 1987.

[62] Kirill N. Alekseev, Gennady P. Berman, David K. Campbell, Ethan H. Cannon, and Matthew C. Cargo. Dissipative chaos in semiconductor superlattices. *Phys. Rev. B*, 54:10625–10636, 1996.

[63] S. W. Teitsworth, R. M. Westervelt, and E. E. Haller. Nonlinear oscillations and chaos in electrical breakdown in ge. *Phys. Rev. Lett.*, 51:825–828, 1983.

[64] Guanrong Chen and Xing Huo Yu. *Chaos control: theory and applications.* Springer, 2003.

[65] Jan Awrejcewicz and Claude-Henri Lamarque. *Bifurcation and chaos in nonsmooth mechanical systems.* World Scientific, 2003.

[66] Richard J. Field and László Györgyi, editors. *Chaos in chemistry and biochemistry.* world Scientific, 1993.

[67] Benno Hess. Order and chaos in chemistry and biology. *Fresenius' Journal of Analytical Chemistry*, 337:459–468, 1990.

[68] Werner Lauterborn and Eckehart Cramer. Subharmonic route to chaos observed in acoustics. *Phys. Rev. Lett.*, 47:1445–1448, 1981.

[69] N. Fletcher, R. Perrin, and K. Legge. Nonlinearity and chaos in acoustics. *Acoustics Australia*, 18:1–9, 1990.

[70] Jürgen Moser. *Stable And Random Motions In Dynamical Systems: With Special Emphasis On Celestial Mechanics.* Princeton University Press, 2001.

[71] Edward N. Lorenz. *The Essence of Chaos.* University of Washington Press, Seattle, 1995.

[72] J. P. Eckmann and D. Ruelle. Ergodic theory of chaos and strange attractors. *Rev. Mod. Phys.*, 57:617–656, 1985.

[73] Ippei Shimada and Tomomasa Nagashima. A numerical approach to ergodic problem of dissipative dynamical systems. *Progress of Theoretical Physics*, 61(6):1605–1616, 1979.

[74] G. Benettin, L. Galgani, A. Giorgilli, and J.-M. Strelcyn. Lyapunov characteristic exponents for smooth dynamical systems and for hamiltonian systems; a method for computing all of them. *Meccanica*, 15:9–20, 1980.

[75] Alan Wolf, Jack B. Swift, Harry L. Swinney, and John A. Vastano. Determining lyapunov exponents from a time series. *Physica D: Nonlinear Phenomena*, 16(3):285 – 317, 1985.

[76] F. Verhulst. *Nonlinear differential equations and dynamical systems.* Springer, 1985.

[77] Lei Yu, Edward Ott, and Qi Chen. Transition to chaos for random dynamical systems. *Phys. Rev. Lett.*, 65:2935–2938, 1990.

[78] D. V. Anosov. Geodesic flows on a compact riemann manifold of negative geodesic curvature. *Proc. Steklov Inst. Math*, 90:1, 1967.

[79] R. Bowen. Markov partitions for axiom a diffeomorphisms. *Amer. J. Math.*, 92:725, 1970.

[80] Celso Grebogi, Stephen M. Hammel, James A. Yorke, and Tim Sauer. Shadowing of physical trajectories in chaotic dynamics: Containment and refinement. *Phys. Rev. Lett.*, 65:1527–1530, 1990.

[81] Stephen M Hammel, James A Yorke, and Celso Grebogi. Do numerical orbits of chaotic dynamical processes represent true orbits? *Journal of Complexity*, 3(2):136 – 145, 1987.

[82] John David Crawford. Introduction to bifurcation theory. *Rev. Mod. Phys.*, 63:991–1037, 1991.

[83] Gerard Iooss and Daniel D. Joseph. *Elementary Stability and Bifurcation Theory*. Springer-Verlag, 1980.

[84] Réka Albert and Albert-László Barabási. Statistical mechanics of complex networks. *Rev. Mod. Phys.*, 74:47–97, 2002.

[85] S. Boccaletti, V. Latora, Y. Moreno, M. Chavez, and D.-U. Hwang. Complex networks: Structure and dynamics. *Physics Reports*, 424(4-5):175 – 308, 2006.

[86] M. E. J. Newman. *Networks: An Introduction*. Oxford University Press, 2010.

[87] H. Jeong, H. Jeong, B. Tombor, R. Albert, Z. N. Oltvai, and A.-L. Barabasi. The large-scale organization of metabolic networks. *Nature*, 407:651–654, 2000.

[88] Reka Albert, Hawoong Jeong, and Albert-Laszlo Barabasi. Internet: Diameter of the world-wide web. *Nature*, 401:130–131, 1999.

[89] Steve Lawrence and C. Lee Giles. Searching the world wide web. *Science*, 280(5360):98–100, 1998.

[90] Ramon Ferrer i Cancho, Christiaan Janssen, and Ricard V. Solé. Topology of technology graphs: Small world patterns in electronic circuits. *Phys. Rev. E*, 64:046119, 2001.

[91] Richard J. Williams and Neo D. Martinez. Simple rules yield complex food webs. *nature*, 404:180–183, 2000.

[92] Christof Koch and Gilles Laurent. Complexity and the nervous system. *Science*, 284(5411):96–98, 1999.

[93] Adilson E. Motter and Ying-Cheng Lai. Cascade-based attacks on complex networks. *Phys. Rev. E*, 66:065102, 2002.

[94] Réka Albert, István Albert, and Gary L. Nakarado. Structural vulnerability of the north american power grid. *Phys. Rev. E*, 69:025103, 2004.

[95] Thomas A. Vilgis and Gert Heinrich. Dynamics of heterogeneous polymer networks. *Phys. Rev. E*, 49:2167–2174, 1994.

[96] M. E. J. Newman. Scientific collaboration networks. i. network construction and fundamental results. *Phys. Rev. E*, 64:016131, 2001.

[97] S. Redner. How popular is your paper? an empirical study of the citation distribution. *Eur. Phys. J. B*, 4(2):131–134, 1998.

[98] Stanley Wasserman and Katherine Faust. *Social network analysis: methods and applications*. Cambridge University Press, 1994.

[99] Bruno Latour. *Reassembling the Social: An Introduction to Actor-Network-Theory*. Oxford University Press, 2005.

[100] Romualdo Pastor-Satorras and Alessandro Vespignani. Epidemic spreading in scale-free networks. *Phys. Rev. Lett.*, 86:3200–3203, 2001.

[101] Parongama Sen, Subinay Dasgupta, Arnab Chatterjee, P. A. Sreeram, G. Mukherjee, and S. S. Manna. Small-world properties of the indian railway network. *Phys. Rev. E*, 67:036106, 2003.

[102] Andrea DAriano, Dario Pacciarelli, and Marco Pranzo. A branch and bound algorithm for scheduling trains in a railway network. *European Journal of Operational Research*, 183(2):643 – 657, 2007.

[103] W. Li and X. Cai. Statistical analysis of airport network of china. *Phys. Rev. E*, 69:046106, 2004.

[104] B. Bollobás. *Random Graphs*. Cambridge University Press, 2001.

[105] D. J. Watts and S. H. Strogatz. Collective dynamics of 'small-world' networks. *Nature*, 393:440, 1998.

[106] R. Pastor-Satorras and A. Vespignani. *Evolution and Structure of the Internet: A Statistical Physics Approach.* Cambridge University Press, 2004.

[107] D.B. West. *Introduction to Graph Theory.* Prentice-Hall, 1995.

[108] Wai-Kai Chen. *Graph Theory and its Engineering Applications.* World Scientific, 1997.

[109] David Gries and Fred B. Schneider. *A Logical Approach to Discrete Math.* Springer-Verlag, 1993.

[110] P. Erdös and A Rényi. On random graphs. *Publicationes Mathematicae*, 6:290–297, 1959.

[111] P. Erdös and A Rényi. On the evolution of random graphs. *Magyar Tud. Akad. Mat. Kutató Int. Közl.*, 5:17–61, 1960.

[112] Duncan J. Watts. *Small worlds: the dynamics of networks between order and randomness.* Princeton University Press, 1999.

[113] Albert-László Barabasi and Réka Albert. Emergence of scaling in random networks. *Science*, 286:509, 1999.

[114] R. Albert, H. Jeong, and A.-L. Barabäsi. Error and attack tolerance of complex networks. *Nature*, 406:378–382, 1999.

[115] Albert-Lszl Barabsi, Rka Albert, and Hawoong Jeong. Mean-field theory for scale-free random networks. *Physica A: Statistical Mechanics and its Applications*, 272(1-2):173 – 187, 1999.

[116] Edward N. Lorenz. Deterministic nonperiodic flow. *J. Atmos. Sci.*, 20:130, 1963.

[117] O. E. Rössler. An equation for continuous chaos. *Physics Letters A*, 57(5):397 – 398, 1976.

[118] Govindan Rangarajan and Mingzhou Ding. Stability of synchronized chaos in coupled dynamical systems. *Physics Letters A*, 296(4-5):204 – 209, 2002.

[119] Louis M. Pecora. Synchronization conditions and desynchronizing patterns in coupled limit-cycle and chaotic systems. *Phys. Rev. E*, 58(1):347–360, 1998.

[120] Peter Ashwin, Jorge Buescu, and Ian Stewart. Bubbling of attractors and synchronisation of chaotic oscillators. *Physics Letters A*, 193(2):126 – 139, 1994.

[121] Shankar C. Venkataramani, Brian R. Hunt, and Edward Ott. Bubbling transition. *Phys. Rev. E*, 54:1346–1360, 1996.

[122] Juan G. Restrepo, Edward Ott, and Brian R. Hunt. Spatial patterns of desynchronization bursts in networks. *Phys. Rev. E*, 69:066215, 2004.

[123] Shankar C. Venkataramani, Brian R. Hunt, Edward Ott, Daniel J. Gauthier, and Joshua C. Bienfang. Transitions to bubbling of chaotic systems. *Phys. Rev. Lett.*, 77:5361–5364, 1996.

[124] Sun, J., Bollt, E. M., and Nishikawa, T. Master stability functions for coupled nearly identical dynamical systems. *EPL*, 85(6):60011, 2009.

[125] Sorrentino, F. and Porfiri, M. Analysis of parameter mismatches in the master stability function for network synchronization. *EPL*, 93(5):50002, 2011.

[126] Gene Howard Golub and Charles F. Van Loan. *Matrix computations*. Johns Hopkins University Press, 1983.

[127] Nicholas Metropolis, Arianna W. Rosenbluth, Marshall N. Rosenbluth, Augusta H. Teller, and Edward Teller. Equation of state calculations by fast computing machines. *The Journal of Chemical Physics*, 21(6):1087–1092, 1953.

[128] David P. Landau and Kurt Binder. *A guide to Monte Carlo simulations in statistical physics*. Cambridge University Press, 2000.

[129] W. K. Hastings. Monte carlo sampling methods using markov chains and their applications. *Biometrika*, 57:97, 1970.

[130] Mauricio Barahona and Louis M. Pecora. Synchronization in small-world systems. *Phys. Rev. Lett.*, 89:054101, 2002.

[131] S. Kirkpatrick, C. D. Gelatt, and M. P. Vecchi. Optimization by simulated annealing. *Science*, 220(4598):671–680, 1983.

[132] Kurt Binder and DieterW. Heermann. *Monte Carlo Simulation in Statistical Physics*. Springer, 2010.

[133] W.H.Press, S. A. Teukolsky, W. T. Vetterling, and B. P. Flannery. *Numerical Recipes in C*. Cambridge University Press, 1993.

[134] James F. Heagy, Louis M. Pecora, and Thomas L. Carroll. Short wavelength bifurcations and size instabilities in coupled oscillator systems. *Phys. Rev. Lett.*, 74(21):4185–4188, 1995.

[135] Kenneth S. Fink, Gregg Johnson, Tom Carroll, Doug Mar, and Lou Pecora. Three coupled oscillators as a universal probe of synchronization stability in coupled oscillator arrays. *Phys. Rev. E*, 61:5080–5090, 2000.

List of Publications

1. *Desynchronization Bifurcation of Coupled Nonlinear Dynamical Systems*,
   Suman Acharyya and R. E. Amritkar,
   Chaos **21**, 023113 (2011) [arXiv:1101.3130].
   http://link.aip.org/link/doi/10.1063/1.3581154

2. *Synchronization of Coupled Nonidentical Dynamical Systems*,
   Suman Acharyya and R. E. Amritkar,
   Europhysics Letters **99**, 40005 (2012) [arXiv:1111.5408].
   http://dx.doi.org/10.1209/0295-5075/99/40005